Design, Development and Characterisation of Piezoresistive and Capacitive Polymeric Pressure Sensors for use in Compression Hosiery

Vasileios Mitrakos

A thesis submitted for the degree of Master of Science by Research in Electrical Engineering

Heriot-Watt University
School of Engineering & Physical Sciences (EPS)
Institute of Sensors Signals & Systems (ISSS)
December 2014

Supervisors:
Professor Marc P. Y. Desmulliez, Head of ISSS, School of Engineering & Physical Sciences, Heriot-Watt University
Dr Philip Hands, Chancellor's Fellow, Institute of Integrated Micro and Nano Systems, School of Engineering, University of Edinburgh
Dr Lisa Macintyre, Lecturer, School of Textiles & Design, Heriot-Watt University

Abstract

The work in this thesis was focused in developing a flexible and cost-effective pressure sensor capable of detecting pressure variations within the low working range (0-6kPa) of compression hosiery. For this cause, both piezoresistive and capacitive pressure sensors were developed and characterised, utilising conductive and non-conductive polymeric elements to sense compressive loads.

In the first case, the developed piezoresistive sensor is composed of a conductive filler - polymer composite, with a force-dependent conductivity, encapsulated in between a structured and unstructured configuration of electrodes. Initially, as the sensing element of the sensor a multi-walled carbon nanotubes-polydimethylsiloxane (MWCNT-PDMS) composite was tested. A fabrication process is also proposed for developing the MWCNT-PDMS composite which involves a series of successive direct ultrasonications and shear mixing in order to disperse the two constituents of the composite, with the use of an organic solvent. Developing the composite over a range of different filler concentrations revealed a sharp step-like conductivity behaviour, typical amongst percolating composites. The MWCNT-PDMS sensor exhibited a positive piezoresistive response when subjected to compression, which was substantially enhanced when structured electrode layers were utilised. A Quantum Tunnelling Composite (QTC) material was also tested as the sensing material, which displays a large negative piezoresistive response when deformed. The QTC pressure sensor exhibited an improved performance, which was similarly significantly increased when a structured electrode was employed.

In the second case, a parallel-plate capacitive pressure sensor was developed and characterised, which successfully provided a pressure sensitivity within the working range of compression hosiery. The sensor employs an ultra-thin PDMS blend film, with tuneable Young's modulus, as the dielectric medium of the capacitor, bonded in between two rigid copper-coated glass layers. A casting process is also presented, involving the use of a sacrificial mould, in order to pattern the polymeric film with a micro-pillar structure to assist the deformation of the medium under compressive loads. The performance of the sensor with regards to the polymeric film thickness, structure and mechanical softness was explored. Overall, the combination of an ultra-thin dielectric medium with a very low Young's modulus and a microstructured surface resulted in a capacitive pressure sensor with a good performance within the desired pressure regime.

ACADEMIC REGISTRY
Research Thesis Submission

Name*:*	VASILEIOS MITRAKOS		
School/PGI:	EPS/ISSS		
Version: *(i.e. First, Resubmission, Final)*	Final	Degree Sought (Award **and** Subject area)	MSc by Research in Electrical Engineering

Declaration

In accordance with the appropriate regulations I hereby submit my thesis and I declare that:

1) the thesis embodies the results of my own work and has been composed by myself
2) where appropriate, I have made acknowledgement of the work of others and have made reference to work carried out in collaboration with other persons
3) the thesis is the correct version of the thesis for submission and is the same version as any electronic versions submitted*.
4) my thesis for the award referred to, deposited in the Heriot-Watt University Library, should be made available for loan or photocopying and be available via the Institutional Repository, subject to such conditions as the Librarian may require
5) I understand that as a student of the University I am required to abide by the Regulations of the University and to conform to its discipline.

* *Please note that it is the responsibility of the candidate to ensure that the correct version of the thesis is submitted.*

Signature of Candidate*:*		Date:	

Submission

Submitted By *(name in capitals):*	VASILEIOS MITRAKOS
Signature of Individual Submitting:	
Date Submitted:	

For Completion in the Student Service Centre (SSC)

Received in the SSC by *(name in capitals):*			
Method of Submission *(Handed in to SSC; posted through internal/external mail):*			
*E-thesis Submitted (**mandatory for final theses)***			
Signature:		Date:	

Acknowledgments

I would like to thank Professor Marc Desmulliez, Dr Philip Hands and Dr Lisa Macintyre for believing in me and giving me the chance to work on this project, under the premises of both Heriot-Watt University and the University of Edinburgh. I am grateful to their constant support and guidance throughout the duration of this programme, without which, the completion of this challenging project would be impossible. These past months, although intense, were amongst the best and most fulfilling in my life and I truly look forward on continuing my studies under their supervision.

At this point, I would also like to express my gratitude to Marc Leonard for his involvement and the training he provided me for the equipment in the MISEC cleanroom, as well as, Giuseppe Schiavone for his assistance during the measurement stage of the sensors and Dr Adam A. Stokes for providing me access to his laboratory for the use of the micromilling equipment.

Last, but no least, I would like to thank my family and friends for their unconditional support and my girlfriend Dorothea for believing in me and my work. Her influence in helping me cope with the demands of this project was invaluable.

Table of Contents

Abstract ..... **i**

Acknowledgments ..... **iii**

List of Figures ..... **vi**

1. Chapter 1: General introduction **1**

1.1 Introduction 1

1.2 Pressure garments and compression hosiery 1

1.3 Pressure range of compression hosiery 3

1.4 Existing commercial pressure sensing technology for compression hosiery and pressure garments 5

1.5 Objectives and thesis outline 8

2. Chapter 2: Theory of piezoresistive and capacitive sensing **10**

2.1 Introduction 10

2.2 Piezoresistive sensing 10

2.3 Conductive filler-polymer nanocomposites 12

2.4 Percolation theory and effective medium theory 13

2.5 Polymer matrix and filler particles materials in conductive percolating polymer composites 17

2.5.1 Choice of the polymer matrix 17

2.5.2 Filler particle material 18

2.5.3 Dispersion of carbon nanotubes in the polymer matrix 20

2.6 Quantum Tunnelling Composite (QTC) 21

2.7 Flexible piezoresitive sensors 23

2.8 Capacitive sensing 26

2.8.1 The parallel-plate capacitor 26

2.8.2 Categorization of the parallel-plate capacitive sensors 28

2.9 Parallel-plate capacitive sensors 29

2.9.1 MEMS capacitive sensors 29

2.9.2 Flexible polymer-based capacitive sensors 31

2.10 Low pressures sensing issue and other novel ultra-sensitive pressure sensors 35

3. Chapter 3: Piezoresistive pressure sensors **37**

3.1 Introduction 37

3.2 Materials chosen and sensor design 37

3.3 Experimental work 39

3.3.1 Aluminium plates design and development 39

3.3.2 Fabrication process of carbon nanotubes-PDMS nanocomposite 42

3.4 Results and discussion 45
3.4.1 Carbon nanotubes-PDMS composite percolation threshold 45
3.4.2 Developed protrusions of the aluminium substrates 47
3.4.3 Electrical conductivity of the composites under compressive loads 48
3.4.3.1 Experimental setup 48
3.4.3.2 MWCNT-PDMS sensor vs pressure 51
3.4.3.3 QTC sensor vs pressure 52
4. Chapter 4: Capacitive pressure sensor 55
4.1 Introduction 55
4.2 Materials chosen and sensor design 55
4.3 Experimental 57
4.3.1 Creation of the polymer mould 57
4.3.2 Polymer blends and spin coating 61
4.3.3 Bonding copper-coated substrates and mould release 65
4.4 Results and discussion 69
4.4.1 Photoresist and polymer thickness as a function of spin speed 69
4.4.2 Polymer structures de-moulding results 72
4.4.3 Capacitance measurements as a function of applied pressure 75
4.4.3.1 Experimental setup 75
4.4.3.2 Sensors pressure sensitivity results 78
5. Chapter 5: Conclusions and future work 84
5.1 Summary and conclusions 84
5.2 Future work 87
5.2.1 Improving the sensitivity of MWCNT-PMDS and QTC sensors and an alternative sensor design 87
5.2.2 Improving the conformability of the capacitive pressure sensors and potential for embedding it in compression hosiery 89
5.2.3 Proposed design of a stand-alone garment-sensor system for low pressure monitoring applications 90
References 93

List of Figures

Figure 1.1: Photographs of (a) knee-length compression hosiery and (b) pressure garments in various designs 1
Figure 1.2: Illustration of compression hosiery knitted configuration 3
Figure 1.3: Illustration of a Class II compression hosiery 3
Figure 1.4: The PicoPress sensor 6
Figure 1.5: The Tekscan I-scan system 7
Figure 1.6: Pliance X system during use in pressure garment 8
Figure 2.1: The structure (a) of a piezoresistive semiconductor sensor and (b) a silicon-membrane based pressure sensor configuration and sensing principle 11
Figure 2.2: Illustration of change in resistivity of percolating composites as a function of filler concentration by weight. 14
Figure 2.3: Percolating omposite resistivity as a function of the geometric factor *t* and filler concentration φ. 17
Figure 2.4: Structure of a multi-walled carbon nanotube 19
Figure 2.5: QTC material 21
Figure 2.6: FN quantum tunnelling between the spikes of two neighbouring nickel particles. 22
Figure 2.7: Resistance drop of a QTC material when subjected to compression 23
Figure 2.8: A MWCNT-PDMS strain sensor 24
Figure 2.9: MWCNT-PDMS composite relative resistance versus pressure and filler concentration 24
Figure 2.10: QTC material as a switch in wearable electronics applications 25
Figure 2.11: Parallel plate capacitor 27
Figure 2.12: A MEMS capacitive pressure sensor 29
Figure 2.13: Illustration of the fabrication process of the MEMS pressure sensor 30
Figure 2.14: Flexible parallel-plate capacitive polymeric pressure sensors 32
Figure 2.15: All-elastomer capacitive pressure sensors. 33
Figure 2.16: High performance flexible strain sensors 34
Figure 2.17: Illustration of fabrication process and working principle of (a) the pressure sensitive organic transistor sensor and (b) the Au nanowires-piezoresistive sensor 35
Figure 3.1: The commercial QTC "pill" product 37
Figure 3.2: Piezoresistive pressure sensor design 38
Figure 3.3: Illustration of envisaged embedding to garment 39
Figure 3.4: The micromilling equipment in action 40
Figure 3.5: Multi-element geometry designed for patterning via the micromilling equipment 41
Figure 3.6: Dispersion of MWCNTs in toluene solution via direct ultrasonication 42
Figure 3.7: Shear mixing of the solution and evaporation of toluene 44
Figure 3.8: Designed setup for measuring the MWCNT-PDMS composites 45
Figure 3.9: MWCNT-PDMS nanocomposite percolating behaviour 46
Figure 3.10: Examination of the protrusion features via optical profilometry 47
Figure 3.11: Scaling down the size of the protrusions and resultant features 48
Figure 3.12: Photograph of developed aluminium structures, with attached wiring, and bonded composite film on a flat aluminium substrate 49

Figure 3.13: Photographs of (a) MAT-400 die-bonder equipment and setup and (b) pressure sensor during measurement 50
Figure 3.14: MWCNT-PDMS pressure sensor response to compression 51
Figure 3.15: QTC pressure sensor with flat top electrode layer. 53
Figure 3.16: QTC sensors performance improved significantly when a structured electrode layer was utilised. 53
Figure 4.1: Capacitive pressure sensor design 56
Figure 4.2: Spin-coating of AZ photoresist 58
Figure 4.3: UV exposure of wafers 59
Figure 4.4: The photomask utilised to develop the photoresist mould 60
Figure 4.5: The photoresist moulds after exposing and development 61
Figure 4.6: PDMS blend Young's modulus as a function of Sylgard 184 concentration by weight 62
Figure 4.7: Sylgard 184 and Sylgard 527 after initial preparation 63
Figure 4.8: Sylgard 184 and Sylgard 527 first degassing prior to mixing 64
Figure 4.9: PDMS films after de-moulding via the triple bath procedure 66
Figure 4.10: The e-beam evaporator equipment 67
Figure 4.11: Ti/Cu coated glass slides 68
Figure 4.12: Bonded Ti/Cu-coated glass slides on the PDMS blend film prior to de-moulding 69
Figure 4.13: Photoresist thickness as a function of spin speed 70
Figure 4.14: Photoresist mould recesses height size over different geometries 70
Figure 4.15: PDMS film thickness 71
Figure 4.16: Developed PDMS film thickness measurements via optical profilometry. 72
Figure 4.17: Manually de-moulded PDMS structures of a circular pillar-geometry 73
Figure 4.18: De-moulded structured PDMS films via the triple bath process 74
Figure 4.19: De-moulded structured PDMS blend films via the triple bath process 75
Figure 4.20: The precision weight set that was utilised to exert the desired pressures... 76
Figure 4.21: Experimental setup connected to the impedance analyser 77
Figure 4.22: The second experimental setup 78
Figure 4.23: Capacitive response of the developed pressure sensors within the working range of compression hosiery 79
Figure 4.24: Capacitive response of a type 10:1 pressure sensor over repeated measurements: (a) in terms of pressure; (b) in terms of cycle. 81
Figure 5.1: A proposed alternative pressure sensor design 88
Figure 5.2: Illustration of proposed fabrication process of a conformable sensor 89
Figure 5.3: Proposed design of (a) stand-alone garment-sensor system as a unit cell and (b),(c) in interconnected multi-cell configurations 91

Chapter 1:
General introduction

1.1 Introduction

In this chapter, compression hosiery and pressure garments are introduced and their importance in treating a number of serious medical conditions is noted. Their working pressure range, as well as the importance of monitoring their performance and the limitations of current commercial sensors utilised for this task, are also discussed. The motivation and the objectives of this research are outlined in the final section; a motivation that stems from the need of a flexible and cost-effective pressure sensing system that can comply with the requirements for this application.

1.2 Pressure garments and compression hosiery

Utilizing medical garments that apply a degree of pressure to treat a number of medical conditions, such as varicose veins, leg ulcers and hypertrophic scars, is considered as one of the key aspects in the healing therapy of such ailments [1]. These medical garments are generally divided into two categories, namely pressure garments and compression hosiery (Fig. 1.1), depending on their respective medical application and method of construction.

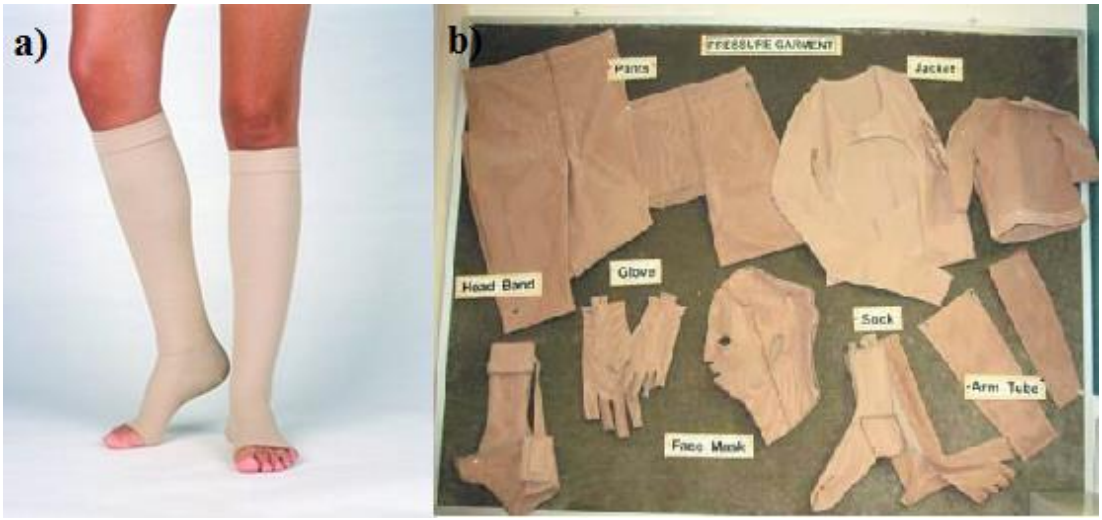

Figure 1.1: Photographs of (a) knee-length compression hosiery and (b) pressure garments in various designs **[2] [3]**

Pressure garments are used primarily in patients suffering from hypertrophic scars inflicted by burns [4]. These garments, designed to be worn on different parts of the body, compress the burn scar site to facilitate a more rapid healing of the damaged tissue and thus block the development of hypertrophic scars [5] [6].

By applying pressure, the damaged tissue's swelling, redness and rigidity drop significantly over time and the full recovery of the tissue becomes feasible. The effect of pressure, although not fully understood, is attributed to a number of factors that include the improved collagen synthesis control [7], its quicker production [8] and the realignment of existing collagen bundles of the tissue [9] [10]. A way to control the amount of pressure delivered to the patient is achieved by the insertion of polyethylene foam paddings in the garment, with varying thicknesses according to the amount of pressure required [11].

Compression hosiery, on the other hand, is utilized to treat or prevent medical conditions such as venous leg ulcers, varicose veins, lymphoedema and chronic venous insufficiency, as well as reduce the risk of thrombosis [12] [13]. Again the hosiery exerts a certain amount of pressure on the leg and forces a portion of the veins to narrow resulting in the reduction of the volume of blood in the veins. Consequently, the calf muscle pump begins to work more efficiently, enabling an easier bloodstream pump to the heart, which leads to a higher tissue oxygenation and better micro circulation [14].

A prime example of one of the most serious conditions that can be treated with compression hosiery is Chronic Venous Insufficiency (CVI), characterised by oedema, hyperpigmentation, lipodermatosclerosis, white atrophy and ulcers on the leg [15]. In CVI, the pump in the calf muscle is unable to reduce venous pressure (referred as venous hypertension) during walking due to damaged or collapsed vein valves, leading to increased capillary pressure.

Compression hosiery began to develop upon the discovery of rubber and most importantly the ability to mix rubber threads with other types of materials [15]. The yarns employed in compression hosiery are of a flexible nature, and are developed by combining materials such as polyimide, cotton and other multifilament fibres to enable large tensile strains [16]. The knitted configuration of compressive hosiery usually utilizes two types of yarns: an inlaid high strain yarn which exerts the required pressure and provides elasticity to the fabric, and a finer non-elastic yarn that forms the base knit structure and the covering layer of the hosiery (Fig. 1.2).

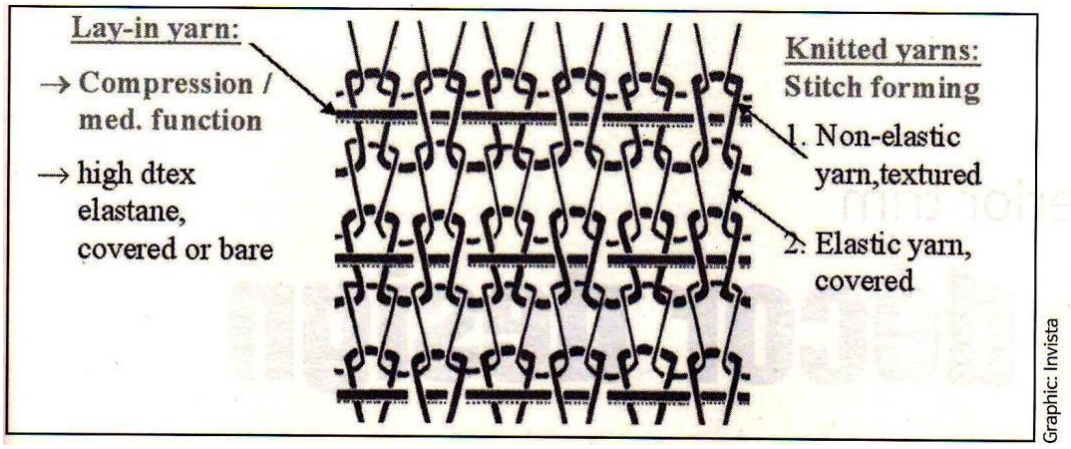

Figure 1.2: Illustration of compression hosiery knitted configuration [15]

1.3 Pressure range of compression hosiery

The knitted configuration of compression hosiery is designed to exert a pressure gradient on the leg of decreasing magnitude by height (Fig. 1.3), generally varying from as low as 0.5 kPa (5 mmHg) at the thigh to as high as 6 kPa (50 mmHg) at the ankle [17] [18] [19].

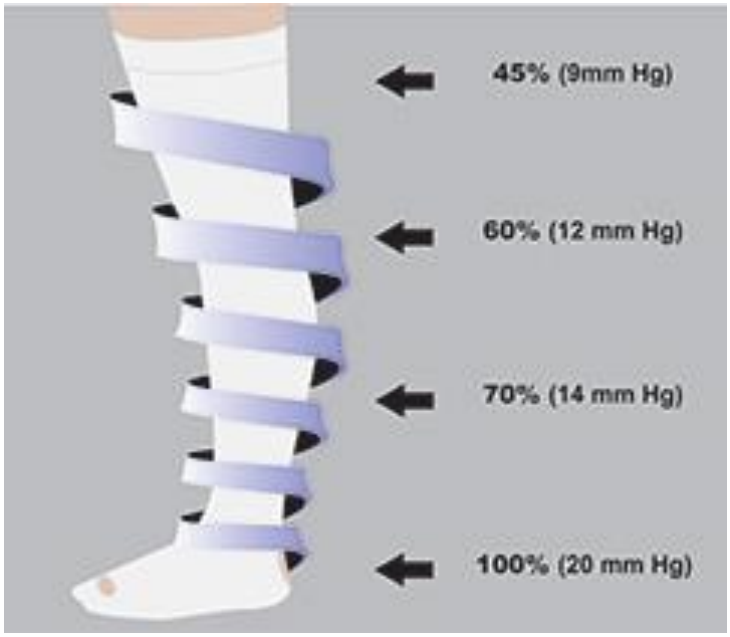

Figure 1.3: Illustration of a Class II compression hosiery that applies a mild pressure gradient from thigh to ankle **[20]**

The physical mechanism of how compression hosiery exerts pressure unto the body can be described by Laplace's law [21]:

$$P = T/r \tag{1.1}$$

The amount of pressure on the tissue P, is proportional of the fabric's tension T and inversely proportional to the leg radius r. Therefore, under a constant tension and increasing radius the compression hosiery exerts a decreased pressure and vice versa.

The application of a pressure gradient lies in the increased blood and lymph velocity achieved in the venous system, and thus the improved leg oxygenation, when the pressure is greatest at the ankle [22]. The increased blood circulation has a significant impact on the relief a patient experiences, from swelling and other associated leg ailments. Moreover, the graduated configuration of compression hosiery has been also reported [23] to reduce ankle swelling, vein pooling and venous distention on the leg.

Compression hosiery was initially designed in 1949 to assist blood circulation on the venous system when it was observed that compression increased venous flow in venous deficiency conditions [24]. The positive effect of compression treatment via compression hosiery was further demonstrated 3 years later when it was shown that this type of garments substantially decreased the occurrence of pulmonary oedema in operated patients [25].

It was not before 1977 however that compression hosiery, with the typical graduated pressure design, were first introduced when it was observed that a pressure of decreasing magnitude leads to a significant decrease of deep venous thrombosis [26]. Despite the positive observations, compression hosiery were not widely utilized in hospitals to treat venous conditions due to the fact that the reported finding were not supported by any physiological mechanisms [27]. Ultimately, a finding that urged to reconsider the usage of compression hosiery in clinical conditions came in 1994 when a meta-analysis of venous deficiency treatments revealed that venous thromboembolism significantly decreased when such hosiery were used [28].

Compression hosiery are also divided into four compression classes (Table I), depending on the maximum amount of pressure the patient's condition requires [14] [29], and are available in many forms and styles such as thigh length stockings, knee length stockings and tights.

Class	Pressure level	Specified Ankle Pressure (mmHg) [1mmHg=133.3Pa]	Suggested Medical Application
I	Light	10-15	Prevent varicose veins, relieve heaviness and fatigue
II	Mild	16-22	Treat mild varicosities, aching, swelling and thrombosis prophylaxis
III	Moderate	23-32	Treat moderate varicose veins, light and dependency oedema, mild or moderate CVI, and post- sclerotherapy
IV	Strong	34-46	Treat serious varicose veins, severe oedema/CVI, leg venous ulcer, lymphedema, and post- erysipelas
V	Very Strong	≥49	Treat severe post-thrombotic syndrome, severe lymphedema, elephantiasis

Table I: Compression hosiery classes and medical application [14] [29]

1.4 Existing commercial pressure sensing technology for compression hosiery and pressure garments

A major concern regarding compression hosiery and compression garments is the lack of a systematic monitoring of pressure delivered to the patient, and therefore, the absence of an optimal grade of compression [30].

Delivering a smaller than required pressure gradient has been reported [12] to insufficiently assist blood circulation, while applying excessive pressures blocks the blood flow and has the reverse effects of reduced deep vein flow velocity and decreased subcutaneous tissue flow [23]. Thus, measuring accurately the exact interface force between skin and garment is important in order to enable the monitoring of treatment efficiency and minimize the complications associated with excess pressure and incorrect pressure gradient [31].

Due to the requirements to monitor low pressure variations in compression hosiery, most of the commercially available pressure sensors either fail to accurately measure the applied pressure, as their measurement range lies higher than the range required (0-6kPa) [18], or are too expensive or time consuming to be used routinely in the clinical environment.

Typical examples of such commercial pressure sensors include:

The PicoPress sensor, as shown in Figure 1.4, which is a large pneumatic sensor consisting of a pressure transducer connected with a polyurethane foam-based sensor [32]. The sensor is placed around the limb and the exerted pressure on the inflated balloon is directly transmitted to the transducer. Due to the large design of the sensor and electro-pneumatic nature, its spatial resolution is limited around the circumference of the leg within a fixed height and the performance of the sensor is marred by the hysteresis and low accuracy [32] [33].

Figure 1.4: The PicoPress sensor **[34]**

The widely used Tekscan I-scan piezoresistive sensors, which employ a resistive ink sandwiched in between two layers of plastic film (Fig. 1.5) [31] [32] . A matrix of these sensors comprises the complete system, providing good spatial resolution. The I-scan sensors come in a variety of shapes and configurations depending on the application and the optimization required. However, these sensors require extensive and elaborate calibration in order to produce an acceptable pressure measurement in terms of accuracy

[32]. Part of this calibration includes de-trapping of air pockets captured between the plastic layers via manual squeezing and conditioning by applying the maximum expected load in a bladder tester.

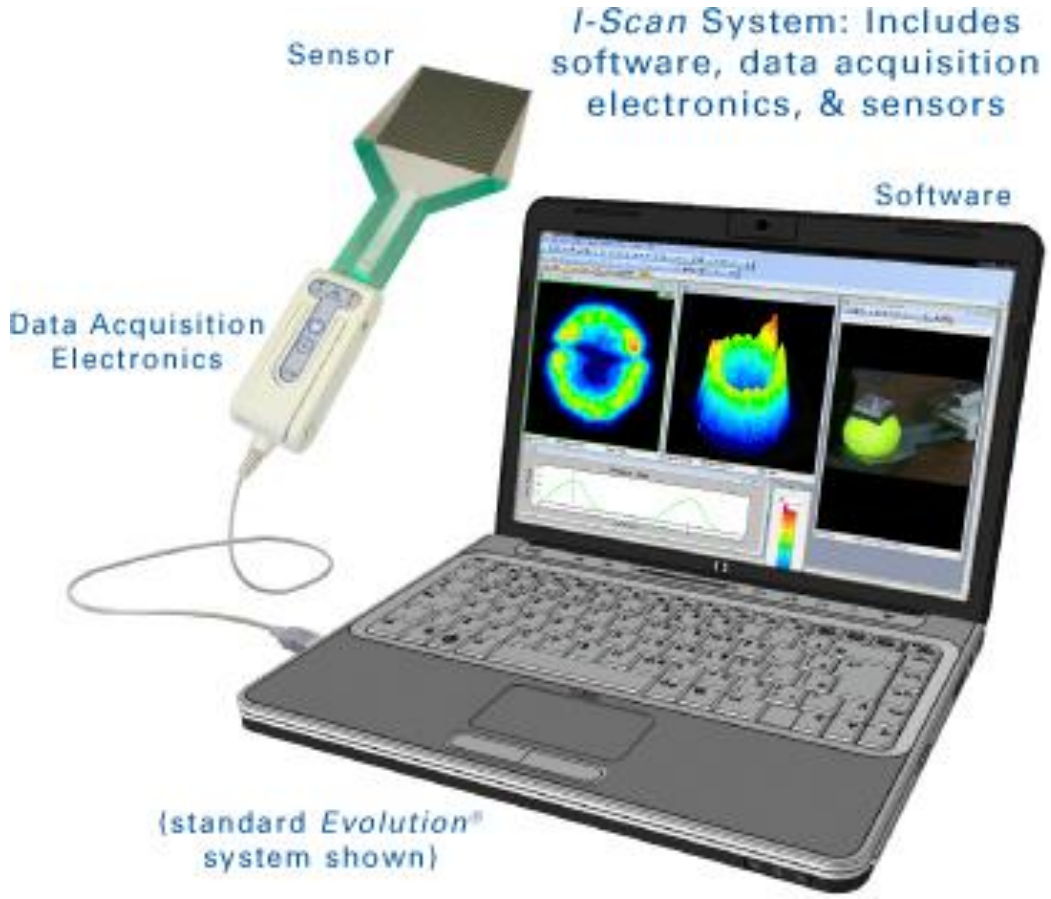

Figure 1.5: The Tekscan I-scan system, which includes the sensor, data acquisition electronics adapter and software **[35]**

And finally the Pliance X System which is a thin (<1mm thick) capacitive pressure sensor with small sensing area of 10mm^2 that utilizes a conductive strip for connection to an electronic analyser (Fig. 1.6) [36]. The sensor exhibits superior pressure sensitivity (detects pressure variations of as low as ~0.3kPa on the range of 0-10kPa), can be interconnected with other Pliance X sensors to form a matrix providing excellent spatial resolution, and due to the presence of the extended conductive strip, can be easily inserted in to compression hosiery. However, the price of the complete system is on the range of approximately US$ 21,000 (including the electronic analyser and software), making it impractical for monitoring the desired interface pressure at a patient level even in a clinical environment [36]

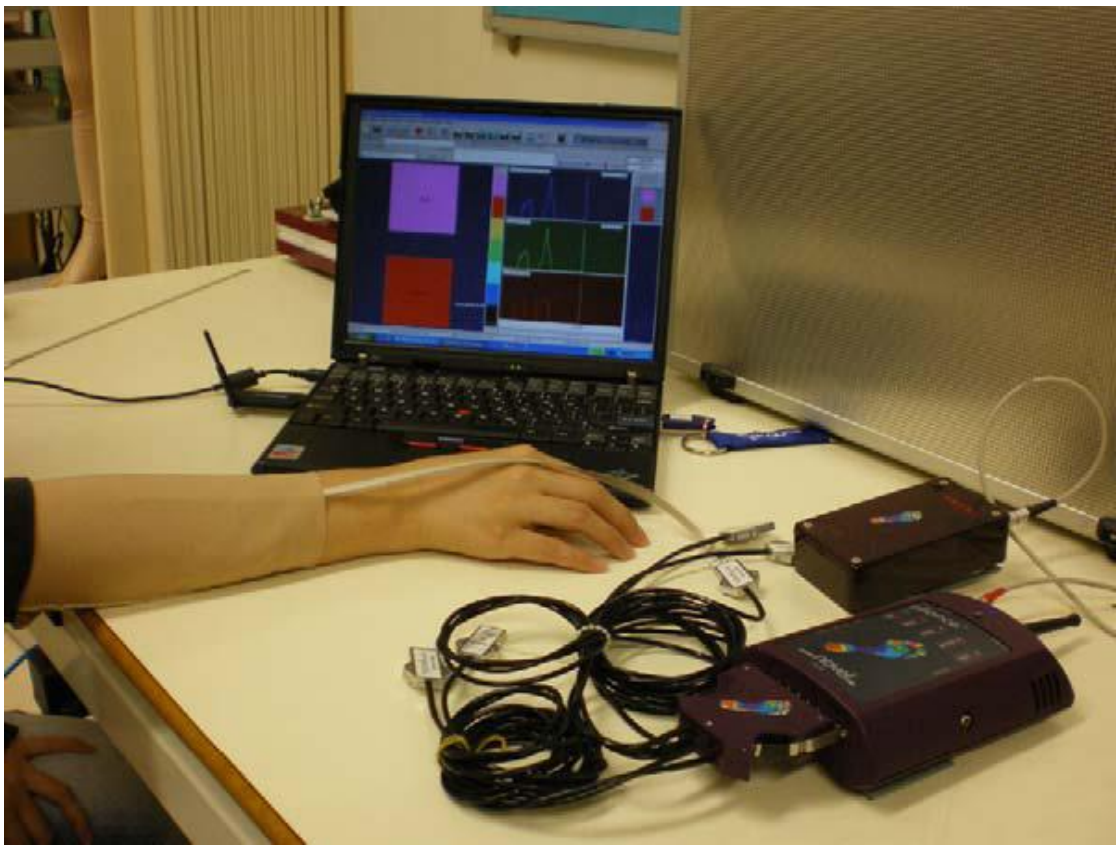

Figure 1.6: Pliance X system during use in pressure garment **[36]**

1.5 Objectives and thesis outline

Ideally, an interface pressure sensor for the use in compression hosiery and pressure garments in general, should be cost-effective, small, thin, flexible and sensitive enough to detect pressures within the range of 0-6kPa (0-50mmHg) [37] [38] [39]. Moreover, it should be suitable to be embedded unto the compression hosiery, be highly conformed to the body contour and ideally be part of the fabric itself.

Since none of the commercially available sensors can fully comply with the aforementioned requirements, a number of cost-effective pressure sensors designs were explored in this thesis, with the aim to be potentially insertable in compression hosiery and be able to monitor the low interface pressure between fabric and skin. The main goal of this work was to develop a pressure sensor capable of detecting the low pressures delivered by compression hosiery. In order to address this issue, two different types of flexible pressure sensors technologies were evaluated: piezoresistive pressure sensors and capacitive pressure sensors.

In the case of piezoresistive sensors, two conductive polymeric composites, Multi-Walled Carbon nanotubes-Polydimethylsiloxane (MWCNT-PDMS) composite and Quantum Tunnelling Composite (QTC), were developed and evaluated within a novel design for compression hosiery embedding. A parallel-plate capacitor sensor was also developed and characterised. This sensor utilises a soft and ultra-thin structured insulating PDMS blend, with tuneable Young's modulus, as the sensor's connecting dielectric medium.

The thesis is divided into 5 chapters and is outlined as follows:

Chapter 2 examines the fundamentals of piezoresistive and capacitive sensing. Concepts affiliated with conductive polymeric composites, flexible piezoresistive and capacitive sensors, such as percolation, effective medium theory, quantum tunnelling and parallel-plate capacitors in capacitive sensing, amongst many, are explored. Examples for both cases of existing pressure sensors in these fields of research are also presented.

Chapter 3 is an experimental chapter and focuses on conductive filler-polymer composites and their sensitivity under axial loading. A carbon nanotube-PDMS nanocomposite preparation technique is presented, as well as the fabrication process of micro-structured rigid layers that encompass the sensor. The pressure sensitivity of the PDMS nanocomposite and QTC material is explored with respect to the rigid micro-structured layer features.

Chapter 4 is an experimental chapter and examines a parallel plate capacitor pressure sensor that utilizes a micro-structured PDMS blend with tuneable Young's modulus. All the steps of the development process are presented which include: the preparation of the PDMS blend, moulding, release and bonding to conductive substrates. The pressure sensitivity is measured and discussed for different blend compositions and structure features.

Chapter 5 gives an overview of the developed sensors sensitivity and their technical applicability in compression hosiery embedding. Strategies for improving the required sensitivity of both categories of the developed sensors are explored. Finally, a general sensor-garment system design is also presented and discussed.

Chapter 2:
Theory of piezoresistive and capacitive sensing

2.1 Introduction

This chapter deals with the fundamentals of piezoresistive and capacitive sensing in flexible applications that employ polymers as the sensing elements. In the first half of the chapter, conductive filler-polymer composites are introduced and the piezoresistive nature governing their conduction is discussed, followed by recent developments in flexible sensor applications of these composites. Similarly in the second half, capacitive sensing under the same context is introduced, along with a number of polymer-based parallel-plate capacitive sensors utilised to detect pressure variations or strain, via structural deformation. In both cases, materials, fabrication methods and techniques in developing sensors of both categories are discussed, as well as the challenges of detecting pressure variations in the low working range of compression hosiery.

2.2 Piezoresistive sensing

Materials that possess the ability to change their internal electrical resistance when subjected to mechanical deformation induced by stress or tensile strain are defined as piezoresistive [40]. Piezoresistive sensors, in turn, are electromechanical sensing systems that utilize the stress-dependant electrical resistance behaviour of some materials to quantify the changes in pressure or strain in applications where sensing of such measurands is desired.

Amongst the plethora of piezoresistive sensors available, the silicon-based MEMS (micro-electromechanical systems) piezoresistive pressure sensors are the most common and widely used. Typical examples of such sensors include the piezoresistive semiconductor sensor [41] and the silicon-membrane based pressure sensor [42] [43] [44].

In the first case (Fig. 2.1a), the sensor is composed of two semiconductor materials and relies on carrier diffusion to measure applied pressures [44]. As the system is subjected

to deformation, charge carriers from the p-type region diffuse into the n-type region inducing a change of the resistivity of the sensor [45].

In the latter case, the sensor utilizes a thin silicon membrane diaphragm covering a sealed cavity, which serves as sensing element of the system (Fig 2.1b). Four piezoresistive thin film elements are deposited onto the surface of the membrane in a Wheatstone bridge configuration. When a pressure is applied to the sensor, the membrane deformation leads to a change of resistance of the four elements which are measured independently.

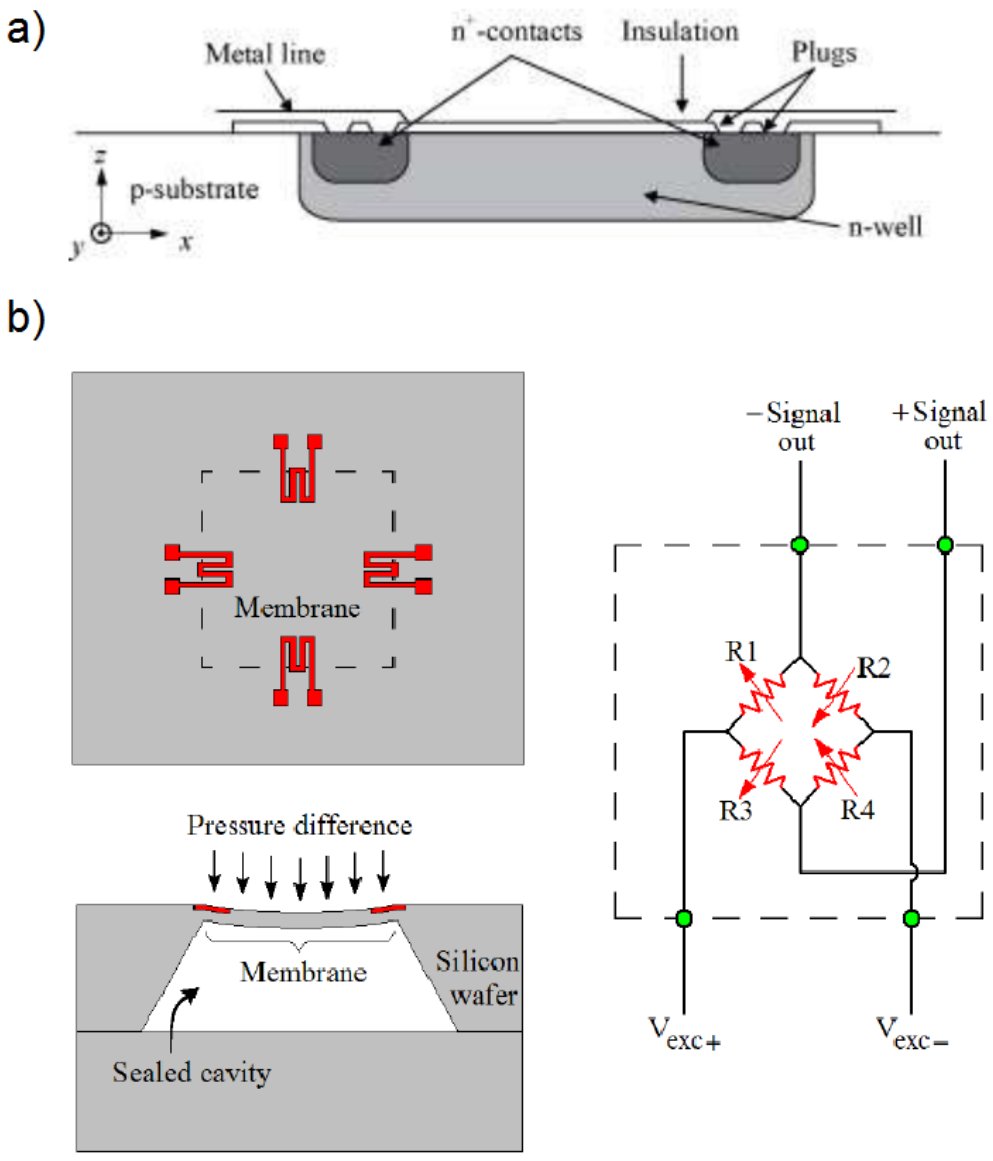

Figure 2.1: The structure (a) of a piezoresistive semiconductor sensor and a (b) silicon-membrane based pressure sensor configuration and sensing principle **[41] [42]**

The rigid and non-conformable nature of these silicon-based MEMS piezoresistive sensors, as well as the demanding and costly fabrication processes they require, have led to the emergence of a new class of flexible piezoresistive sensors based on conductive polymer composites. Utilising these composites as the piezoresistive element can be traced back to 1986 when Lundberg and Sundqvist discovered that the resistivity of a polymer containing carbon particles exhibit sensitivity to deformation, when subjected to applied pressure or due to swelling in the presence of certain chemical solvents [46] [47].

The existence of a material that is intrinsically flexible with a deformation-dependant conduction behaviour, and can also be integrated to sensory systems utilising simple procedures such as mould casting (soft lithography), has had a tremendous impact on the development of flexible sensors in recent years, as shown in the next sections.

2.3 Conductive filler-polymer nanocomposites

Composites are materials defined as multi-component systems where two or more components, of different physical and chemical properties, are blended together in such a way that at least one of the components serves as the *matrix* of the system, constituting the major continuous phase, whilst the others are minor constituents of the system, referred as the *fillers* [48]. Both *matrix* and *filler* constituents retain however their identities as they do not merge into one another or dissolve, but act in concert providing in the end a more desirable combination of properties [49].

Interest in these multi-component systems, especially polymer nanocomposites, has grown rapidly in recent years since it is relatively straightforward to modify the properties of a material by just inserting the appropriate amount of a different material [50]. Generally, a composite is considered a nanocomposite if the filler has at least one dimension in the nanometre scale. Interest in the nanocomposites stems from their ability to exhibit the desired property enhancement at very small filler concentration, due to the increased surface and aspect ratios, which reduces significantly the cost of the final composite material. Furthermore, nanocomposites have been shown to be more compatible with ink-jetting and other printable deposition techniques, compared to their latter larger filler particle micro-composite counterparts [51].

In polymer nanocomposites the most commonly used fillers are metallic nanoparticles, nanosilicas and carbon based nanoparticles. The attributes ascribed to the polymer by the nanoparticles can be remarkable, with the potential to produce a whole new generation of materials with specifically tuned properties. They represent a material class radically different compared to conventional materials [52] [53] [54].

2.4 Percolation theory and effective medium theory

Manipulation of the electrical conductivity stands as one of the most important properties for polymeric composites. Polymers are generally by nature electrically insulating materials. A way to make them conductive is by inserting a conductive filler particle to the polymeric matrix. The conduction in these polymeric composites is the result of either a strong field-effect such as tunnelling, field emission and space-charge limited transport or the formation of continuous conducting networks, due to direct contact of the filler particles spanning the whole material; a phenomenon known as percolation [55]. In the case of non-percolating composites, the resulting current/voltage behaviour of the composite is non-linear; in the case of percolating composites, current/voltage behaviour is predominately ohmic.

Significant drop in the resistivity of a composite via the addition of carbon-based fillers such as carbon black, carbon nanotubes, graphite and graphene has been well documented over the last few years [56]. Carbon-based fillers are generally preferred in polymeric composites over their metal particles counterparts as the latter tend to oxidize their surfaces, producing an insulating layer. Moreover, the resulting composite utilising carbon-based fillers is also lighter [57]. The fact that this type of polymer-filler composites exhibits the ability to vary conductivity accordingly to one's needs has led to the development of a wealth of novel sensor systems the past years, including but not limiting to, strain sensors, pressure sensors and chemical sensors, described later.

Generally in these composites, a major drop in resistivity is observed at a critical concentration of the conductive filler which is referred as the percolation threshold, and many conductive polymer composites exhibit this behaviour [58]. Percolation theory stands on the principle that, beyond the critical filler concentration, a conductive pathway is formed that completely spans the composite. In addition, percolation theory

assumes that the electrical conductivity arises solely due to the direct contact of the filler particles.

More specifically, when a small weight fraction of the filler particles is randomly inserted into the polymeric matrix (Fig. 2.2 region A), contact amongst neighbouring particles is insignificant and therefore the composite remains insulating [59]. However, if the filler weight fraction in the composite is increased, the direct contact amongst neighbouring filler particles also rises, leading to an exponential increase in conductivity; a point commonly referred as the percolation threshold (Fig. 2.2 region B). The step-like behaviour in the composite conductivity is attributed to the formation of a complete conductive pathway of neighbouring filler particles in direct contact (Fig. 2.2 regions B and C).

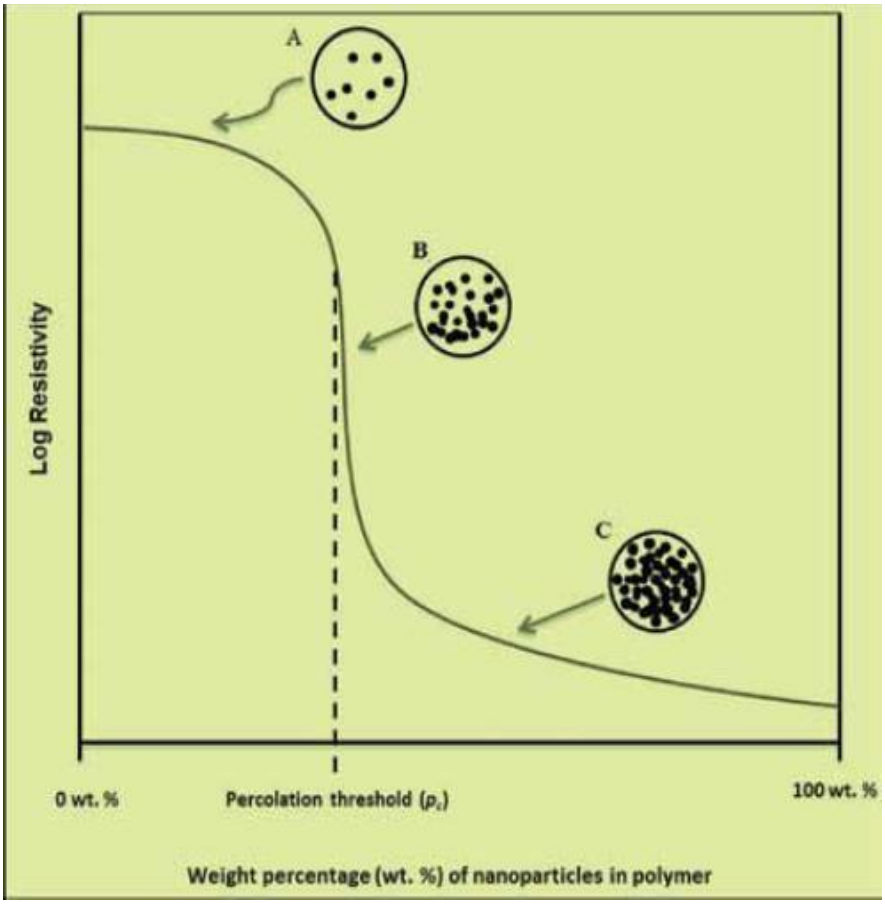

Figure 2.2: Illustration of change in resistivity of percolating composites as a function of filler concentration by weight. Region A represents the insulating state of the composite, region B the percolation threshold at which a conductive pathway is formed and resistivity drops exponentially, and region C the change in resistivity when a large number of conductive pathways has already formed **[60]**

According to percolation theory the relation between the conductivity σ of a composite and the filler concentration p, near the percolation threshold p_c, is given by the following equation [61]:

$$\sigma \propto (p - p_c)^t \tag{2.1}$$

The equation 2.1 only holds for $p>p_c$, and the exponent t has a different value according to the geometry of the filler [62].

Percolation theory, albeit a successful model for describing the conductivity behaviour of polymer composites, only applies if the conductivity ratio σ_h/σ_l of the low and high conductivity phases of the composite is infinite [63]. In addition, the model fails for filler concentration very near or below the percolation threshold and only exhibits good results for composites with randomly and non-aggregated filler particles of smooth, ellipsoidal or spherical shape (Fig 2.3). Percolation theory's failure to accurately describe the electrical behaviour of a composite below the percolation threshold led to the development of another theory, the effective medium theory [64] [65].

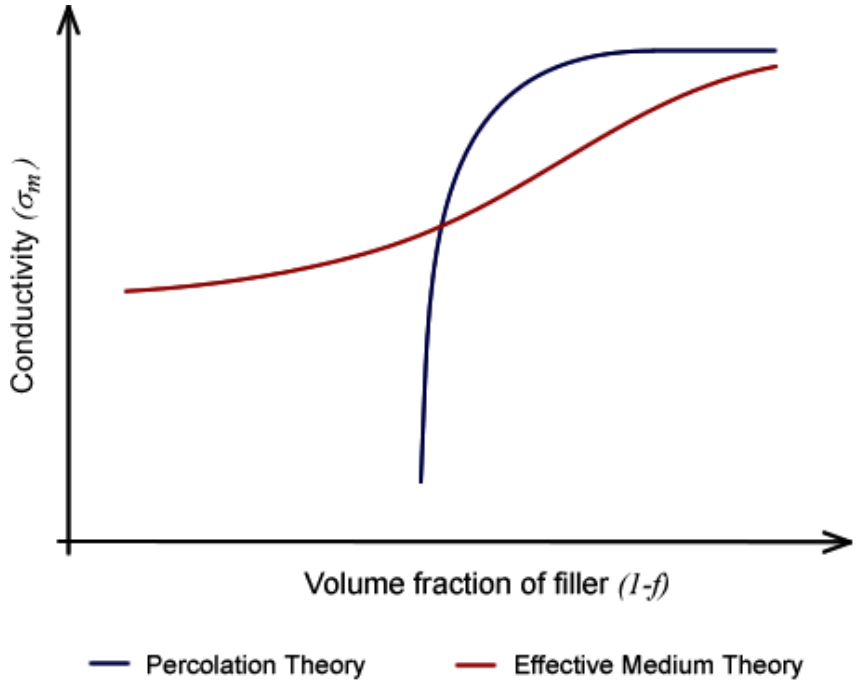

Figure 2.3: Effective medium theory and percolation theory curves bellow and above percolation threshold **[63]**

Effective medium theory is based on a model that associates each pair of nearest neighbouring filler particles with a resistance, which in total, form a network with a random resistance distribution. This resistance network in turn is described by an average value, and thus the original inhomogeneous composite is represented by an ordered and homogenous medium, called effective medium, with the same macroscopic properties as the composite. Effective medium theory works best with composites of finite conductivity ratio and describes only and successfully the behaviour of a

composite below the percolation threshold, as it predicts no sharp percolation threshold (Fig. 2.3).

A complete mathematical model that effectively describes a composite's conductivity below and above the percolation threshold, as a function of the concentration of the filler, was developed by MacLachlan in 1987 via the Generalised Effective Medium Theory (GEM) which united the percolation theory and effective medium theory under one equation [66].

The GEM equation is given by the following expression:

$$\frac{(1-\varphi)\left(\sigma_l^{1/t}-\sigma_m^{1/t}\right)}{\sigma_l^{1/t}+\frac{1-\varphi_c}{\varphi_c}\sigma_m^{1/t}}+\frac{\varphi\left(\sigma_h^{1/t}-\sigma_m^{1/t}\right)}{\sigma_h^{1/t}+\frac{1-\varphi_c}{\varphi_c}\sigma_m^{1/t}}=0 \tag{2.2}$$

Where φ is the filler concentration (by volume fraction) and φ_c is the concentration of the filler at the percolation threshold. The symbols σ_l and σ_h relate to the low conductivity constituent, the polymeric matrix, and the high conductivity constituent, the filler, respectively. The subscript *m* represents the effective medium.

Finally the factor *t*, as in percolation theory, varies according to the geometric shape of the filler particle. In the case of ellipsoid-shaped filler particles *t* is calculated via the expression $t=\varphi_c/(1-L)$, where the demagnetisation factor *L* is 1/3 for spheres 1/2 for flat discs [67]. For more complex particle geometries (i.e. thin rods) *t* can only be calculated by fitting it to experimental data [68] .

The conductivity of the composite can be therefore estimated by solving GEM equation as a function of $\sigma_m(\varphi)$ and by fitting experimentally the filler σ_h and polymer σ_l individual conductivities, the percolation threshold φ_c, and the geometric factor *t*. The composite's conductivity can be expressed by the following equation (Fig. 2.4):

$$\sigma_m(\varphi)=\left\{\frac{1}{2a}\left[R(\varphi)+\sqrt{R^2(\varphi)+4ahl}\right]\right\}^t \tag{2.3}$$

Where

$$a=\frac{1-\varphi_c}{\varphi_c},\ h=\sigma_h^{\frac{1}{t}},\ l=\sigma_l^{\frac{1}{t}}\ and\ \ R(\varphi)=\varphi(h-l)(a+1)+al-h$$

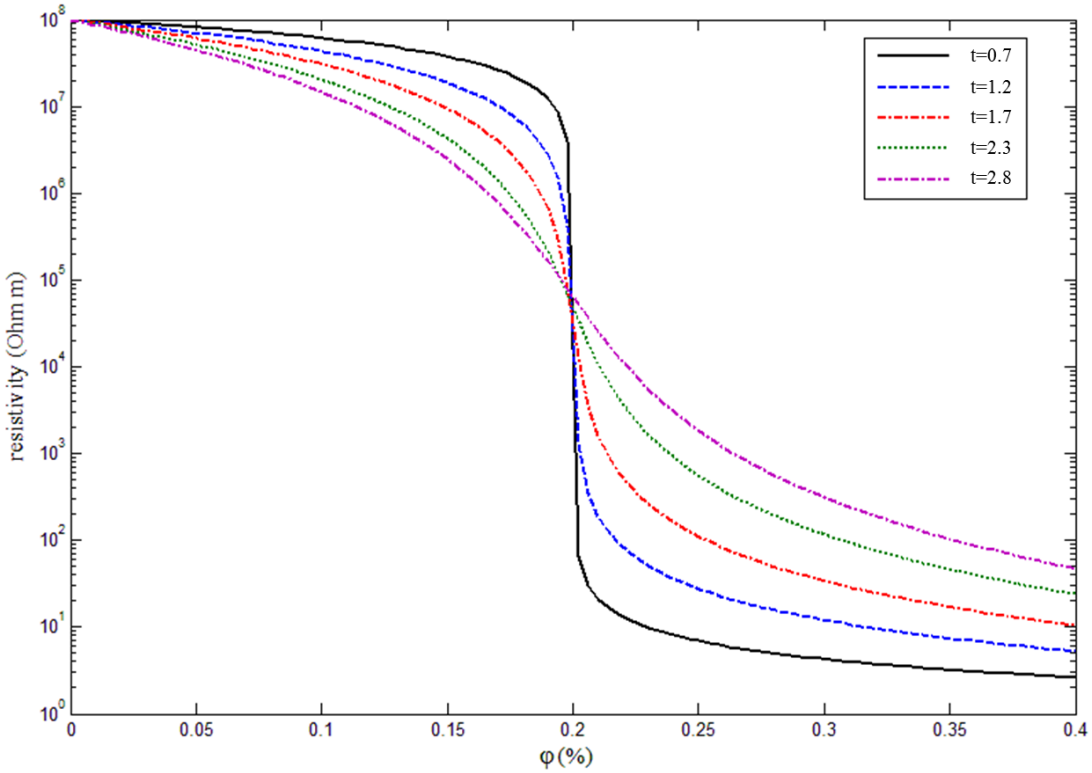

Figure 2.4: Percolating omposite resistivity as a function of the geometric factor t and filler concentration φ. Equation 2.3 was solved and plotted via Matlab for $\sigma_l = 10^{-8}$ Ω·m, $\sigma_h = 1$ Ω·m , $\varphi_c = 0.2\%$, t = 0.7-2.8. Smaller values of t lead to a sharper percolation threshold

2.5 Polymer matrix and filler particles materials in conductive percolating polymer composites

2.5.1 Choice of the polymer matrix

Plastics and elastomers with diverse properties can be used as the matrix of the nanocomposite. Poly(ethylene) (PE) [69], poly(methyl methacrylate) (PMMA) [70], poly(L-lactide) (PLLA) [71], polycarbonate [72], have been used as the matrix constituent of carbon-based nano-filler composites to produce flexible sensors such as strain gauges with the ability to withstand excessive strain of orders of magnitude larger than that of standard metallic gauges [73].

Poly(dimethylsiloxane) (PDMS) is a silicone-based elastomer, which in comparison with the aforementioned polymers, exhibits superior mechanical elasticity capable of withstanding structurally large strains over 100% [74]. The vast majority of flexible sensors are based on PDMS elastomeric structures since it is non-conductive, with a low

Young's modulus of 1.7MPa, suitable for micro-processing, chemically inert and biocompatible material, making it ideal for biomedical sensors [75] [76].

Moreover, owing to its great flexibility PDMS can be easily mounted on curved surfaces. Generally, PDMS structures serve as a protective layer for fluidic channels and encapsulants [76], but a number of fully elastomeric strain, pressure and tactile sensors exploiting conductive PDMS structures have been reported that utilize single or multi-walled nanotubes [77], graphene [78] and carbon black [79] as the filler particles.

Amongst the advantages of using PDMS, is the fact that the initial fluid state of the material makes it possible to develop composites with various filler concentrations. The material can be processed at room temperature and gives excellent control over the desired film thickness. PDMS is also an inert material and due to its low polarity surface has hydrophobic characteristics which make it less prone to degradation over time, thus ensuring a long and stable device operation [80].

2.5.2 Filler particle material

Carbon fillers that are utilized in polymeric nanocomposites, include graphite, carbon black, graphene and carbon nanotubes.

Graphite has a multi-layer planar structure, and the carbon atoms that comprise each of these layers are arranged in a lattice of a hexagonal geometry, the most stable form of carbon [81]. Utilising graphite as the filler constituent in polymeric composites usually involves the use of graphite intercalated composites of micron-sized particles, in which atoms of alkali metals are intercalated between carbon layers that leads to the increase of the interlayer spacing of the graphite and weakening of the interlayer interactions [82].

Carbon black, on the other hand, is an amorphous form of carbon, with a spherical geometry with a radius of tens or hundreds nanometres, and is highly aggregated [83]. Regarded as a zero-dimension (0D) carbon nanofiller due to its low aspect ratio, carbon black is used extensively in polymeric nanocomposites due to its abundant availability, low cost and good electrical conductivity. However, large weight fractions of carbon black, in the range of 10-20%, are required in order to reach the percolation threshold

which leads to a heavy reinforcement of the polymeric matrix, effectively making it a rather stiff composite unsuitable for flexible applications [84] [85].

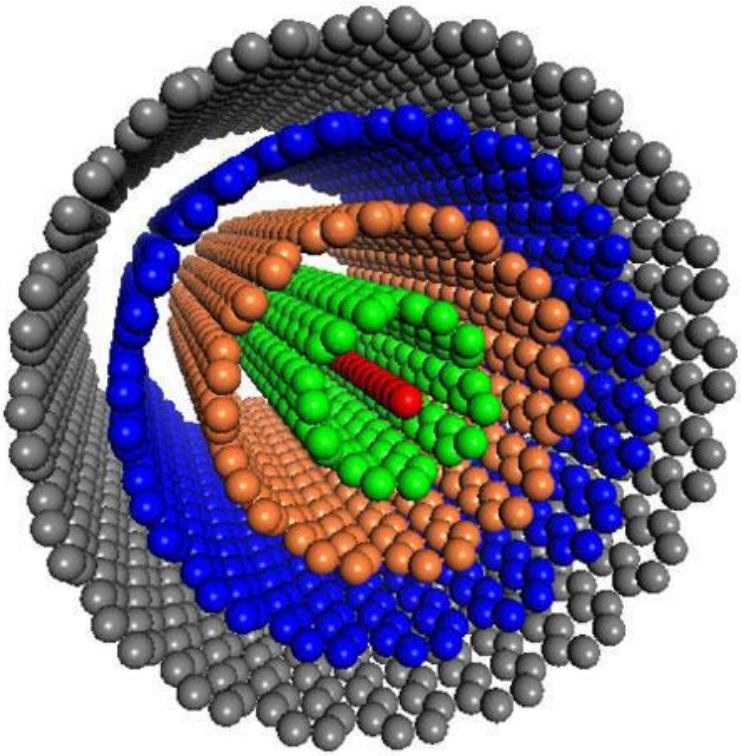

Figure 2.5: Structure of a multi-walled carbon nanotube **[86]**

Carbon nanotubes, on the other hand, are cylindrical nanostructures with high aspect ratios, which exhibit exceptional electrical and mechanical properties [87]. Ever since their discovery by Iijima in 1991 a great deal of research has been committed into unravelling their unique properties [88]. Regarded as 1D nanofillers, carbon nanotubes have an one-atom-thick layer of graphite, known as graphene, wrapped around itself into a cylinder with a 1 nanometer diameter and a micron sized length [89]. They are classified as single-walled (SWCNTS) and multi-walled (MWCNTS) nanotubes, depending on whether there is only one cylindrical layer of graphene for the first case, or a multitude of concentric cylindrical graphene layers (multi-SWCNTs shells) for the latter case (Fig. 2.5).

Carbon nanotubes are generally found in a highly aggregated form of aligned ropes that are strongly held together by van der Waals forces, and thus a de-aggregation process is required during dispersion. Due to their high aspect ratios, polymeric nanocomposites that utilize carbon nanotubes exhibit a very low percolation threshold (0.5% to 2%) with superior electrical properties, probably owing to the formation of a more efficient conducting network [90].

Finally, when carbon-based polymeric nanocomposites are subjected to mechanical deformation their respective conductivity varies accordingly to the applied stress or strain; an effect that stems from the filler particles' change of geometry or interconnections under deformation [91]. Manipulating this piezoresistive response of carbon-based polymeric nanocomposites has led to the development of numerous flexible sensors, as will be presented in section 2.7.

2.5.3 Dispersion of carbon nanotubes in the polymer matrix

In order to develop a filler-polymer conductive composite, the filler constituent of the system must be thoroughly mixed within the polymer matrix. This process known as dispersion requires the uniform spreading of individual nanotubes throughout the continuous polymer matrix so as to produce a good and isotropic composite conductivity. The aforementioned process poses a significant challenge since carbon nanotubes tend to form highly aggregated agglomerates due to the inter-tube van der Waals attraction that holds them together and acts within a range of a few nanometers [92].

Overcoming this attraction by simple manually stirring of the carbon nanotubes into the polymer leads to poor dispersion due to insufficient shear local force. A number of physical processes, including shear mixing, micro-bead milling, mechanical stirring and ultra-sonic agitation, have been employed to separate the carbon nanotubes from each other [93] [94] [95]. Although these processes appear distinctively quite different, they all share the same principle with regards to breaking down the carbon nanotube agglomerates, which is the introduction upon the nanotubes bundles of physical shear stress. Generally, as the filler aggregates are introduced into the polymer they experience shear stresses provided by the polymer during the mixing process. The external force applied leads to the flow of the medium, which generates the required mechanical energy necessary to separate the aggregates [96].

However, usually due to the highly viscous nature of the polymer matrix an additional process is employed to assist the dispersion of carbon nanotubes [96] [97] . This process involves the use of a common organic solvent at some stage of the dispersion process.

The organic solvent chosen has to be able to dissolve the polymer easily and monodisperse the carbon nanotubes. The process involves the preparation of two solutions, one containing the polymer and the other the carbon nanotubes, sharing the same solvent. Both solutions are individually mixed via mechanical stirring or sonication, before they are combined into one solution. Mechanical stirring or sonication is employed again to mix the final solution, followed by solvent evaporation. In the case of PDMS and carbon nanotubes nanocomposites, suitable solvents to assist the dispersion process include toluene, chloroform, dimethylformamide and terahydrofuran, amongst many [98-101].

2.6 Quantum Tunnelling Composite (QTC)

Quantum tunnelling composite is a nickel-polymer composite developed exclusively by Peratech Inc. The composite displays a unique conduction response when subjected to mechanical deformation. The patented manufacturing process of the composite involves the uniform dispersion of micron-sized nickel particles with spiky surface morphology into a polymeric silicone rubber matrix (Fig. 2.6), employing a low mechanical energy mixing process that minimizes damage to the spikes [102] [103].

During this process, the particles are completely coated by the polymeric matrix and the resulting composite acts as an insulator when no stress is applied, even at very high loadings. The composites are electrically insulating to filler loadings as high as 25% by weight which, in conventional polymeric carbon-based composites, far exceeds their percolation threshold.

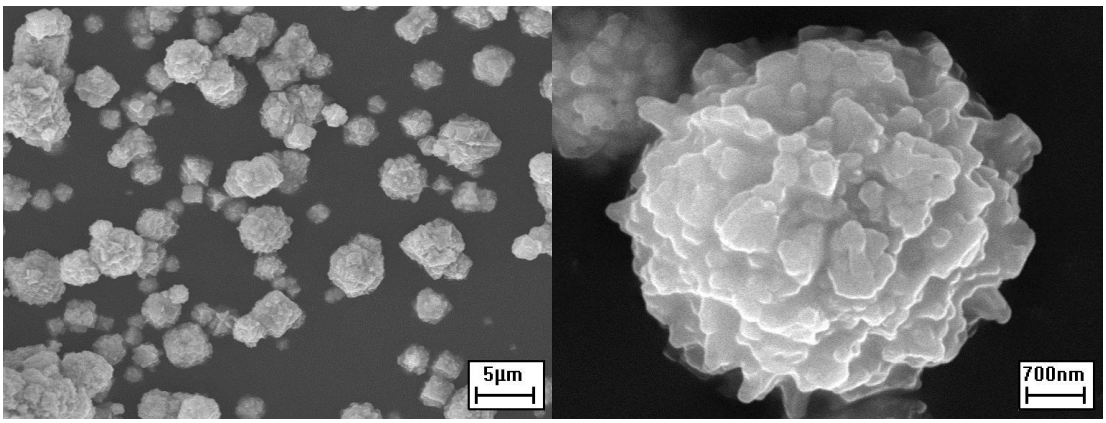

Figure 2.6: Raw nickel powder prior to mixing with elastomer matrix **[63]**

The physics governing electrical conduction in QTC materials differ substantially from conventional percolating nanocomposites [63] [102]. In this case, conduction is dominated by quantum tunneling between nickel particles facilitated by local field enhancement from the spikes.

More specifically, the existence of the spikes increases the charge density, which leads to high local electric fields. When pressure is applied to the composite, the distance between neighbouring spikes decreases and therefore the potential barrier width between two spikes drops accordingly. This effect increases dramatically the possibility of the charge carriers tunnelling according to the Fowler-Nordheim (FN) tunnelling phenomenon through the connecting elastomer matrix. FN tunnelling is a quantum tunnelling effect via the triangular potential barrier formed by the matrix sandwiched between the metal spikes (Fig. 2.7).

QTC exhibits a large piezoresistive effect, as the electrical resistance of the material can drop by over 7 orders of magnitude when compressed (Fig 2.8) [102]. Furthermore, the QTC resistivity drops reversibly even when the material is stretched, bent or twisted; a behaviour that differs substantially from their percolating counterpart composites, for which their resistivity increases when subjected to tensile strains. Also, the current-voltage behaviour of QTC is highly non-linear, with an exponential drop in resistivity as compressive loading increases.

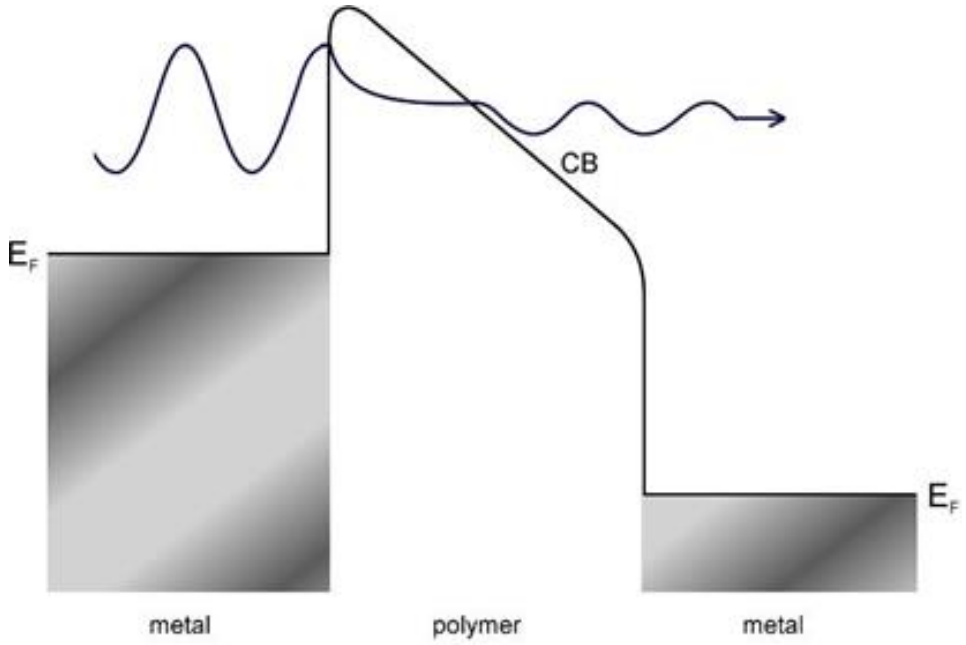

Figure 2.7: FN quantum tunnelling between the spikes of two neighbouring nickel particles **[63]**

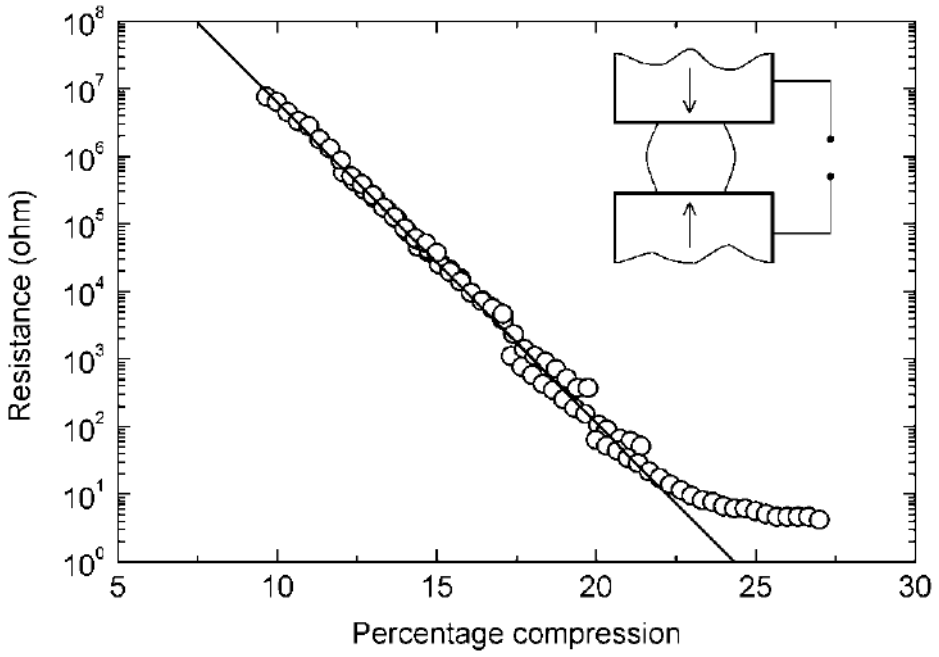

Figure 2.8: Resistance drop of a QTC material when subjected to compression **[102]**

However, despite their impressive characteristics, QTC is not without drawbacks [63]. The trapping of carriers due to the trapping sites of the amorphous polymeric matrix, leads to continual upwardly drifting currents when a constant voltage is applied. QTC exhibits hysteresis after the first voltage sweep, meaning that the material displays electrical history-dependant behaviour. Finally QTC exhibits creep behaviour as well. When strained the material slowly reduces its thickness, due to the viscoelastic behaviour of the polymeric matrix.

2.7 Flexible piezoresitive sensors

Carbon-based percolating polymer composites are mainly employed for flexible strain sensors and rely on the breaking of the percolating network of the filler particles [104-110]. However a number of piezoresistive pressure sensors, employing CNT-PDMS composites, have also been reported [111] [112] [113].

The carbon nanotubes which are the filler of the composite are preferred as they exhibit a percolation threshold at very low concentrations compared to other filler materials such as carbon black or metal particles. In that respect the composite still keeps a low Young's modulus for flexible sensors applications [110]. Moreover, PDMS is the

dominant material utilized as the composite's polymeric matrix due to its superior characteristics. Therefore, the resultant CNT-PDMS composites retain a high flexibility, which makes them an ideal candidate for the development of flexible sensors [104].

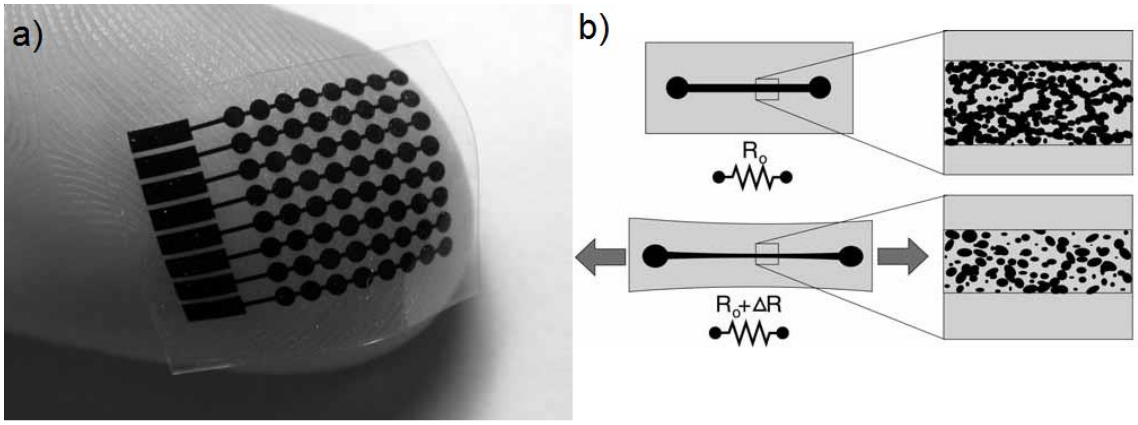

Figure 2.9: (a) A MWCNT-PDMS strain sensor. (b) When the sensor is subjected to tensile strain its resistance increases as the number of available conductive pathways decreases **[104]**

When strain is applied to the composite, the average spacing between conductive particles increases and thus the number of available conductive pathways decreases , which leads to an increase of the resistance (Fig. 2.9) [114]. This type of CNT based flexible strain sensors exhibit a superior performance over their silicon-based MEMS counterparts, as the flexible PDMS matrix of the composite allows large strains (>1%), as high as 100%, to be monitored consistently [115].

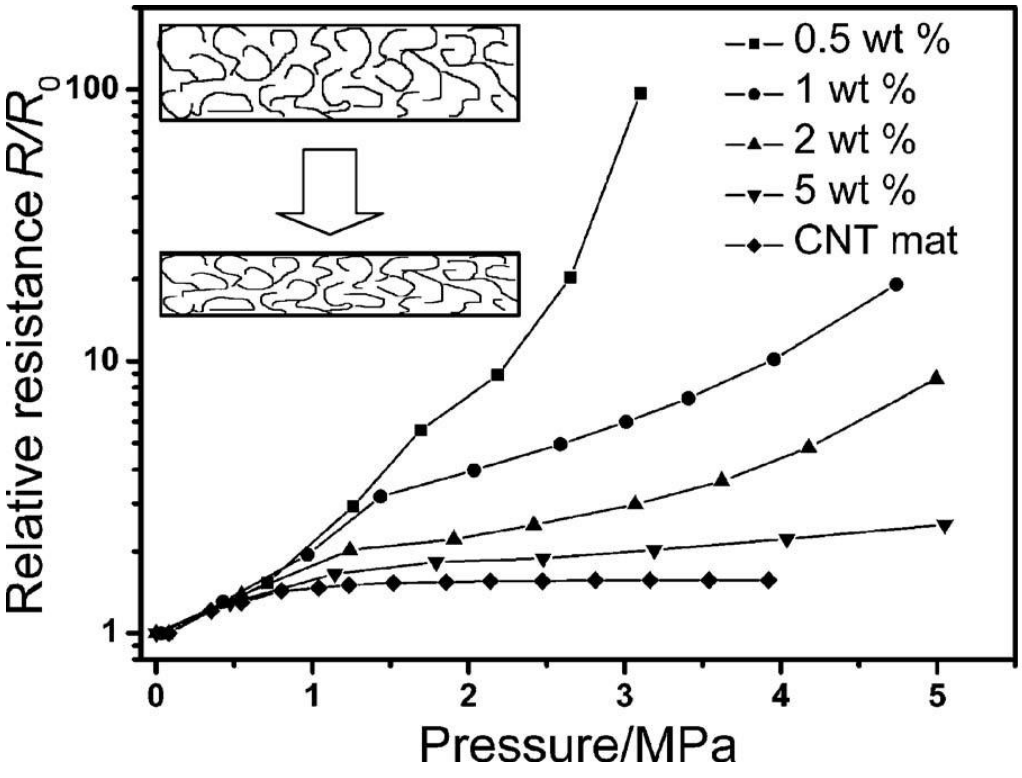

Figure 2.10: MWCNT-PDMS composite relative resistance versus pressure and filler concentration **[111]**.

Interestingly, in the case where CNT-polymer composites have been used for pressure sensing, the composite exhibits also an increase in resistivity with applied pressure (Fig. 2.10) [111] [112] [113].

As the material is compressed, the CNTs experience bending which deteriorates their intrinsic electronic properties and increases the resistivity of the composite significantly [108]. Moreover, the formation of new conductive networks and the destruction of existing ones under external pressure play also a significant role [116] [117].

In conventional composites with low aspect ratio particles (spherical particles), compression leads primarily to the formation of new conductive pathways, due to the very high percolation threshold (>30% by volume) that results in small average difference between fillers [118], and thus an increase in the conductivity. In CNT-based composite however, where the average distance between fillers is larger due to a much lower filler concentration, the amount of existing pathways that are destroyed is significantly larger over their newly formed counterparts, which leads to an increase of the resistivity.

The combination of these two phenomena leads to a significant positive piezoresistive effect, i.e. an increase in relative resistance, in the composite under compressive loads. At this point, it is also important to note that the piezoresitive response of the CNT-based composite can be improved substantially if the filler concentration is low and just below the percolation threshold, as the low-loading composites experience much larger curvatures and therefore exhibit enhanced pressure sensitivity [111].

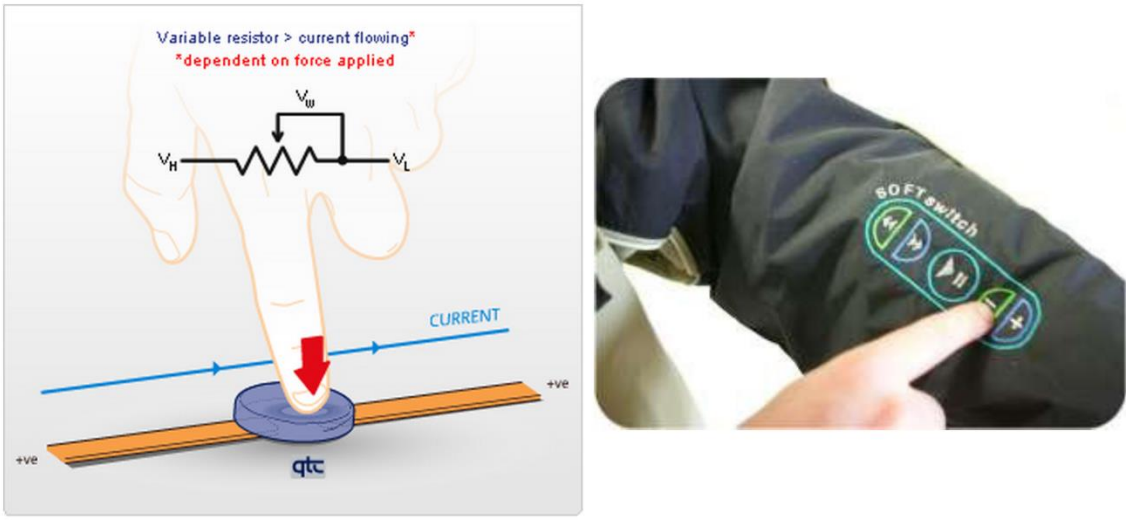

Figure 2.11: QTC material as a switch in wearable electronics applications **[119]**

Finally in the case of QTC composites, the material is patented and distributed exclusively by Peratech Inc. Due to its enormous piezoresitive response to external forces, the composite is primarily used as a switch in electronics systems and especially in wearable electronics applications (Fig. 2.11) [120].

A significant advantage of the material, over its carbon-based composite counterparts, is the resilience that it exhibits to wear that ensures a long working lifetime. This effect directly stems from the non-contact tunnelling conduction mechanism between the spiked nickel-particle fillers, which effectively shields and protects the particles' structures even after extended use [121].

Moreover, the QTC material exhibits a substantial electrical response when exposed to chemical vapours [63] [122] [123] and is a strong contender for the fabrication of an electronic nose [124]. In this case, the vapour sensor is composed of a QTC material developed in granule form with similar properties as the bulk form, which in turn, is compressed between permeable frits to produce a porous structure and introduce an initial resistance to the system. In the presence of a chemical vapour the sensor structure swells and expands leading to an increase in resistance. This response is dependent on the chemical vapour type, as well as its concentration.

2.8 Capacitive sensing

2.8.1 The parallel-plate capacitor

Capacitors, invented by Cuneus and Mussenbroek in 1746, are amongst one of the first electrical devices to be developed [125] and rely on the ability of an electrical system to store electrical charge. The concept of capacitance however can be understood in a more fundamental basis by examining the definition expressed by Maxwell in 1873 [126].

The capacitance between two conductors is defined as the charge induced on one of the electrodes versus the potential difference between them that induced it:

$$C_{ij} = \frac{Q_{ij}}{V_i - V_j} \tag{2.4}$$

Where the indexes i and j denote the two electrodes respectively, C_{ij} the capacitance of the system measured in Farad, Q_{ij} the charge induced on the i^{th} electrode (a -Q_{ij} charge is induced on the other), while V represents the electrode's potential.

Considering a two-electrode electrical system, the capacitance between them is dependent on a number of parameters such as the shape and size of the electrodes, their spatial distance, as well as the medium in which they operate. In most cases, only simple structures can be solved analytically without employing approximate techniques such as Finite Element Method (FEM) [125].

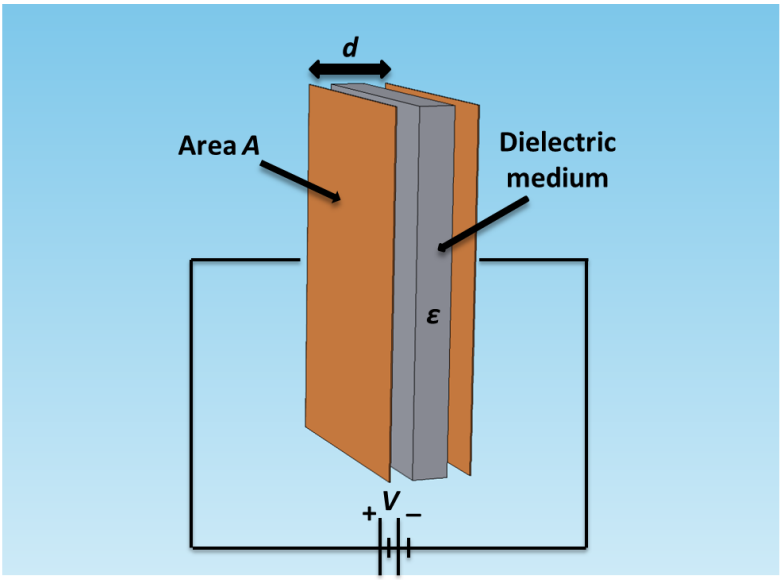

Figure 2.12: Parallel plate capacitor

The most common and simple configuration of a capacitor is that of an electrical system consisting of two flat parallel plates of conductors, held in close proximity to one another with an insulating dielectric medium in between them (Fig. 2.12). In this case, if the distance between the electrode plates is considerably smaller than their surface area, then the capacitance of the system can be approximated by the following equation:

$$C = \varepsilon_r \varepsilon_0 \frac{A}{d} \tag{2.5}$$

Where ε_0=8.85·10^{-12} F/m the vacuum's permittivity, ε_r the relative permittivity of the dielectric medium, A is the surface area of electrode plate and d the distance between the two plates.

2.8.2 Categorization of the parallel-plate capacitive sensors

Due to the simplistic form of a parallel-plate capacitor, the aforementioned geometry is heavily used to develop capacitive sensors. These sensors rely on manipulating one of the physical parameters of equation 2.5, while holding the others parameters constant. Three categories can be defined for the sensors: the ε-type, the A-type and the d-type.

The ε-type capacitive sensors, as the name suggests, rely on taking advantage of the relative permittivity of the dielectric medium of the sensor as a sensing principle. They are mostly used to characterize materials, especially as liquid-level gauges and humidity sensors [127] [128]. An example of the former sensor can be found in [127], which utilizes a set of two isolated probes to measure the interface level of non-conductive liquids. In this configuration, the probes and the liquid are effectively the parallel plates and the dielectric layer of the capacitor's structure respectively. However, due to the fact that the performance of ε-type capacitive sensors is hindered by the anisotropic and temperature-dependant behaviour of most mediums' relative permittivity, their usage is limited.

A-type sensors are utilized as motion encoders that measure the change of position of a target with high-resolution [127] [129]. The operating principle of this type of sensors is based on variations of the effective area of the capacitor plates. By decreasing or increasing the effective area of the two plates the capacitance of the system alters accordingly. An example of such a sensor has been reported in [129], where a moveable pick-up plate is employed to capture motion and position of a target. The sensitivity of this type of sensors relies on the system mechanical accuracy and therefore any defects on the surface or geometry of the electrode plate have a strong influence on their performance.

The most widely used parallel-plate capacitive sensor amongst the three categories is the d-type sensor, mainly employed in sensing structural deformation. Capacitive sensors of this kind generally utilize conductive plates that deform axially under a compressive load or lateral strain. This deformation results in a reduction of the capacitor thickness and thus an increase of its respective capacitance. The sensitivity of such capacitive sensors largely depends on the capacitive change. Designing a d-type sensor requires therefore an ultra-thin dielectric medium.

A wealth of different capacitive pressure or strain sensors has been developed over the past years due to their low power consumption, good DC response and high sensitivity [130] [131] [132]. However, the main reason behind the huge interest in this type of sensor lies in the fact that small, compact, ultra-thin and highly sensitive pressure or strain sensors can be developed by taking advantage of this principle, with a vast and versatile field of applications spanning from interactive electronics [133], biomedicine and device implants [134] to robotics and aeronautics [135].

2.9 Parallel-plate capacitive sensors

2.9.1 MEMS capacitive sensors

Capacitive pressure sensors are generally preferred over their piezoresistive counterparts as they exhibit a higher pressure sensitivity, lower power consumption and better stability [136] [137]. One of the most typical examples of existing capacitive pressure devices is a silicon-based Micro-electromechanical system (MEMS) capacitive pressure sensor that is composed of a thin and flexible conductive diaphragm and suspended above a fixed back electrode plate (Fig. 2.13) [136-140].

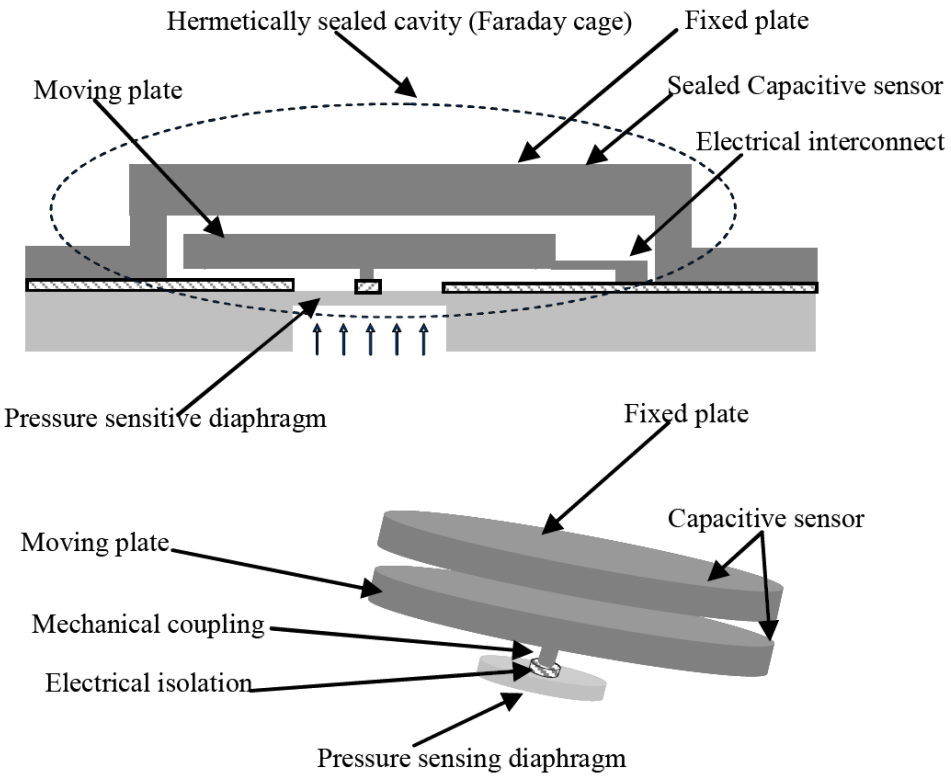

Figure 2.13: A MEMS capacitive pressure sensor structure that utilizes a moveable plate connected to a thin diaphragm to sense small pressure variations in the range of 0-10kPa **[141]**

When the device is subjected to compressive loading, the diaphragm deflects leading to a decrease of the air gap and therefore an increase in the capacitance between diaphragm and the fixed back plate. Thus the applied pressure to the sensor is sensed by the capacitance change introduced by the deflected diaphragm's state and its pressure sensitivity is dependent on the shape and size of the diaphragm.

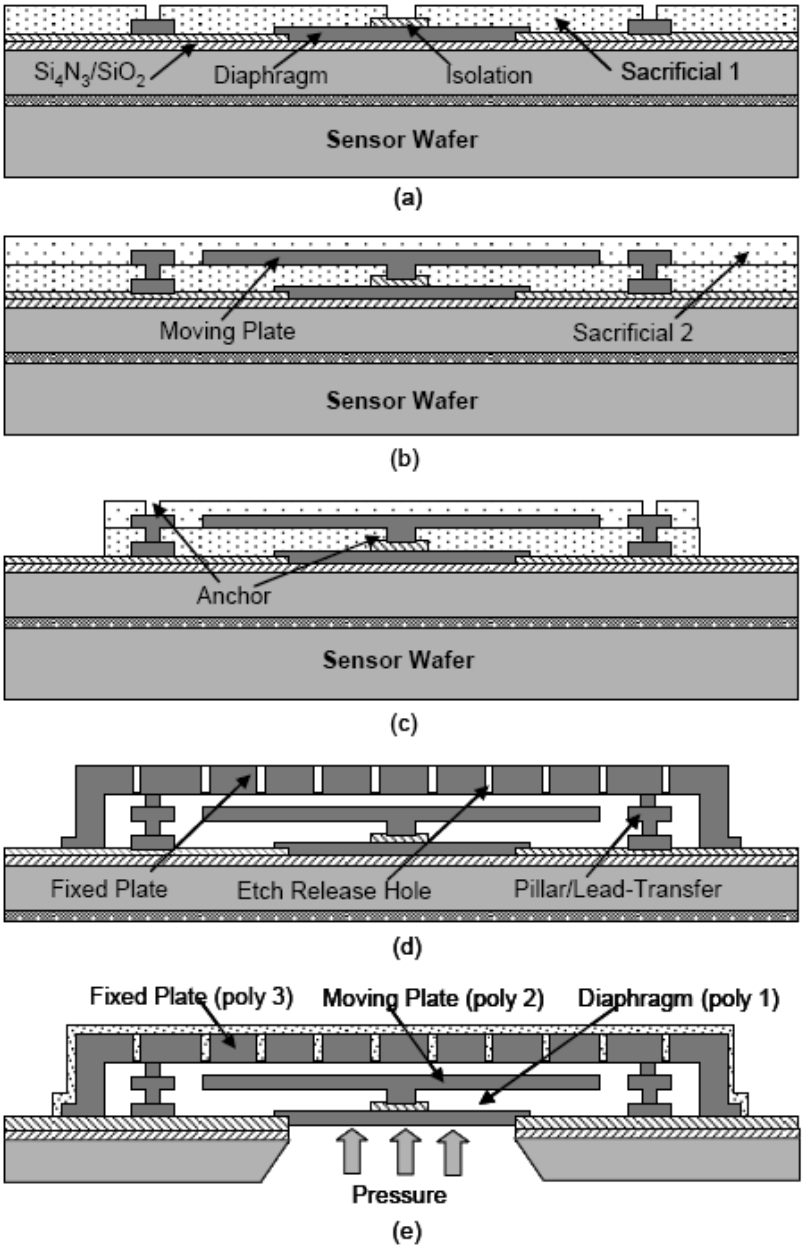

Figure 2.14: Illustration of the fabrication process of the pressure sensor depicted in Figure 2.12, which involves **[141]**: (a) a polysilicon layer deposition and doping on a pre-patterned composite silicon oxide/silicon nitride layer to form the diaphragm; (b) deposition and doping of a second polysilicon layer, via patterning a sacrificial oxide layer, to form the moveable plate; (c) patterning of a second sacrificial oxide layer to form the sensing gap and cavity; and (d) deposition of a third polysilicon layer to form the fixed plate and HF etching of the sacrificial layers via perforating holes in the structure, (e) followed by an additional etching process in order to expose the diaphragm of the device.

Despite the fact that this type of sensor exhibits a high pressure sensitivity, its robustness, large size and complex fabrication process (Fig 2.14) deem it impractical for flexible and cost-effective pressure sensing [142]. More specifically, the high sensitivity is achieved by scaling down the diaphragm's thickness and air gap, and by increasing substantially its size, which makes its behaviour non-linear with limited dynamic range.

However, the most limiting factor of MEMS capacitive pressure sensors lies in their complete inflexibility and zero conformity on curved surfaces due to the silicon-based material used as the structural basis of the device [143].

2.9.2 Flexible polymer-based capacitive sensors

In contrast to MEMS capacitive pressure sensors which are mainly composed of metals or semiconductors that considerably limit their flexibility, polymer-based capacitive pressure sensors possess a number of advantageous material characteristics such as mechanical flexibility, optical transparency, biocompability and chemical stability that broaden their potential applicability significantly [144]. Moreover, polymer-based sensors can be developed by employing both soft lithography techniques, such as cast moulding, and conventional photolithography processes, for increased resolution and limited feature size.

Although distinctively different parallel-plate capacitive sensor devices have been developed the past years, they all share the same structural principle. In order to allow large capacitance changes over deformation and a flexible sensor design, a soft polymer is utilized as the main structural material that acts either as the dielectric medium in between the capacitor plates or as a substrate, encapsulant or both.

Arguably, the most widely utilized polymer for this purpose is PDMS, which exhibits an intrinsically low Young' modulus of 1.7MPa for large deformations and excessive tensile strains without structural failure as presented in section 2.5.1. However, besides PDMS, other polymeric material are used in the development of flexible capacitive sensors such as polyimide, ultra-flexible epoxy resins, polyurethane, polybutyrate amongst many [145-148].

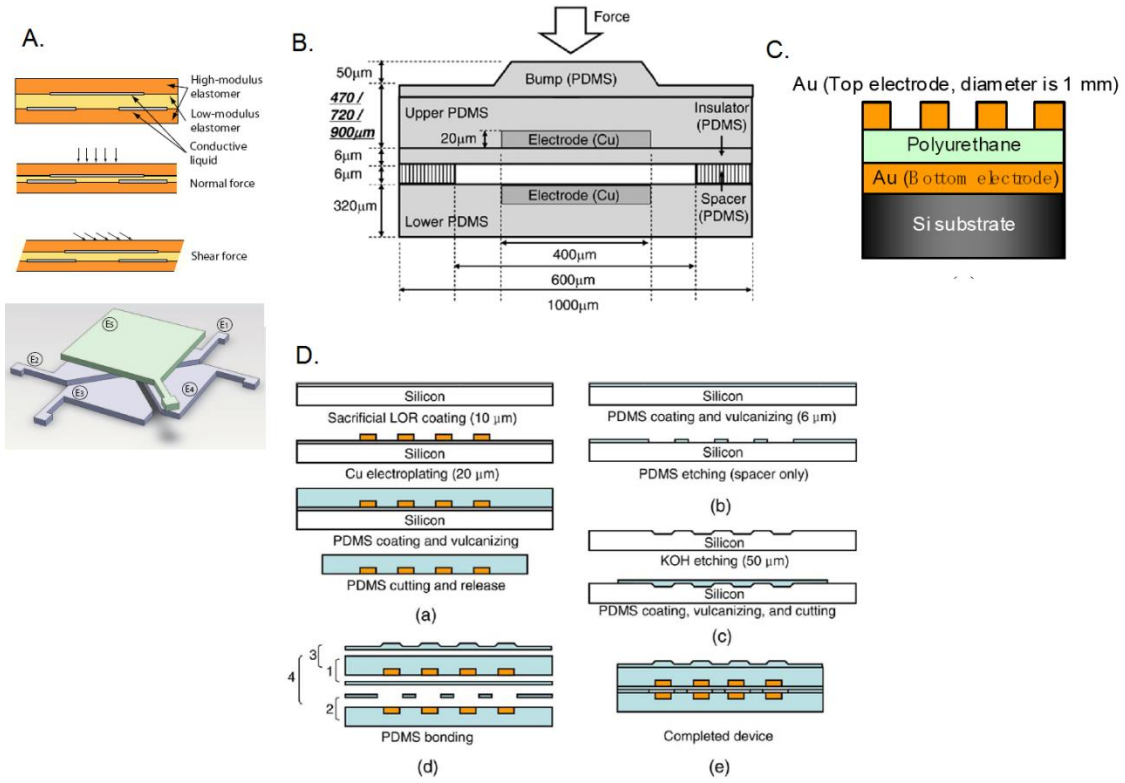

Figure 2.15: Flexible parallel-plate capacitive polymeric pressure sensors that utilize (A) polybutyrate , (B) PDMS and (C) Polyurethane polymers as the structural material respectively, and a fabrication process flow (D) which includes both photolithography and soft lithography processes **[147] [148] [149]**

Typical examples of such a flexible capacitive pressure sensor can be found in [147] [148] [149]. The structuring of these devices follows a similar and simple parallel-plate geometry where the electrodes of the capacitor are encapsulated by a soft polymer (Fig. 2.15). Scaling down the sensor size, whilst retaining measurable capacitance change over compressive loads, is achieved by ensuring that the distance amongst plates is on the micrometre-scale.

The pressure sensor which utilizes a polymer bump and an air gap between the plates to enhance its sensitivity (Fig. 2.15 A,D), demonstrates a good example on how the typical photolithography processes (photoresist deposition, exposing and development, substrate etching, metal deposition) and soft lithography processes (polymer spin coating, casting, moulding, de-moulding, bonding) can be employed to develop a flexible capacitive sensor [149].

In addition, a common technique employed to achieve good spatial resolution is by designing the top and bottom electrode plates into perpendicular-oriented to one another rows of conductor strips that overlap on fixed locations. This way, the total sensor is the result of a multi-element lattice configuration that provides good spatial resolution, as each sensor from the matrix is electrically individually accessible.

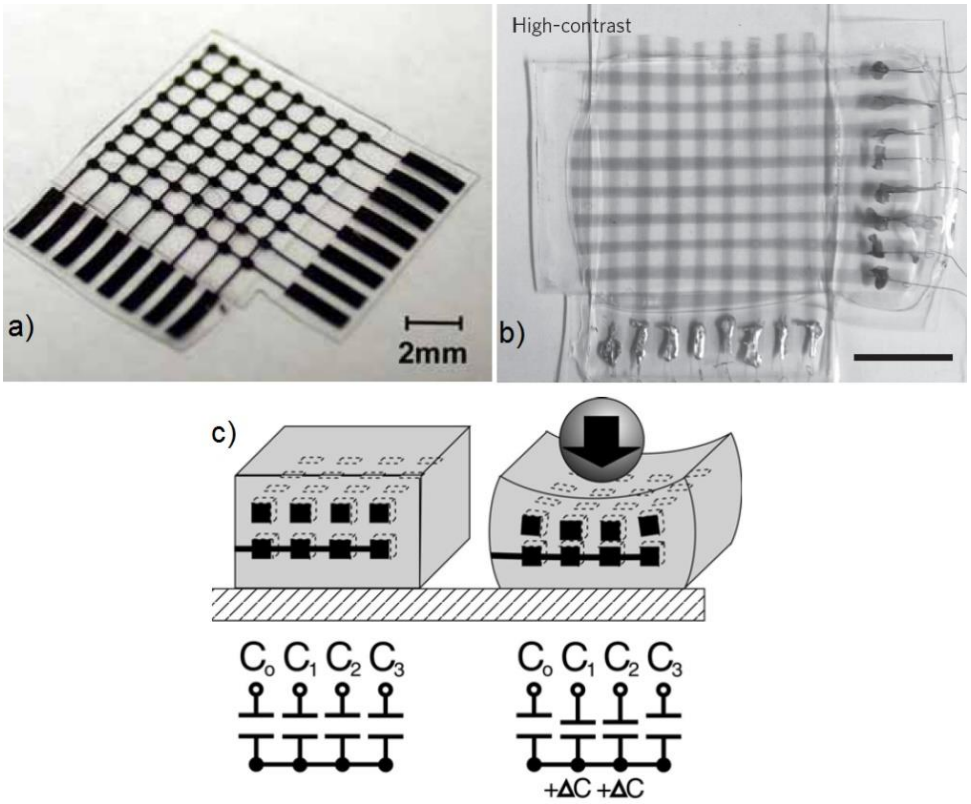

Figure 2.16: All-elastomer capacitive pressure sensors that utilize respectively a MWCNT-PDMS (a) and SWCNT-PDMS (b) composite as the conductive plates of the capacitor, encapsulated in PDMS. Both sensors are designed in a perpendicular-oriented double row configuration to provide spatial resolution (c) **[104] [150]**

Integrating filler-polymer composites into this parallel-plate sensor design has also been demonstrated (Fig. 2.16). The replacement of the metallic electrode plates with conductive CNT-PDMS composites offers an increase in the sensor intrinsic flexibility in applications where lateral deformation is also desired. Examples of such devices can be found in [104] [150]. Furthermore, this type of sensors can also be used as strain sensors; when tensile strains are exerted to the system the CNT-PDMS strips along the strain axis exhibit an increase in resistivity.

However, despite the fact that these all-elastomer capacitive sensors exhibit good flexibility in large areas, their performance is hindered by a non-reliable response and low spatial resolution limited on the millimetre-scale due to the difficulty in developing sub-millimetre features with the processes currently available [151] [152] [153].

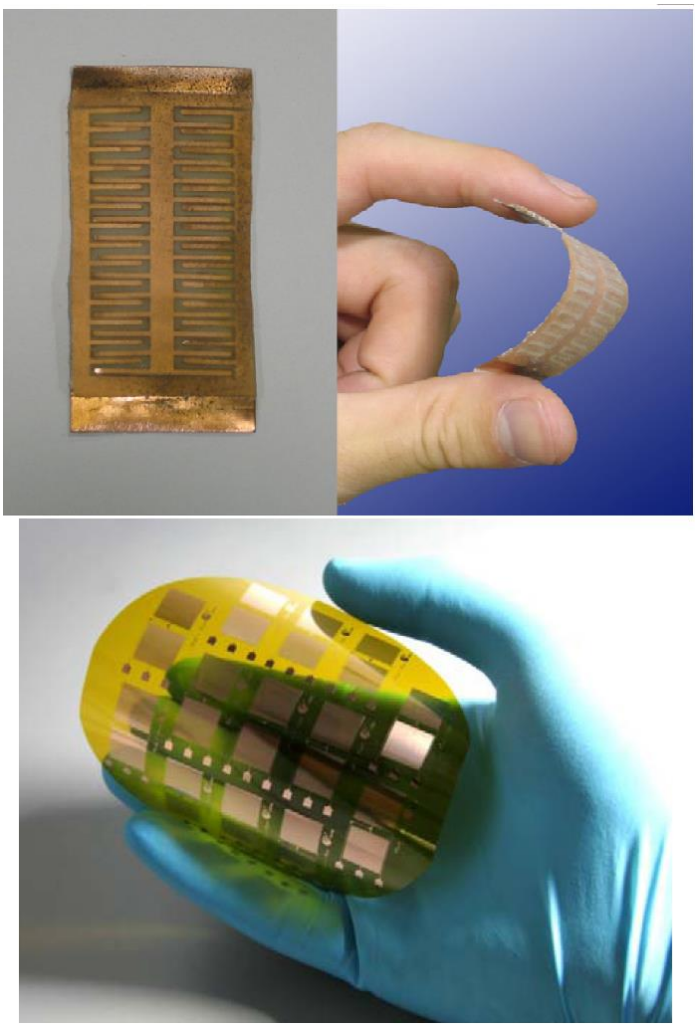

Figure 2.17: High performance flexible strain sensors that employ an interdigitated structure configuration encapsulated in a soft polymer **[145] [146]**

Besides the pressure sensing applications, there is also great deal of interest in developing high performance strain sensors based on capacitive sensing (Fig. 2.17). One the most common configuration of a capacitive strain gauge, which coincidentally was also one of the first applications of the flexible polymer as the main structural material, is the interdigitated capacitive strain sensor [145] [146].

In this type of sensor, the two electrodes of the capacitor are structured in a comb formation and the fingers of each comb are set in close proximity. The comb structure is deposited on a flexible substrate and encapsulated in a soft polymeric material, which allows large tensile deformation compared to their typical silicon-based counterparts. Therefore as the sensor is stretched or bent the distance amongst neighbouring fingers widens which leads to a decrease of the sensor capacitance.

2.10 Low pressures sensing issue and other novel ultra-sensitive pressure sensors

Despite the fact that a large number of flexible piezoresitive and capacitive pressure sensors of various designs have been reported the past few years, as shown in the previous sections, developing a sensor with a sensitivity on the low pressure regime (<10kPa) still remains a significant challenge.

Most of the pressure sensors developed out of flexible polymeric materials (capacitive sensors) or conductive composites (piezoresistive sensors) exhibit a pressure sensitivity in the range of 50kPa to 5MPa [109] [111-113] [149-150] [154-155]. The reason behind this can be attributed in the difficulty of either scaling down the structural size to enable a large enough capacitance change for the former case, or in the latter case, developing a conductive composite with a large enough piezoresistive effect on the low pressure regime of 0-10kPa. Flexible pressure sensors that have, however, a response in this regime, although with limited resolution, have been reported in [148] [156] [157].

Up to date, to the best of the author's knowledge, only two flexible pressure sensors have been developed that exhibit exceptional device reliability and pressure sensitivity in the low pressure regime: a flexible-pressure sensitive organic transistor [158] and a piezoresistive sensor utilizing gold nanowires [159].

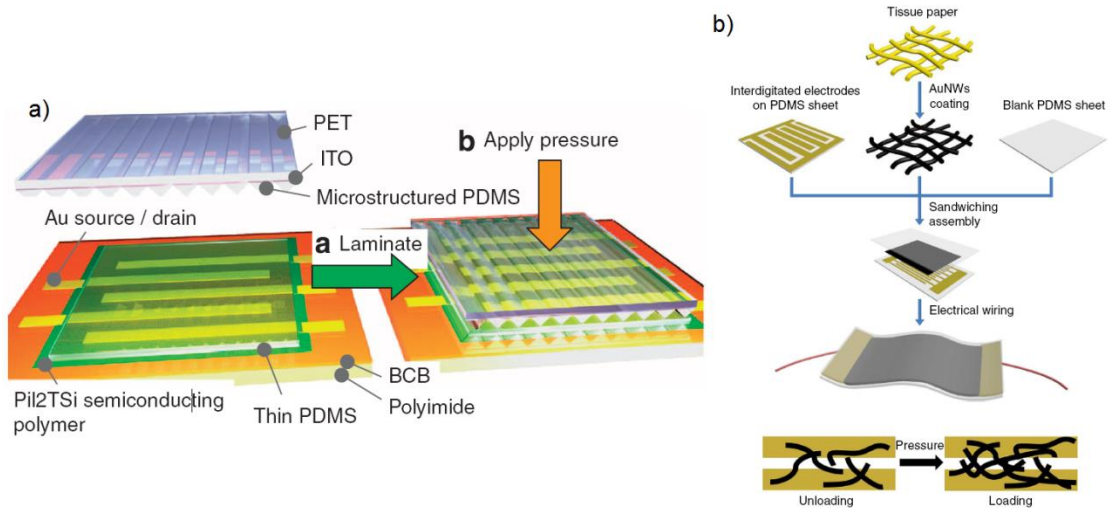

Figure 2.18: Illustration of fabrication process and working principle of the pressure sensitive organic transistor sensor (a) and the Au nanowires-piezoresistive sensor (b) [158] [159]

In the first case (Fig 2.18a), the device is manufactured by laminating successively a number of layers which include: a BSB-coated polyimide substrate, the bottom drain and source gold electrodes of the transistor, a PDMS-coated conjugated polymer (PiI2T-Si) that serves as the semiconductor, and a micro-structured (lines) PDMS layer on a ITO-coated PET film that serves as the gate dielectric. The device operates by transducing the compression of the micro-structured PDMS layer under pressure to a current variation between the drain and source electrodes of the transistor.

In the latter case (Fig 2.18b), high quality ultra-thin (2nm in width with a huge aspect ratio of 10,000) gold nanowires (AuNWs) are deposited onto tissue paper, via successive dip-coating and drying, which in turn is encapsulated in between a patterned with an interdigitated electrode configuration PDMS layer and a 500um-blank PDMS sheet. The sensing mechanism of the sensor relies on the force-dependant contact between the AuNWs and the fingers of the interdigitated electrode configuration.

Both these sensors exhibit exceptional pressure sensitivity in the range of 0-10kPa and beyond. Developing these sensors, however, requires an elaborate and complex procedure which hinders their practical applicability; laminating and structuring a large number layers of quite a different nature in the first case, and applying a costly and demanding fabrication protocol for synthesizing the AuNWs in the latter case [160].

Therefore in this work, in order to develop a cost-effective and simple pressure sensor capable of sensing pressure variations in the low working pressure regime of compression hosiery (0-6kPa), both piezoresistive sensors (utilizing conductive filler-polymer composites) and capacitive parallel-plate sensors (utilizing polymeric structures) were developed and evaluated, by taking into account and employing non-demanding fabrication processes and design configurations. The two categories of the aforementioned sensors are presented in Chapter 3 and Chapter 4, respectively.

Chapter 3:
Piezoresistive pressure sensors

3.1 Introduction

This chapter presents a set of piezoresistive pressure sensors and their respective performance under compressive loads. Initially, the sensors design and the materials utilised to develop them are described, followed by the experimental processes employed to produce the structuring of the sensor and carbon nanotube-based composite. The results over the developed composite percolating behaviour, as well as the sensor pressure sensitivity as a function of composite type and electrode layer structure, are discussed in the final section of the chapter.

3.2 Materials chosen and sensor design

In this work, a pressure sensor was developed that utilizes a piezoresistive filler-polymer composite layer as the sensing component of the device. Two different composites were evaluated for this purpose: a carbon nanotubes-PDMS nanocomposite and a QTC composite.

Figure 3.1: The commercial QTC “pill” product **[161]**

In the first case, as the filler constituent of the composite, MWCNTs were selected due to the better conductivity they provide compared to their SWCNTs counterparts [90]. In addition, from an economic point of view MWCNTs generally are less expensive to purchase than SWCNTs. In the case of the QTC composite, a commercially available product by Peratech, known as the QTC "pill", was utilized and purchased for less than £0.40 per piece (Fig. 3.1).

The structure of the sensor was designed to be embedded in compression hosiery in order to monitor the interface pressure between garment and skin. For cost-effectiveness, the sensor design includes three layers with a total thickness of approximately 1.5 mm. The three layers include a flat rigid conductive substrate, the piezoresistive sensor element and another rigid conductive layer structured with protrusions, all with a surface area of 25mm^2 (Fig. 3.2).

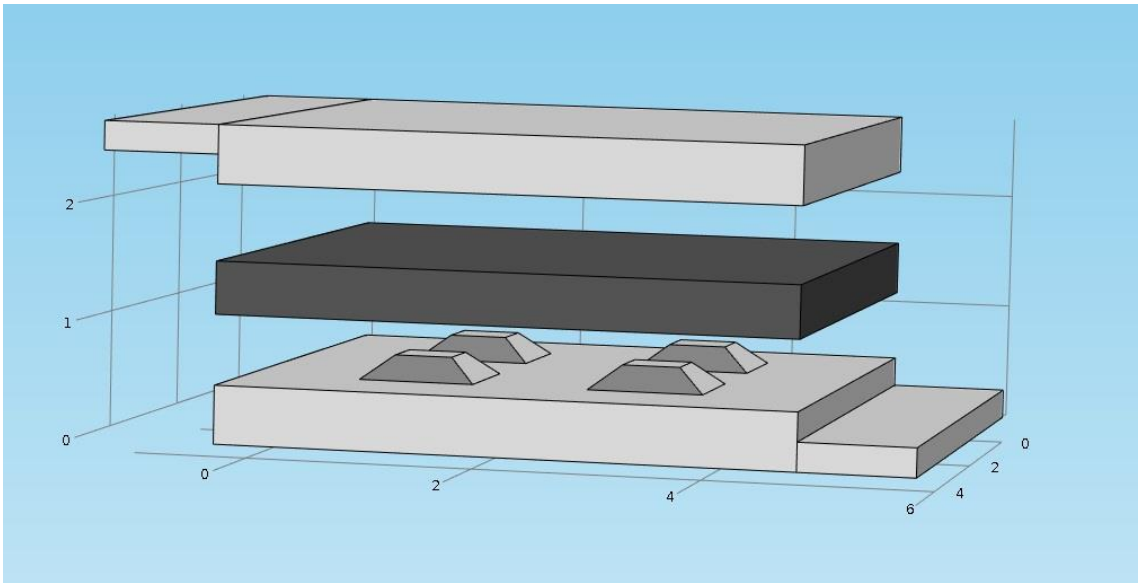

Figure 3.2: Piezoresistive pressure sensor design

The rigid conductive layers, of thickness of 0.5mm, were designed to serve both as the electrodes of the device and limit the piezoresistive layer response only to axial compressive loading. The filler-polymer composite would then sit in between and the total structure would be encapsulated by soft a polymer such as PDMS. Electrode pads, protruding from the edges of the rigid conductive layers with a thickness of 0.25mm, serve as the connecting points of the sensor with an external bias.

The structuring of the surface of the top rigid layer with protrusions provides an augmented pressure effect to the piezoresistive layer. More specifically, if a uniform load is exerted onto the surface of the top layer, this load is evenly transduced unto the

contact surface of the protrusions with the piezoresistive material. However, since the surface of the symmetrical positioned protrusions is significantly smaller, the resulting pressure to the piezoresistive material is accordingly larger. Therefore, protrusions should provide an improvement on the sensors sensitivity under compressive forces.

Attaching the sensor on the compression hosiery, utilizing uncured PDMS poured through the holes of the fabric was first envisaged (Fig. 3.3). The PDMS would subsequently bond with the surface of the encapsulated sensor. In addition, a number of conductive threads could be knitted onto the fabric in a snake-wise fashion to allow stretching of the fabric, which would provide an input signal to the sensor. In a more general approach, the sensor could be interconnected with multiple other similar sensors under a conductive thread single bias that would transverse the fabric vertically, whilst each sensor would retain its own individually-accessible exit signal.

Assuming that the sensors would be sensitive enough, monitoring of the interface pressure between garment and skin, on fixed locations around the leg such as the ankle, calf and thigh, could become feasible.

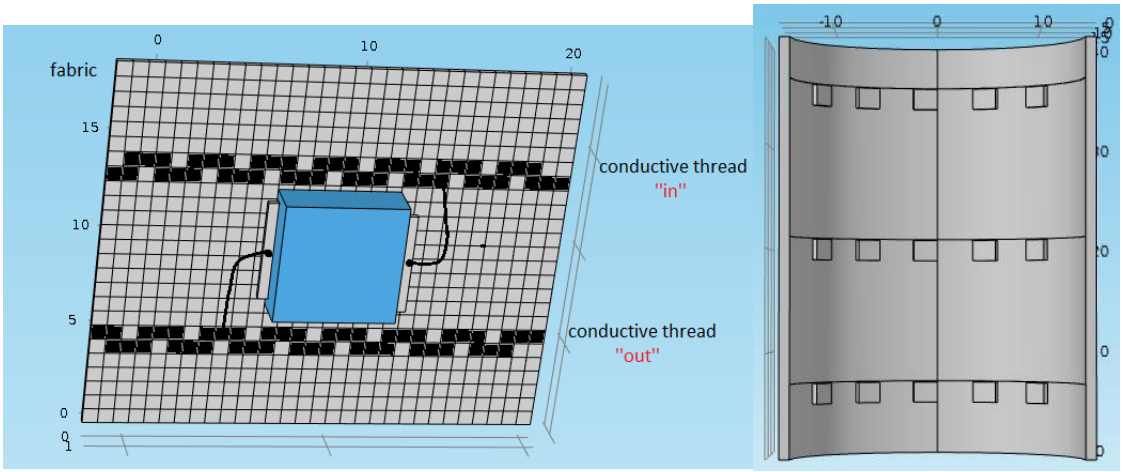

Figure 3.3: Illustration of envisaged embedding to garment: (left) sensor is encapsulated in PDMS, bonded to the fabric and electrically connected via knitted conductive threads of a snake-wise fashion; (right) interconnection of multiple sensors on the compression hosiery that share, latterly and vertically respectively, a common input and output bias

3.3 Experimental work

3.3.1 Aluminium plates design and development

A micromilling machine was employed to develop the rigid conductive layers that encompass the piezoresistive layer (Fig. 3.4). As structural material for the rigid layers,

aluminium was chosen due to its good conductivity, but most importantly, because it is a soft metal that can be milled easily.

The micromilling equipment utilizes a carbide mill tip with 1mm diameter and is capable of milling features with an accuracy of 25 μm. As the pitch distance amongst separate elements is limited by the diameter of the milling tip, in the case of the protrusion-shaped layer with a size of 25mm^2, only four protrusions could be milled upon the aluminium surface. A large flat aluminium block with a thickness of 1 mm was utilized that was firmly attached onto the equipment's frame via double tape. Ensuring that the aluminium block is firmly attached is of great importance since the smallest movement during milling leads to significant variations on the resulting features.

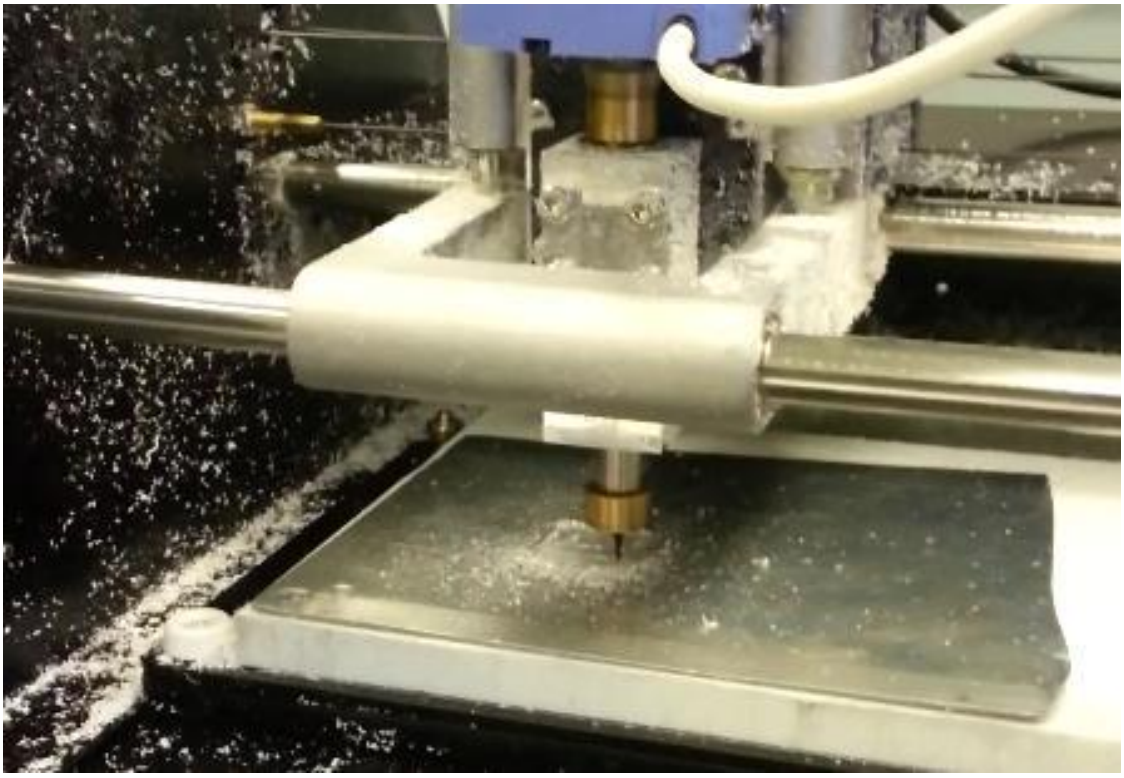

Figure 3.4: The micromilling equipment in action

In order to mill the required pattern, the Autocad^{TM} file containing the desired pattern was loaded onto the equipment's software. A simulation of the milling resulting features was run. The micromilling machine then followed a 3-step procedure in order to mill the sample, which included the following processes: surfacing the sample, roughing the pattern and finally finishing the features.

In the first step, the sample pattern area is initially surfaced by etching away a 25 μm layer providing an initial flat surface. Subsequently, on the next step, a rough shape of the desired features is developed via slowly milling the whole surface repeatedly, on the x and y axis separately, over a step of 25 microns on the z axis. The exact features of the designed pattern are developed on the final step where most of the patterns now empty spaces are skimmed and the milling is focused on the remaining rough features. The whole procedure may take as much as 8 hours for a sample with an area of 9cm^2 and features depth of 0.5 mm, making this process hardly scalable.

.

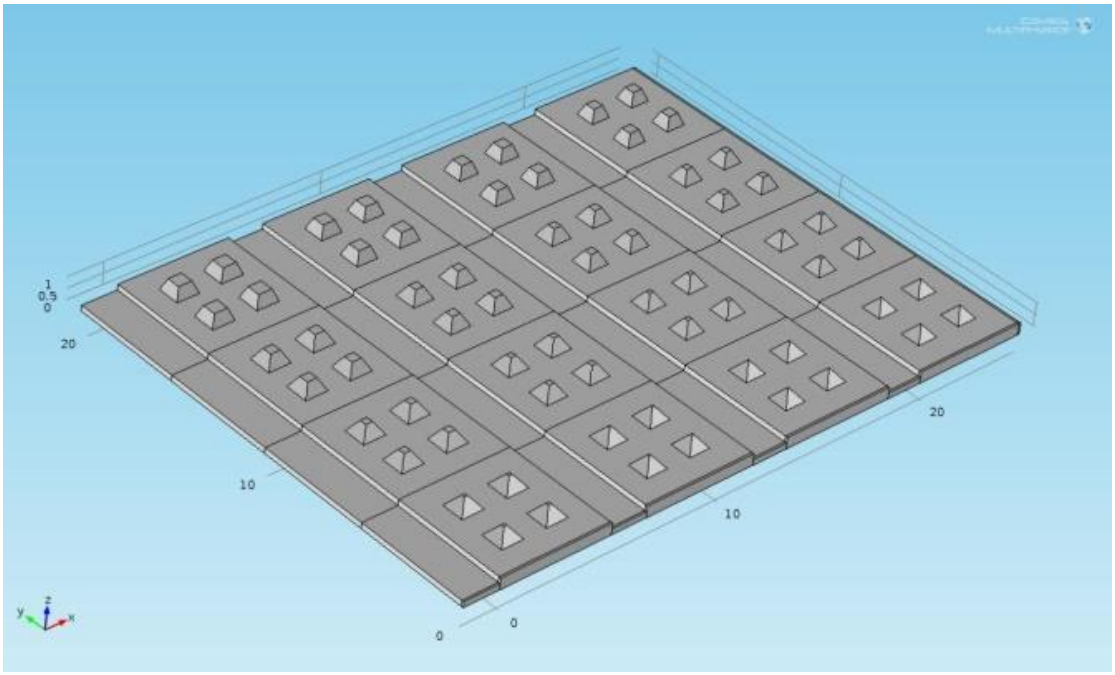

Figure 3.5: The multi-element geometry designed for patterning via the micromilling equipment

The geometry designed for patterning consisted of 16 individual protrusion-shaped substrates with electrode pads, each having protrusion tips surfaces with different area sizes. The tip surface areas ranged from 550x550 μm^2 to as small as 75x75 μm^2, all with a protrusion heights fixed at 0.5mm (Fig. 3.5).

Finally, the individual elements of the resulting patterned aluminium block were separated via the use of a laser cutter. The cutting width of 300μm of the laser beam was taken into consideration while designing the pattern to be milled. The results of the developed features are presented in section 3.4.

3.3.2 Fabrication process of carbon nanotubes-PDMS nanocomposite

As the filler constituent of the composite, multi-walled nanotubes in a powder form were purchased from Sigma Aldrich with a relative purity of carbon at 98% and a density of 2.1g/ml. The outer dimensions and inner dimensions of the nanotubes were respectively 10nm±1nm and 4.5nm±0.5nm, with a length of 3-6μm, as specified from the technical datasheet provided by the supplier. The polymer employed for the development of the nanocomposite was PDMS Sylgard 184 purchased from Dow corning Inc., which includes 2 parts that need to be mixed together on a 10:1 ratio, the elastomer base and the curing agent.

The optimized fabrication process employed to develop the MWNTs-PDMS nanocomposite utilizes 6 distinct steps: (1) ultrasonication of MWCNTS and shear mixing of PDMS elastomer base into toluene individually, (2) ultrasonication of the 2 solution together, (3) shear mixing until solvent evaporation, (4) insertion of PDMS curing agent and shear mixing, (5) degassing of the composite under vacuum, and finally (6) thermally curing the composite. The combination of ultrasonication and shear mixing with the use of an organic solvent was chosen due to the better dispersion results reported in comparison to the first or second process used alone [60] [162] [163].

Figure 3.6: Dispersion of MWCNTs in toluene solution via direct ultrasonication

Initially, the desired carbon nanotubes quantity was inserted into a small vial containing toluene on a 1% weight ratio, utilizing a metallic spatula and a high precision digital scale to monitor the exact material quantity inserted. Toluene was chosen as the common organic solvent of the solutions, due to the great solubility with PDMS and because of the reported good results in assisting carbon nanotubes dispersion [98].

The carbon nanotubes were then dispersed into the toluene solution by ultrasonicating the solution, utilizing a 20kHz high frequency sonicator (Fig. 3.6). High frequency direct sonication was preferred over a sonication bath as the latter yields poor dispersion. Employing high frequency ultrasonication also generates the desired dispersion in significantly shorter amount of time, a couple of minutes instead of hours, as reported in [162].

Ultrasonication was achieved by immersing the tip of the horn probe of the sonicator into the solution and operating the equipment in pulse mode with 10 seconds on, 15 seconds off, for 3 minutes which allowed the solution to settle back after each burst. At the same time, the PDMS elastomer base was dissolved in toluene, in a 10% w/w ratio. The dissolution was achieved by shear mixing the solution for 5 minutes, via the use of a magnetic stirrer at 500 rpm.

Subsequently, the 2 solutions were combined in a large vial, on the desired filler-polymer ratio, and an additional direct ultrasonication step was conducted, in a pulsed mode for 3 more minutes.

In order to remove the organic solvent from the nanocomposite, the solution was then heated at 100 ^{o}C close to the boiling point of toluene, ~110 ^{o}C, and shear mixed, with the use of a magnetic stirrer at 500rpm, until 95-97% of the toluene evaporated (Fig. 3.7). This took approximately 45 minutes for 8g composite. The evaporation was closely monitored during this step via a high precision digital scale.

Beyond this point, it was observed that no more solvent would evaporate from the solution regardless of time. In addition, evaporating the solvent without employing concomitantly shear mixing yielded a very low evaporation rate of 0.003g/min which resulted in the settling and re-agglomeration of the carbon nanotubes at the bottom of the vial after extended amounts of time, larger than 10 minutes.

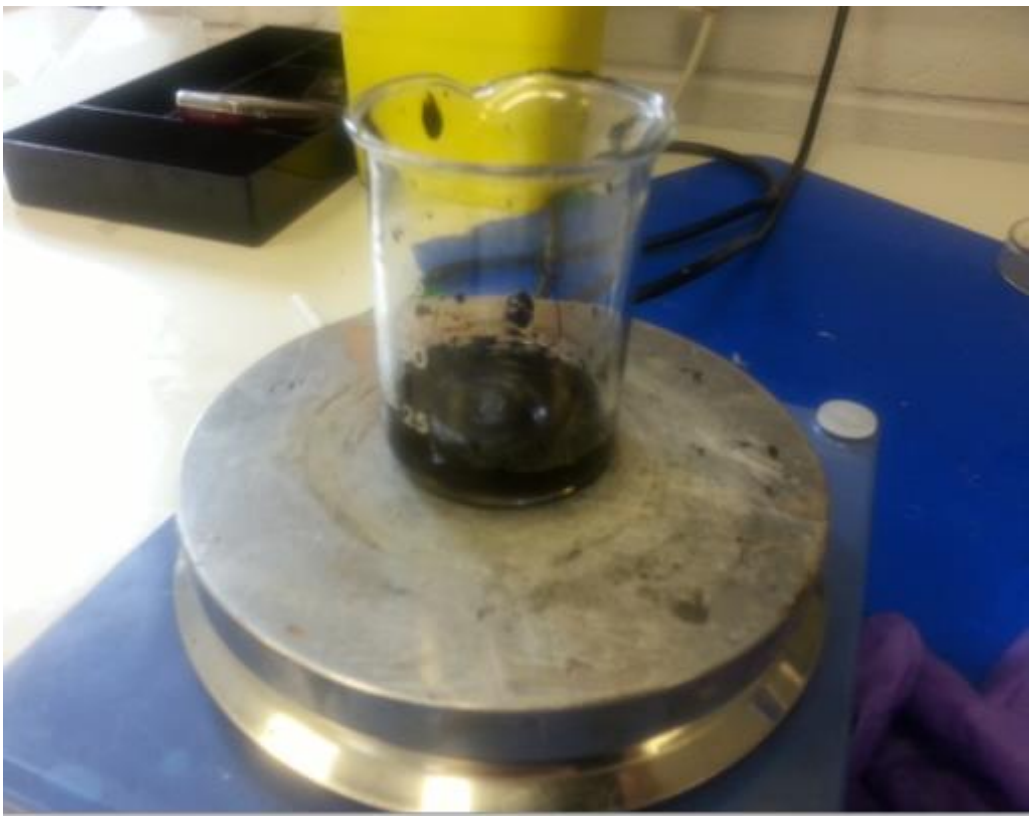

Figure 3.7: Shear mixing of the solution and evaporation of toluene

Afterwards, the solution was cooled down at room temperature by immersing the vial into a cold water bath. The cooling down of the composite prior to the insertion of the PDMS curing agent is necessary in order to avoid thermally curing the composite during mixing. Subsequently the curing agent was added to the solution and the composite was shear mixed for 15 minutes at 500rpm with a magnetic stirrer, at room temperature. In addition, the standard ratio of 10:1 PDMS elastomer base to curing agent was used, as recommended by the manufacturer and used widely in literature [60] [101] [104] [162] [163] [164].

Although it is well documented that manipulating the curing agent-elastomer base ratio has an impact on the resulting Young's modulus as explained later (chapter 4), it was observed that significant variations from the recommended ratio yielded only partially cured composites after the curing process.

Finally, the liquid composite was placed into a dessicator and degassed under vacuum for 45 minutes in order to remove the trapped air pockets within the composite generated during the mixing process.

A glass slide with two copper tracks on a fixed pitch distance of 0.7cm was prepared and an area of 1x0.5cm^2 was isolated which surrounded the pitch of the two copper tracks. A small quantity of the composite was poured within this area and spread repeatedly, using a blade, to form a thin film with a thickness of 0.300±0.100mm (Fig. 3.8a). The MWCNT-PDMS composite was then placed onto a hot plate and left to completely cure for 1 hour at 100^{o}C (Fig 3.8b). The setup was designed to measure the electrical resistance of the developed MWCNT-PDMS nanocomposite.

Figure 3.8: Designed setup for measuring the developed MWCNT-PDMS composites: (a) copper tracks deposition and pitch area isolation, prior to spreading the composite; (b) cured MWCNT-PDMS composite film

3.4 Results and discussion

3.4.1 Carbon nanotubes-PDMS composite percolation threshold

The fabrication process described previously was iterated for a number of different loadings of carbon nanotubes concentrations with regards to the PDMS polymeric matrix, in order to map the percolation threshold of the composite. Carbon nanotubes loadings from 0.2% to 3% were prepared and electrical resistance of the samples was

measured with a digital multimeter Keithley 2000 connected to a DC source, operating at 1V.

Probes were attached to the copper tracks of the glass slides containing the cured composites and the resistance values of a set of 6 MWCNT-PDMS nanocomposites samples per each loading were measured (Fig. 3.9). Errors introduced into the measurements included the difficulty in inserting the exact desired weight fraction of carbon nanotubes into the polymer, the integrity of the Ohmic contacts between the wiring and copper tracks as well between the copper tracks and the cured composite, the degree of organic solvent evaporation during processing which was larger (~97%) at small weight fractions (<0.6%) and smaller (~95%) at bigger weight fractions (>1%).

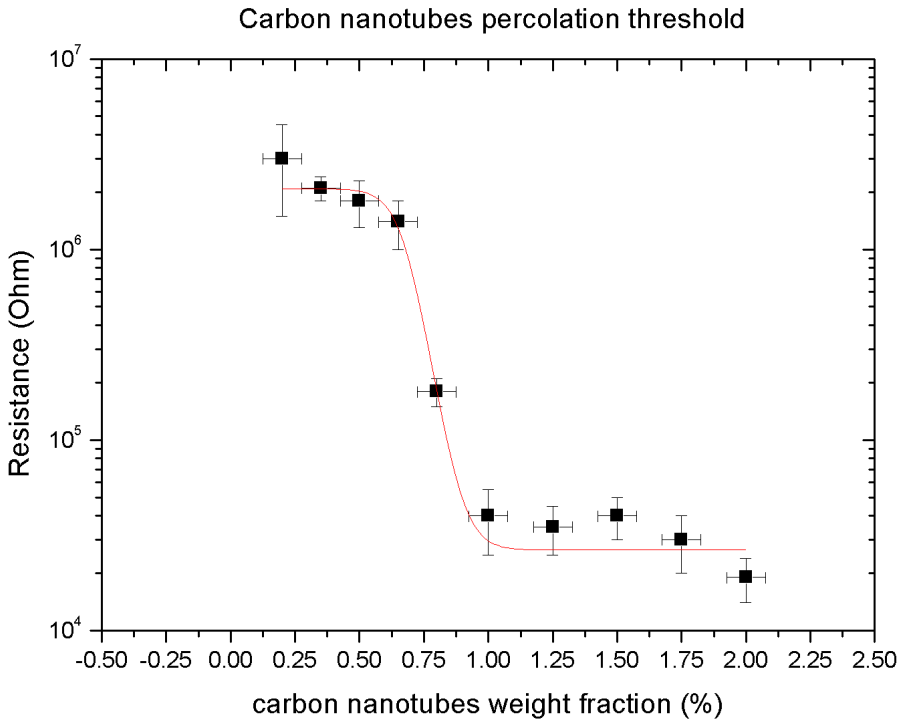

Figure 3.9: MWCNT-PDMS nanocomposite percolating behaviour

The developed MWCNT-PDMS nanocomposite exhibits the typical sigmoidal conductive behaviour from percolating carbon-based polymer composites. As expected, the percolating threshold of the composite was found to be at a very low carbon nanotubes weight fraction of approximately 0.65±0.10% (Fig. 3.9).

Beyond that point the resistance of the composite dropped significantly, by approximately 3 orders of magnitude, signifying the formation of a percolating network spanning the sample. In addition, from the value of 1% w/w of carbon nanotubes to

PDMS, the electrical response of the composite remained stable and exhibited only a minor decrease as expected from percolation theory.

However the rise in the electrical conduction of the composite of the polymer was not as dramatic as reported in the literature, where a change of as large as 9 orders of magnitude has been recorded [164]. Possible reasons for this behaviour are attributed to either the presence of a residual amount of the organic solvent, used to assist the dispersion of the carbon nanotubes into the polymer matrix, which was not evaporated completely blocking the percolating network, or the extended shear mixing of the composite during the evaporation step which might have led to the breaking of the carbon nanotubes and resulting shortening of their length, and therefore to the decreased conductivity of the composite as reported elsewhere [101].

3.4.2 Developed protrusions of the aluminium substrates

As mentioned in section 3.3.1, a large aluminium plate was micro-milled with 16 individual protrusion-shaped electrode pads, separated via a laser-cutter. These protrusions served as an enhanced pressure delivery mechanism from the sensor. Each developed protrusion-shaped electrode layer had distinctive protrusion features with tip surfaces ranging from 550x550um^2 to 75x75um^2. The features of the developed aluminium electrode layers were examined and evaluated utilizing optical profilometry.

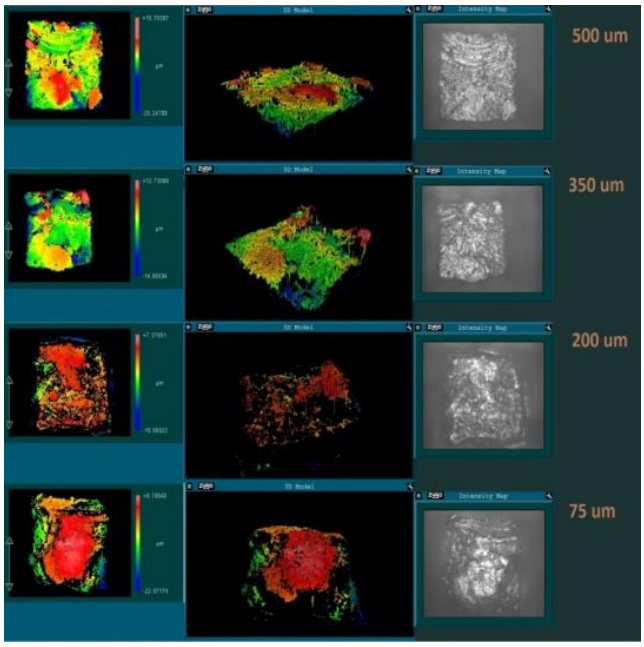

Figure 3.10: Examination of the protrusion features via optical profilometry

After examination via the profilometer equipment Zygo Viewmeter 5200, it became apparent that, regardless of tip size, the micro-milling equipment produces an uneven protrusion surface (Fig. 3.10). The surface of developed protrusions exhibited random small bumps and recesses, with an average height deviation from the surface in the order of 8-15μm. Moreover, for the smaller features of structured electrodes, the tip edges of the developed protrusions became less and less defined, from totally square surfaces for the larger protrusions to almost spherical for the smallest protrusions (Fig. 3.11).

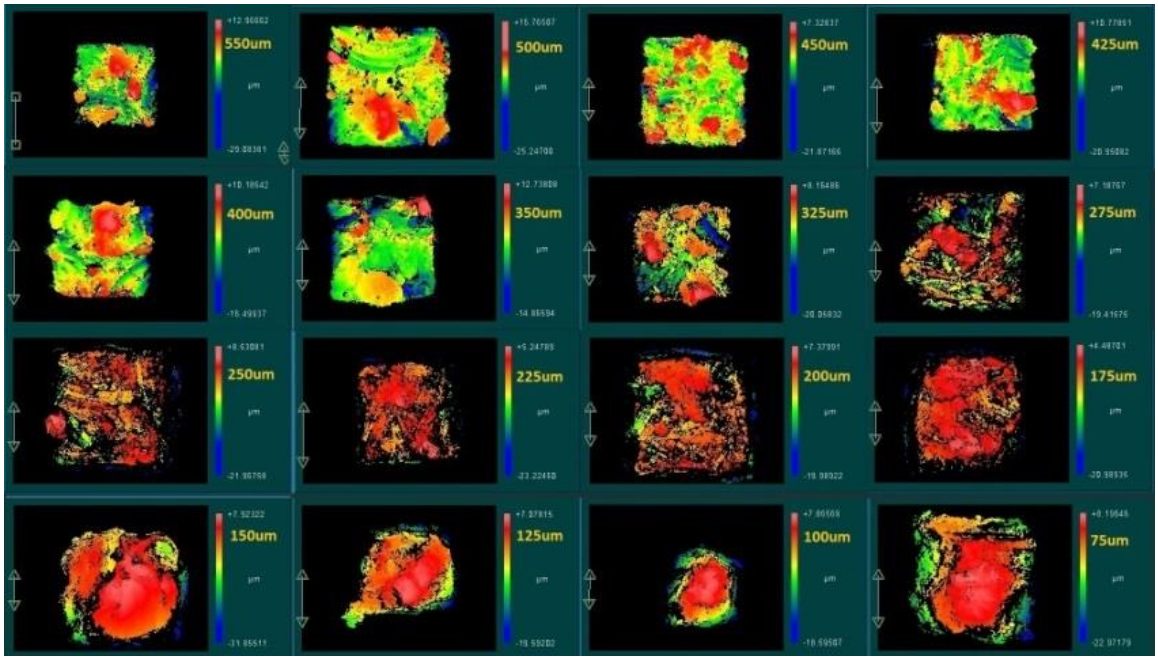

Figure 3.11: Scaling down the size of the protrusions and resultant features

3.4.3 Electrical conductivity of the composites under compressive loads

3.4.3.1 Experimental setup

In order to measure the piezoresistive response of the conductive composites, flat aluminium substrates were utilized to bond them atop and were firmly fixed on a large aluminium plate via double tape.

A thin layer of silver conductive epoxy was doctor-bladed upon the surface of the flat substrates and the composite films were attached upon it. After the silver epoxy had solidified a firm bond was achieved between composite film and the flat substrate, ensuring maximum electrical contact. In addition, using the same conductive epoxy thin wires were bonded to the electrode pads of the aluminium substrates to connect them with the input signal bias (Fig. 3.12).

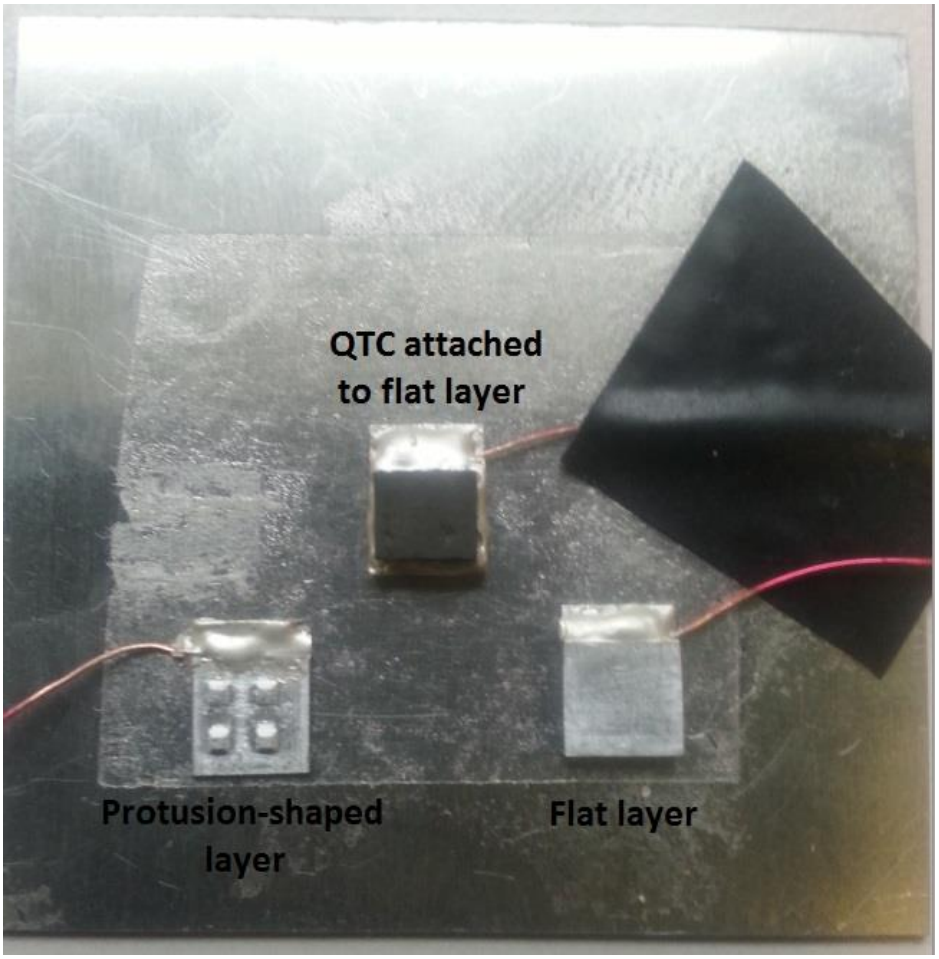

Figure 3.12: Photograph of developed aluminium structures, with attached wiring, and bonded composite film on a flat aluminium substrate

A MAT-400 die-bonder was used as the pressure delivery system. The machine could exert pressure on the surface of the devices (25mm^2) from approximately 40kPa to 1.2MPa, by increment of 5kPa (Fig. 3.13). The die-bonder equipment utilizes a computer-controlled probe with a micro-camera, which is used to position the sensor accurately upon a target, and can exert the aforementioned forces within a user-set time limit.

The reason behind choosing this equipment lies on the observation that none of two composites had any detectable response on the desired low pressure range of 0-6kPa,

when measured with a set of precision weights. Therefore the die-bonder equipment that delivered larger forces was selected to explore the filler-polymer composites behaviour under stress.

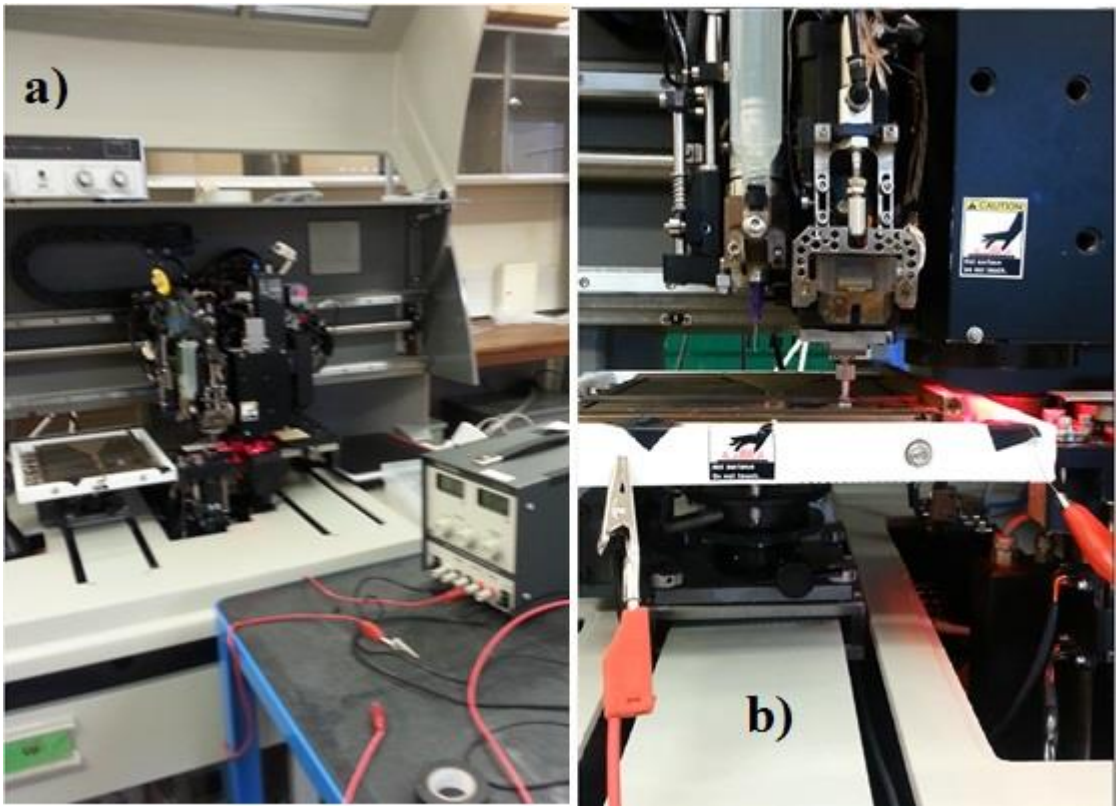

Figure 3.13: Photographs of (a) MAT-400 die-bonder equipment and setup and (b) pressure sensor during measurement

Moreover, in order to evaluate the electrical response of the composites under different protrusion surface areas, a variety of the developed protrusion-shaped aluminium substrates were attached on the composite films surface.

The bonded thin wires of the 2 aluminium layers were then connected to a DC supply operating at 1V and a Keithley 2000 digital multimeter was used, in series to the circuit, to measure the resistance of the device under pressure (Fig 3.13a). Great care was taken at this stage to firmly fix the apparatus wires, so as not to disturb the sensor during measurement.

The probe of the die-bonder would then be positioned on top of the device and the desired pressures would be exerted for a period of 20 seconds. Before each measurement, each sensor was inspected in order to ensure that the structured top layer of the sensor was in the correct position.

3.4.3.2 MWCNT-PDMS sensor vs pressure

In the case of MWCNT-PDMS nanocomposite films, samples with a carbon nanotubes weight fraction near the percolation threshold were chosen since they exhibit the largest sensitivity to applied force, as explained in section 2.6.

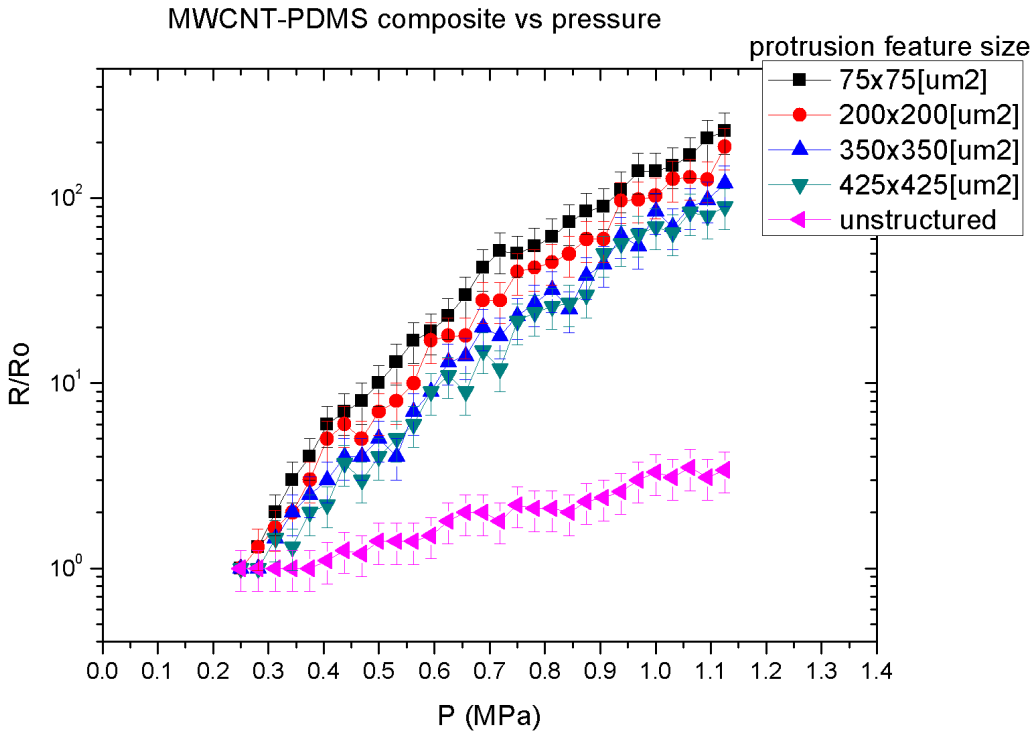

Figure 3.14: MWCNT-PDMS pressure sensor response to compression. The performance of the sensor improved when one of the electrodes was structured with protrusions

As described in section 2.6, the MWCNT-PDMS composite, when subjected to compressive deformation, exhibits a positive piezoresistive response, i.e. an increase in relative resistance. A similar response was observed on this occasion, as the developed carbon nanotubes-based composite exhibited an increase in its relative resistance R/R_o with applied pressure (Fig. 3.14).

More specifically, the MWCNT-composite film was first evaluated utilizing a flat aluminium top layer under compressive loads from 40kPa to 1.2MPa (Fig. 3.14, unstructured data). The composite shows a very limited response with regards to its relative resistance, from 0.4MPa and onwards, reaching its maximum response at approximately 1.2MPa with a final value of the resistance barely 50% more than the initial resistance value. This result is in agreement with the response of a similar

MWCNT-PDMS composite reported in [111] (see Fig 2.9). The pressure resolution is approximately 200kPa.

However, larger variation of resistance was observed in the samples when aluminium plates with protrusions are utilized (Figure 3.14). The electrical resistance of the composite showed a detectable response from pressures as low as 0.25MPa for protrusions with a tip area of 75x75um^2 with values increasing 250 times the initial resistance over the same pressure regime. Changes of resistance were measured for pressure steps as low as 50kPa.

The dynamic range also slightly increased as the surface of the protrusions tip becomes smaller. A detectable shift on a smaller pressure range, of approximately 200kPa, was observed as the protrusion tip surface areas were scaled down from 550x550μm^2 to 75x75μm^2. Overall though, none of the samples exhibited any detectable response for pressures lower than 0.2MPa or for a pressure resolution lower than 50kPa.

3.4.3.3 QTC sensor vs pressure

A better response to pressure was observed for the QTC sensors. The QTC composite was effectively behaving as an electrical insulator until a critical compressive load. Beyond that point the resistance of the composite started to drop exponentially, in agreement with the tunnelling effect dominating the relationship between the neighbouring filler constituents of the composite. As the forces exerted onto the QTC became greater the distance between the spikes of the neighbouring nickel particles became smaller, enabling tunnelling conduction.

As in the previous section, the response to pressure of the QTC composite was first evaluated with a flat aluminium layer (Fig. 3.15). QTC resistance started to drop exponentially, from ~10MΩ to 100Ω, in the pressure range of approximately 0.2MPa to 1.2MPa. The observed electrical behaviour of the QTC composite under pressure was in agreement with similar experiments conducted on QTC pills as reported in [122]. Overall, the lowest variation in resistance, distinguishable from noise, was observed at approximately 50kPa.

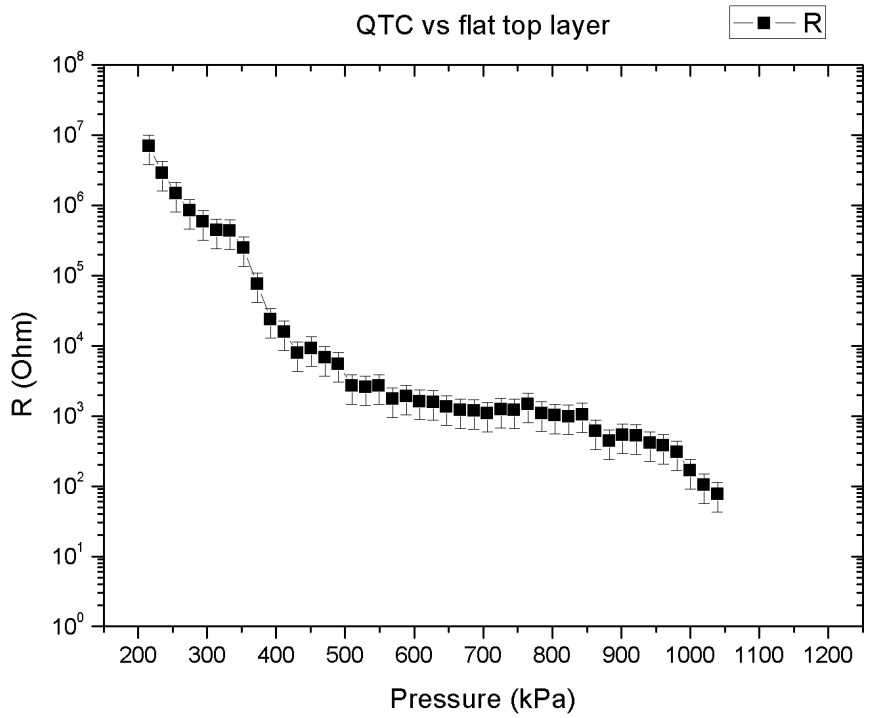

Figure 3.15: QTC pressure sensor with flat top electrode layer. Resistance dropped exponentially over the measured range

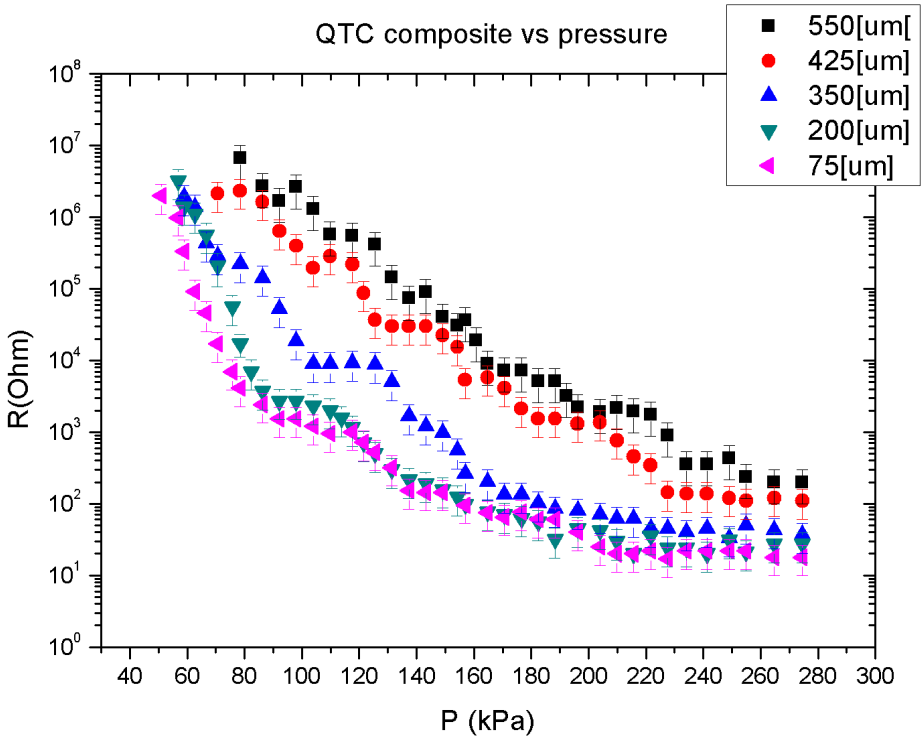

Figure 3.16: QTC sensors performance improved significantly when a structured electrode layer was utilised. Scaling down the size of the protrusions had an additional positive impact on the sensor performance

However, the dynamic range of the sensor increased significantly when protrusion-shaped top layers were used (Fig. 3.16). In this case, the pressure range of the sensor narrowed down to 100-180kPa and pressures as low as 50kPa were recorded. Pressure changes as small as 10kPa were detected and the overall performance of the sensor significantly improved.

Increased dynamic range of the sensors was also observed with the scaling down of the protrusion tip surface areas. The lowest detectable pressure shifted from 100kPa for 550x550μm^2 area tips to approximately 50kPa for the smallest tips of 75x75μm^2. Moreover the pressure range of the sensor also narrowed down with respect to the surface area of the protrusions tips, from 180kPa for the largest protrusion tips to 80kPa for the smallest protrusion tips. Beyond the above pressure region, the resistance of the sensor saturated on a relatively small and stable resistance value of approximately 30-100Ω.

Finally, despite the fact that the QTC composite demonstrated a superior sensitivity compared to the developed MWCNT-PDMS composite, none of the tested samples exhibited any detectable response for pressures lower than 50kPa, and even with the smallest protrusions, pressure resolution less than 10kPa was not distinguishable. In addition, QTC exhibited significant variations in the measured resistances over the same force loads. A strong drift behaviour was also measured, with 10 to 20 seconds necessary to reach a relatively stable resistance value for each pressure measurement. The large variations observed can be attributed to the non-uniform surface of the protrusions. Indicative of the above, is the fact that the resistance variations became larger in the case when aluminium structures with the smallest protrusion geometry were used that also possessed the most non-uniform and less defined surface features.

Therefore, due to the inability of both the MWCNT-PDMS and QTC composite to detect pressure variations on the desired low pressure range of 0-6kPa, a different sensor design was explored and is presented in the next chapter.

Chapter 4:
Capacitive pressure sensor

4.1 Introduction

This chapter presents a capacitive pressure sensor, composed of a microstructured ultra-thin polymeric dielectric medium. As in the previous chapter, the design and materials of the sensor are first introduced, followed by the experimental procedure undertaken to develop it. The results in relation to the sensor polymeric dielectric medium thickness and structuring, as well as the sensor performance under compressive loads in the low pressure regime as a function of the above parameters and others, are discussed in the final section of the chapter.

4.2 Materials chosen and sensor design

In order to achieve a greater pressure resolution within the desired working range of compression hosiery, a parallel plate capacitive pressure sensor design was explored which utilizes a thin structured polymer layer as the dielectric material of the capacitor. PDMS Sylgard 184 elastomer from Dow Corning Inc. was chosen as the deformable material as it exhibits a low Young's modulus of 1.7MPa and is suitable for micro-processing.

To further increase the deformation of the polymeric layer, a PDMS material blend with tuneable Young's modulus was also explored, as explained in the following sections. This blend consists of a mixture of Sylgard 184 elastomer and Sylgard 527 dielectric gel under different ratios, depending on the desired Young's modulus of the final PDMS blend.

The structure of the sensor was designed again so as to be a cost-effective and potentially embeddable device to compression hosiery. The sensor design includes two 18x18mm^2 rigid conductive layers that encompass an ultra-thin polymeric layer (Fig. 4.1).

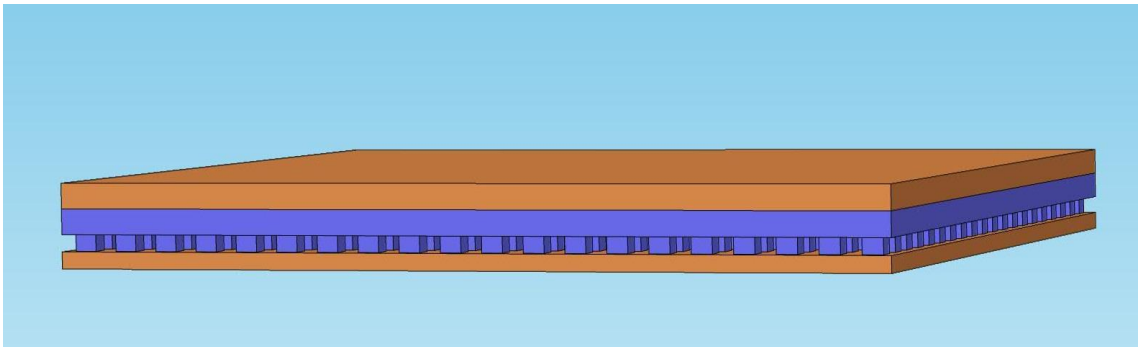

Figure 4.1: **Capacitive pressure sensor design**

Thin films of titanium/copper evaporated onto glass slides were utilised as the conductive top and bottom layers of the parallel-plate capacitor sensor. In addition, the polymeric layer, which lies in between the two conductive plates, was structured with micropillars with a height of approximately 18μm, for a total thickness of the dielectric layer of approximately 33μm. A variety of pillar surface sizes and pitch distances were developed and evaluated, ranging from 30μm to 100μm.

Thinning the polymeric film layer as much as possible, controlling its softness and micro-structuring it, have significant impact to the performance of the sensor. The capacitance change under stress is given by the following equation:

$$\Delta C = C - C_0 = \varepsilon_o \varepsilon_r A \frac{\Delta d}{d \cdot (d - \Delta d)} \tag{4.1}$$

Where *Co* is the sensor initial capacitance, *C* is the sensor capacitance after compression, *A* is the conductive plate surface area, ε_o is the vacuum permittivity, ε_r is the relative dielectric constant and *d* and *Δd* are the initial distance and the compressed distance, respectively.

If one assumes that d>>Δd then the above equation becomes:

$$\Delta C \approx \varepsilon_0 \varepsilon_r A \cdot \frac{\Delta d}{d^2} = C_0 \cdot \frac{\Delta d}{d} \tag{4.2}$$

However considering that the polymeric layer deforms elastically under stress:

$$\sigma = \varepsilon \cdot E = \frac{\Delta d}{d} \cdot E \tag{4.3}$$

Such that

$$\Delta C \approx C_0 \cdot \frac{\sigma}{E} \tag{4.4}$$

The dynamic range of the capacitor is a function of three parameters: the initial capacitance of the device, the Young's modulus of the dielectric layer between the two conductive plates, and the exerted stress. Therefore large initial capacitances of the sensor can be achieved by scaling down the thickness of the polymeric films, whilst utilizing polymers with very low Young's modulus can also substantially increase the sensor capacitive response.

However, the dynamic range can be further increased by micro-structuring the polymeric dielectric layer as reported in [156] [158]. In this case, when pressure is applied upon the top plate of sensor, the exerted force is distributed to the reduced area of the micro-structured pillars, allowing therefore a higher deformation of the polymeric film due to a virtually augmented pressure effect. In this work, all of the aforementioned parameters were taken into account and evaluated during the development of the capacitive sensor.

Finally, following a similar approach as in the previous chapter, the sensor was meant to be embedded to the compression hosiery by attaching it onto the surface of the garment, where the bottom conductive plate would be in direct contact with a conductive thread traversing the garment, whilst the top layer could be connected under a different conductive thread. Similarly, a multitude of such sensors could be interconnected via conductive threads that would span the fabric from top to bottom as in the previous chapter.

4.3 Experimental

4.3.1 Creation of the polymer mould

A casting method was employed, which utilizes a resin-based mould, to develop the structured surface of the polymeric dielectric layer of the parallel-plate capacitor sensor, 3 inch glass wafers were thoroughly cleaned in DI water and Decon 90 detergent in a sonication bath for 60 minutes. The glass wafers were then rinsed in DI water, placed in

a sonication bath for an additional 30 minutes to strip the detergent, and dried firstly by a Nitrogen blow gun and afterwards at a hot plate for 10 minutes at 70^{o}C.

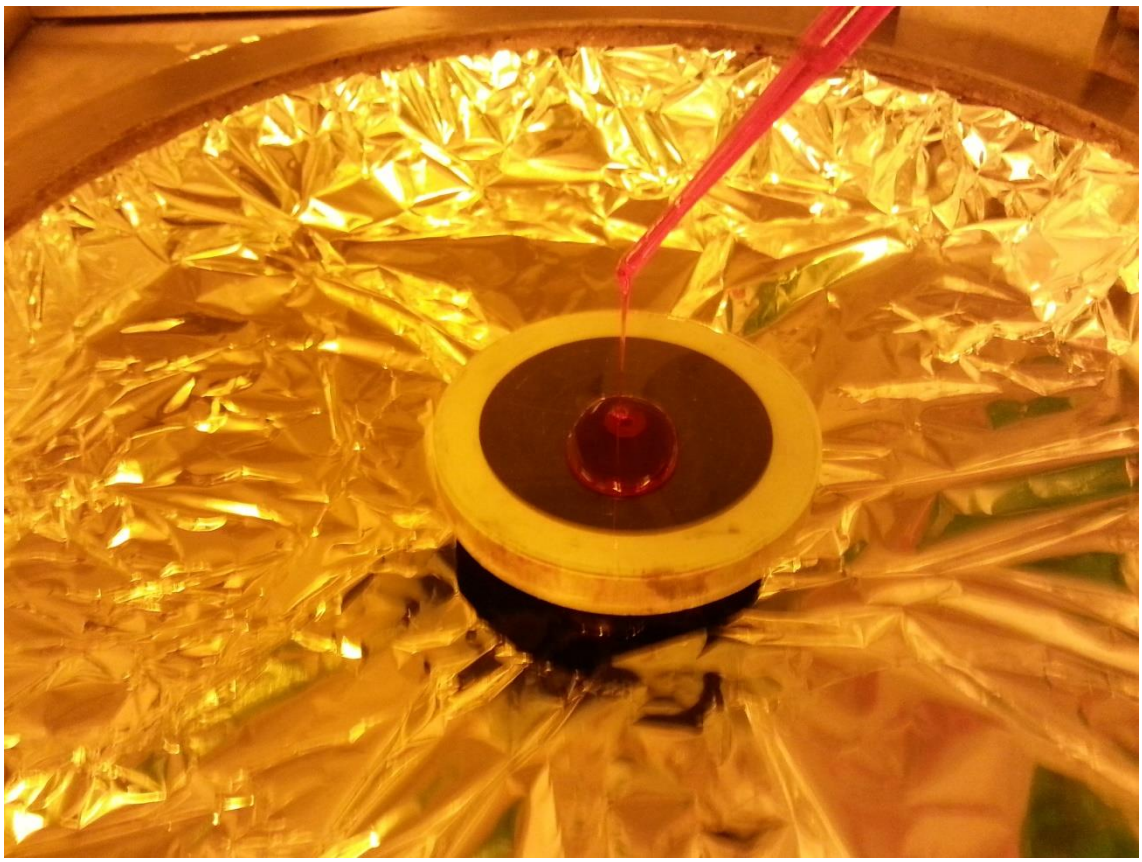

Figure 4.2: Spin-coating of AZ photoresist

More specifically, the cleaned glass wafers to be used, were positioned into a spin coater that held them firmly in place via vacuum, and 3ml of the AZ photoresist were poured centrally utilizing a pipette (Fig. 4.2). At this stage, great care was taken to quickly remove the presence of any trapped air pockets in the liquid photoresist since they would greatly affect the quality of the resultant features of the developed photoresist layer.

The photoresist was then spin coated employing a 2-step process: (1) the spreading stage which ensures that material is uniformly spread on the glass wafer and (2) the thinning stage which subsequently thins the photoresist layer to the desired thickness. In the first stage the spin-coater equipment was set at 400rpm for 20 seconds, whilst in the second stage a variety of spin speeds was tested from 800 to 4000 rpm for the same amount of time with an acceleration of 100rpm/s in both cases.

Subsequently, the spin-coated wafers were left to settle for 10 minutes, afterwards cured on a hot plate for 4 minutes at 100 ^{o}C to polymerize the photoresist and thereafter left again for 2 hours before the exposing stage.

In order to produce the mould out of the cured photoresist, the wafers were placed into a UV lithography equipment (Fig. 4.3) and UV exposed with an exposure dosage of 800mJ/cm^2, utilizing a glass photomask with transparent square features (Fig. 4.4) with sizes from 110μm to 30μm (pitch size ~30μm). This way a negative image of the desired geometry was imprinted onto the spun photoresist, as the UV exposed photoresist areas become dissolvable in positive type photoresist, which could now be used as a mould for the polymer layer of the parallel-plate capacitor sensor.

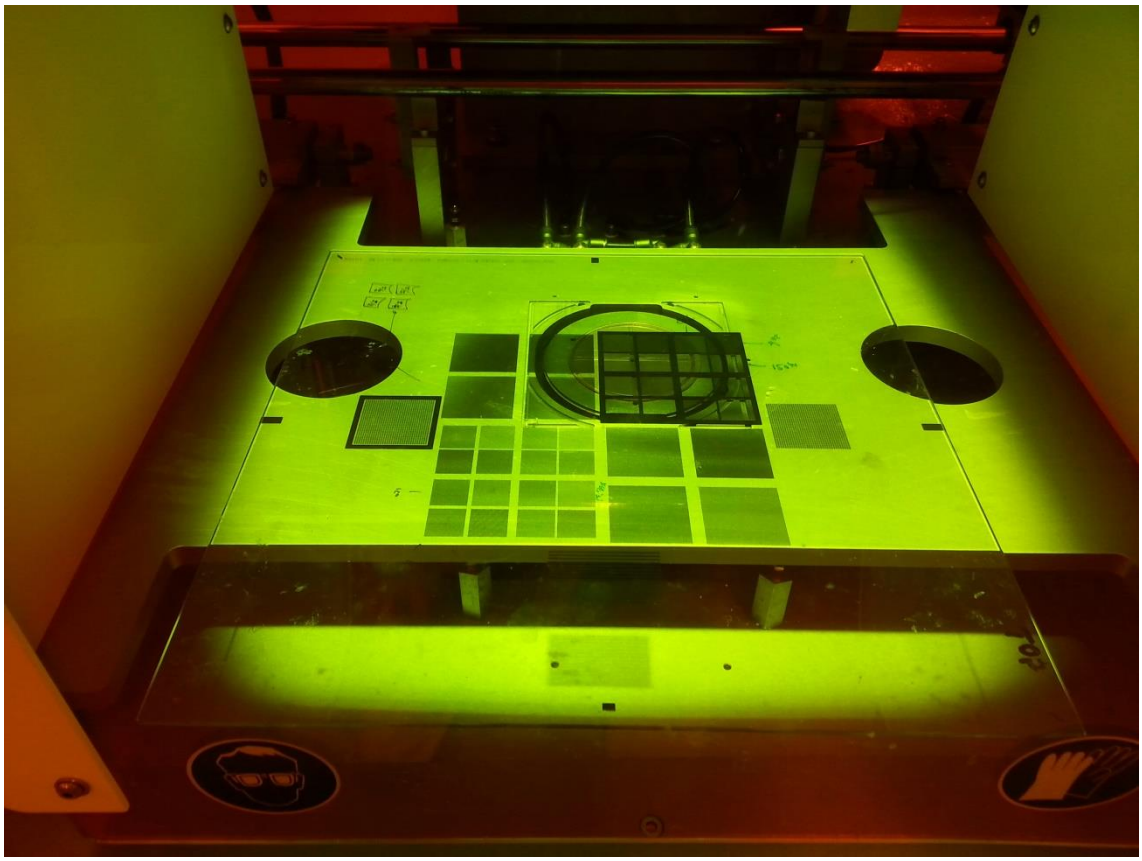

Figure 4.3: UV exposure of wafers

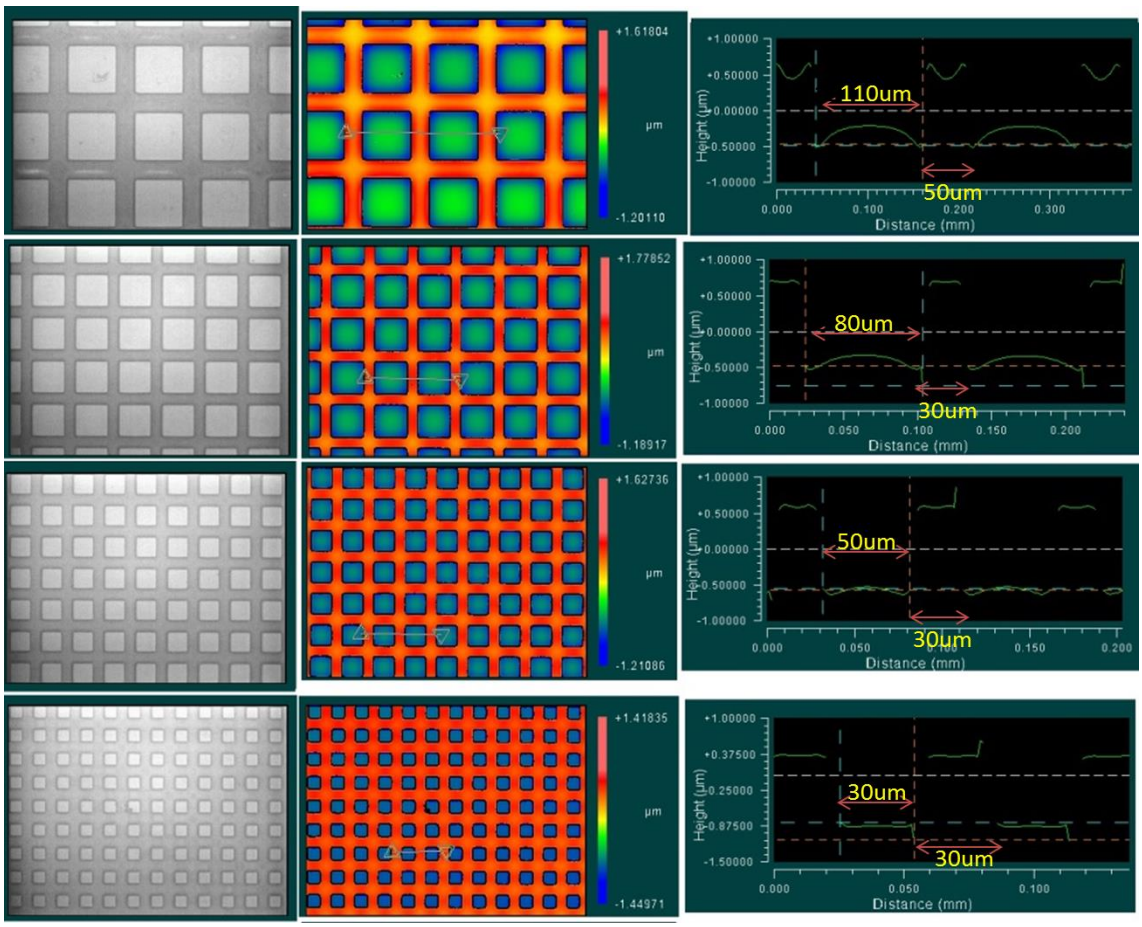

Figure 4.4: The photomask utilised to develop the photoresist mould had 4 different patterns with features ranging from 30µm to 100µm

Finally, in order to reveal the UV imprinted geometry of the photoresist, the exposed wafers were developed into a solution of 3:1 AZ 400 developer to DI water for 6 minutes, rinsed afterwards first with same solution and then with DI water, and blown-dry with a nitrogen gun (Fig. 4.5). Applying mild manual agitation during development helped to further increase the quality of the resultant features of the photoresist mould. Finally, for every developed wafer an evaluation of the quality of their features was conducted via the use of the Zygo Viewmeter 5200 optical profilometer.

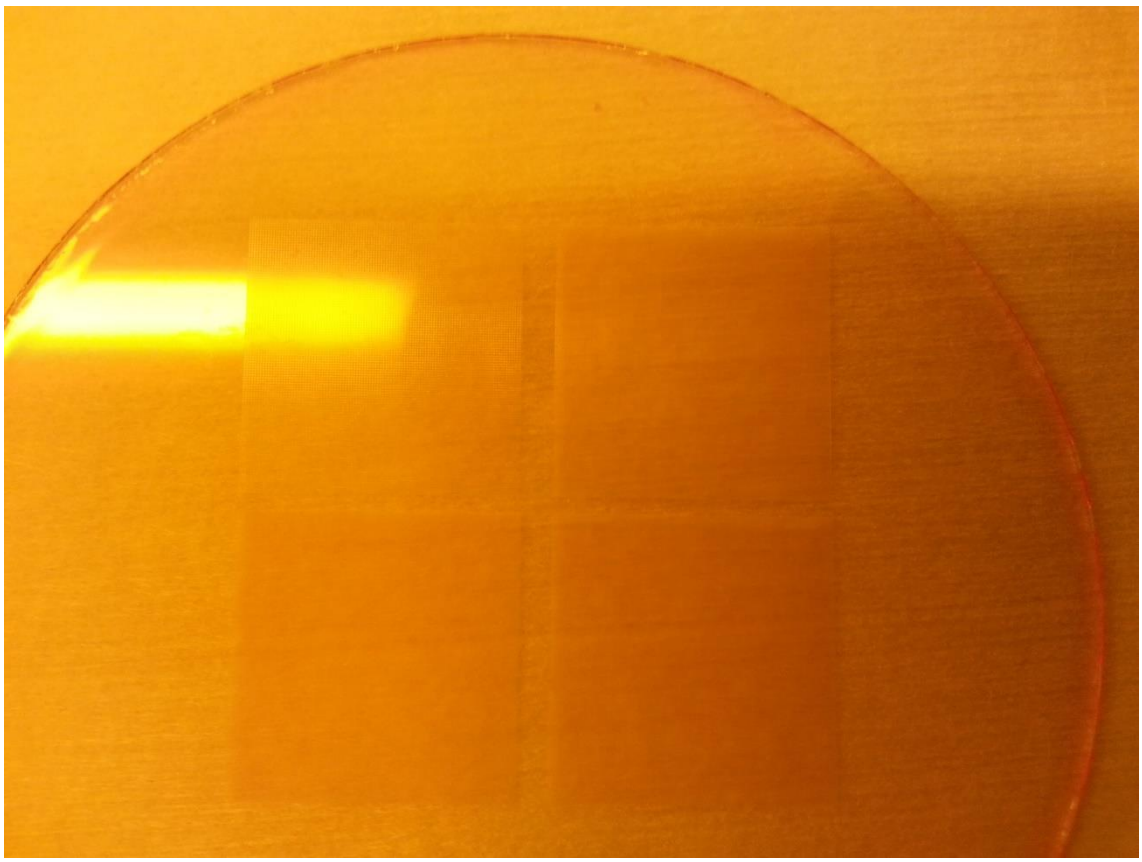

Figure 4.5: The photoresist moulds after exposing and development

4.3.2 Polymer blends and spin coating

PDMS elastomer was initially chosen as the structural material of the deformable dielectric layer of the parallel-plate capacitor sensor. The elastomer was prepared with the standard 10:1 elastomer base to curing agent ratio, as recommended by the manufacturer, and then degassed on a vacuum chamber for 45 minutes to remove trapped air pockets in the material produced during mixing.

A 3ml quantity of the degassed PDMS elastomer was then poured on the glass wafers containing the photoresist moulds and spin coated using a similar 2-step process of spreading and thinning. In the thinning stage, a variety of spin speeds from 500rpm to 4000rpm were tested and evaluated with regards to the resultant thickness of the polymer layer. The wafers were then placed onto a hot plate at 100 ^{o}C for 1 hour to commence the curing of the spin-coated PDMS layer.

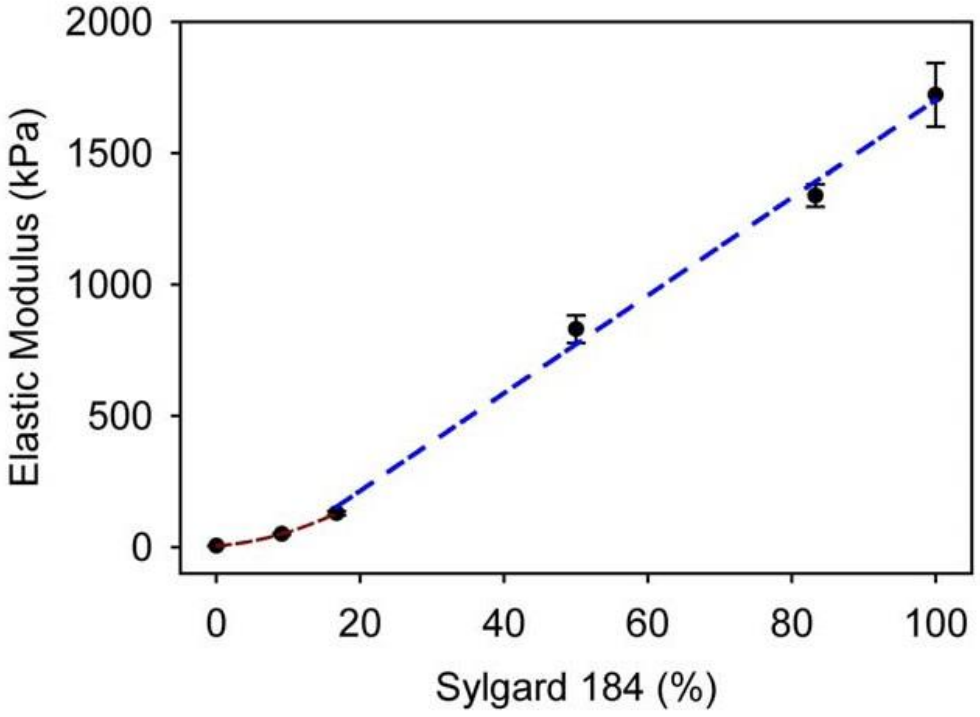

Figure 4.6: PDMS blend Young's modulus as a function of Sylgard 184 concentration by weight [165]

Furthermore, in order to explore the impact of the polymer layer's Young's modulus on the sensor performance, PDMS blends of Sylgard 527 with Sylgard 184 were also prepared and evaluated. Mixing the two aforementioned elastomers together leads to the development of a PDMS composite with tuneable Young modulus from 50kPa to 1.7MPa (Fig. 4.6), as reported in [165], with distinct advantages compared to the common processes employed to decrease the Young's modulus of Sylgard 184 to lower values.

Reducing the Sylgard 184 elastomer's Young's modulus (1.7MPa), usually involves the manipulation of the curing agent/elastomer base ratio from the value 1:10, recommended by the manufacturer, to as low as 1:70 [166-169]. However, reducing the amount of the curing agent in the elastomer, leads to the partial cross-linking of the polymer that leads to the diffusion out of the material of a large amount of free non-crosslinked elastomer; an effect observed also experimentally in this work when the ratio of PDMS Sylgard 184 curing agent to elastomer base was lowered to values less than 1:15.

This effect stems from the fact that the recommended ratio 1:10 is the optimum stoichiometric value of the crosslinking reaction of the polymer [170]. When the above ratio is decreased, the number of non-crosslinked polymer chains that diffuse out of the

material is increased. Moreover, Sylgard 184 elastomer also consisted of fumed nanosilica particles that contribute to as much as 50% of the stiffness of the cured elastomer. These particles exist in both the curing agent and the elastomer base of the material and thus the manipulation of the amount of curing agent does not remove them from the system [171]. Furthermore, a significant variability as large as 600% of the resulting Young modulus values has been reported in literature [166-169], whereas for PDMS Sylgard 184 films that have been prepared on the ratio 1:50, values of the elastic modulus ranging from 8kPa to 50kPa have been recorded.

On the other hand, developing PDMS blends out of Sylgard 527 dielectric gel of Young's modulus 5kPa and Sylgard 184 of Young's modulus 1.7MPa produced elastomers which were completely crosslinked, even in the case of very soft developed elastomers (E=50kPa), in agreement to the reported results of [165]. In this case, the consistency over the mechanical and surface properties of the resultant composite is attributed to the preservation of the stoichiometry of both constituents, the Sylgard 184 and Sylgard 527, which are prepared on the recommended stochiometric ratios (1:10 for Sylgard 184 and 1:1 for Sylgard 527) before mixing (Fig. 4.7). Here also both elastomers were prepared individually and degassed in a vacuum for 45 minutes to remove trapped air pockets prior to mixing (Fig. 4.8).

Figure 4.7: Sylgard 184 (left) and Sylgard 527 (right) after initial preparation

Subsequently the two elastomers were manually mixed together on a fixed ratio and degassed again under vacuum for another 30 min. Finally, the degassed blend was spin coated atop the photoresist moulds and cured on a hot plate at 100 ^{o}C for 1 hour.

In total, 3 different polymeric layers were developed and evaluated: PDMS blend 1:10 Sylgard 184 to Sylgard 527, PDMS blend 1:5 Sylgard 184 to Sylgard 527, and pristine PDMS Sylgard 184, with Young's modulus of 50kPa, 130 kPa and 1.7MPa respectively, as reported in [165].

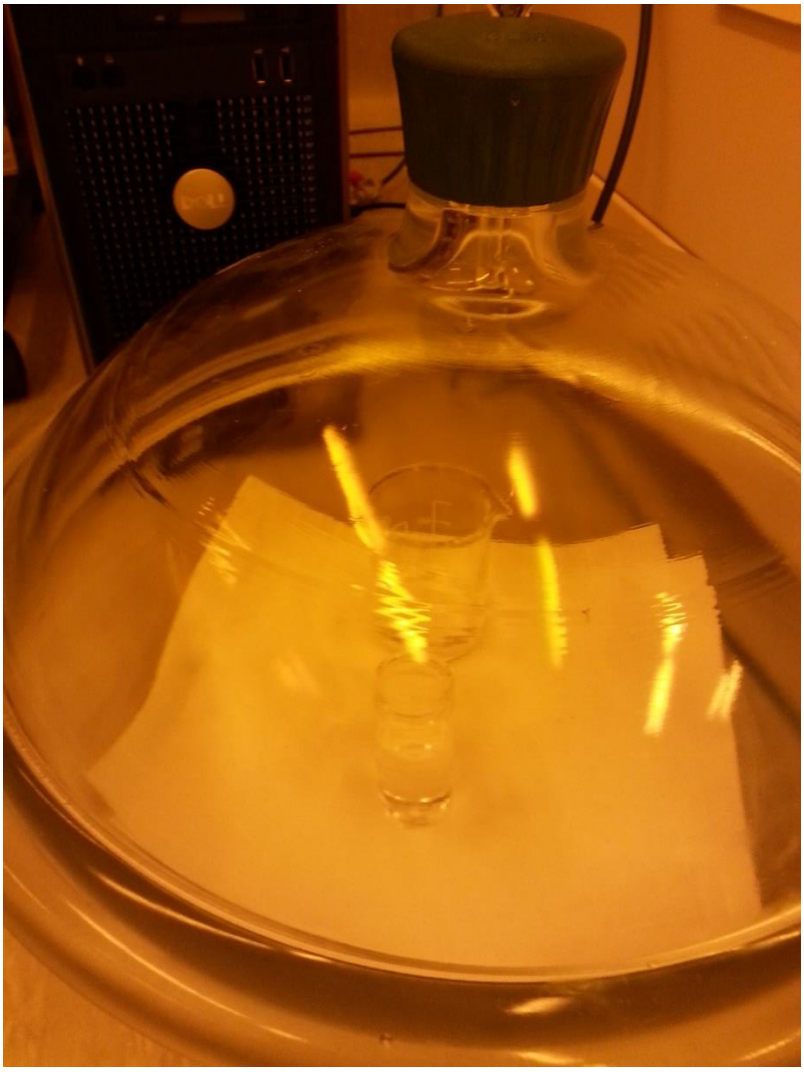

Figure 4.8: Sylgard 184 and Sylgard 527 first degassing prior to mixing

4.3.3 Bonding copper-coated substrates and mould release

Successfully de-moulding the thin cured polymers layers from the structured photoresist moulds proved to be one of the most challenging aspects in the fabrication process of the parallel plate capacitor sensor.

Initially, de-moulding by hand was explored which was only partially successful for the stiffer pristine PDMS Sylgard 184 films. In the case of the softer PDMS blends it utterly failed. In the former case, de-moulding was achieved only for relative thick films, under a DI water bath with a blade and produced significant breakages of the pillar-geometry of the structure.

On the other hand, successful de-moulding results with regards to the quality of developed pillar features were achieved when a triple bath process technique was employed which included an acetone bath, an Isopropyl Alcohol (IPA) bath and a DI water bath. Taking advantage of the AZ 9260 photoresist immediate dissolution in acetone, the glass wafers were inserted into an acetone bath, which resulted in a relatively effortless de-moulding process.

The structured thin polymer films would quickly detach from the wafer, as the photoresist mould dissolved, and float atop the acetone bath surface. The thin films were then collected with a filter and placed firstly in an IPA bath to remove the acetone for less than 1 minute and then on a DI water bath, before they were placed onto a pre-cleaned glass wafer and dried by nitrogen blow (Fig. 4.9).

The above cleaning steps were very important as the presence of acetone on the polymer films for more than 3 minutes deteriorated and destroyed the structured polymeric films. To help de-moulding in less than 1 minute in the acetone bath stage, mild manual agitation was also implemented to drive the acetone into the photoresist mould channels and simultaneously any polymer excess was stripped beforehand from the photoresist mould surface.

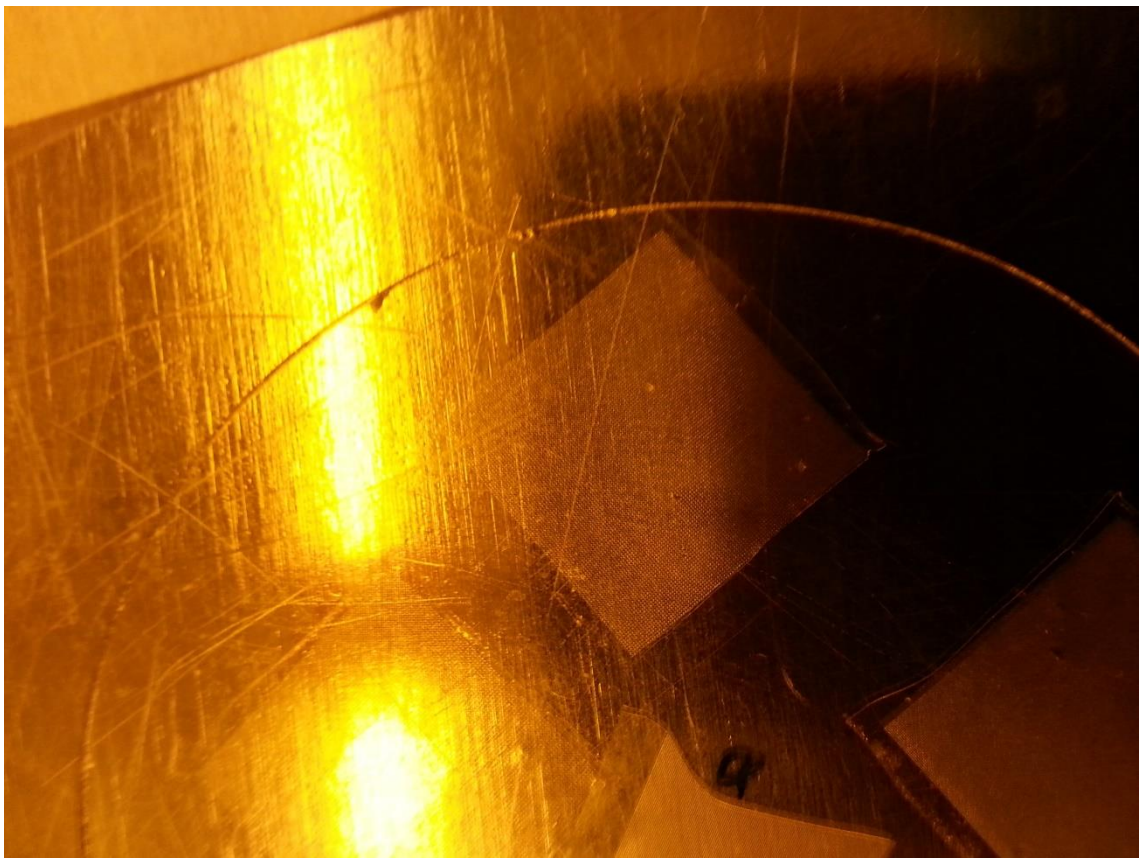

Figure 4.9: PDMS films after de-moulding via the triple bath procedure

However, despite the fact that the aforementioned technique produced undamaged features of the polymeric films, effectively collecting them and placing them flat atop copper-coated glass wafers, for inspection and measurement, was practically difficult. Due to the very thin nature of the films, collecting them from the DI water bath, required great care and delicate handling as otherwise the films would wrap around themselves and would not unbundle without damage.

In the case of the very thin (~30μm) and softer PDMS blends, effectively collecting them without significant damage to the size of the films become almost impossible, as they would wrap more heavily and more easily. More importantly, placing them completely flat unto copper coated glass wafers, which would serve as the bottom electrode plate of the sensor, was extremely difficult to achieve, even for the stiffer and thicker polymer films, as the polymer films would exhibit ondulations on their surfaces.

In order to tackle the above issues and improve the practicality of the device, prior to the triple bath de-moulding process, pre-cleaned copper-coated glass substrates were bonded unto the cured polymer layer.

More specifically, 120μm thick glass slides of the same size (18x18mm^2) as the structured polymeric film were cleaned by the same process and a thin titanium/copper layer was deposited atop their surface. An e-beam evaporator equipment was utilized for this task and the process involved a multitude of steps (4.10).

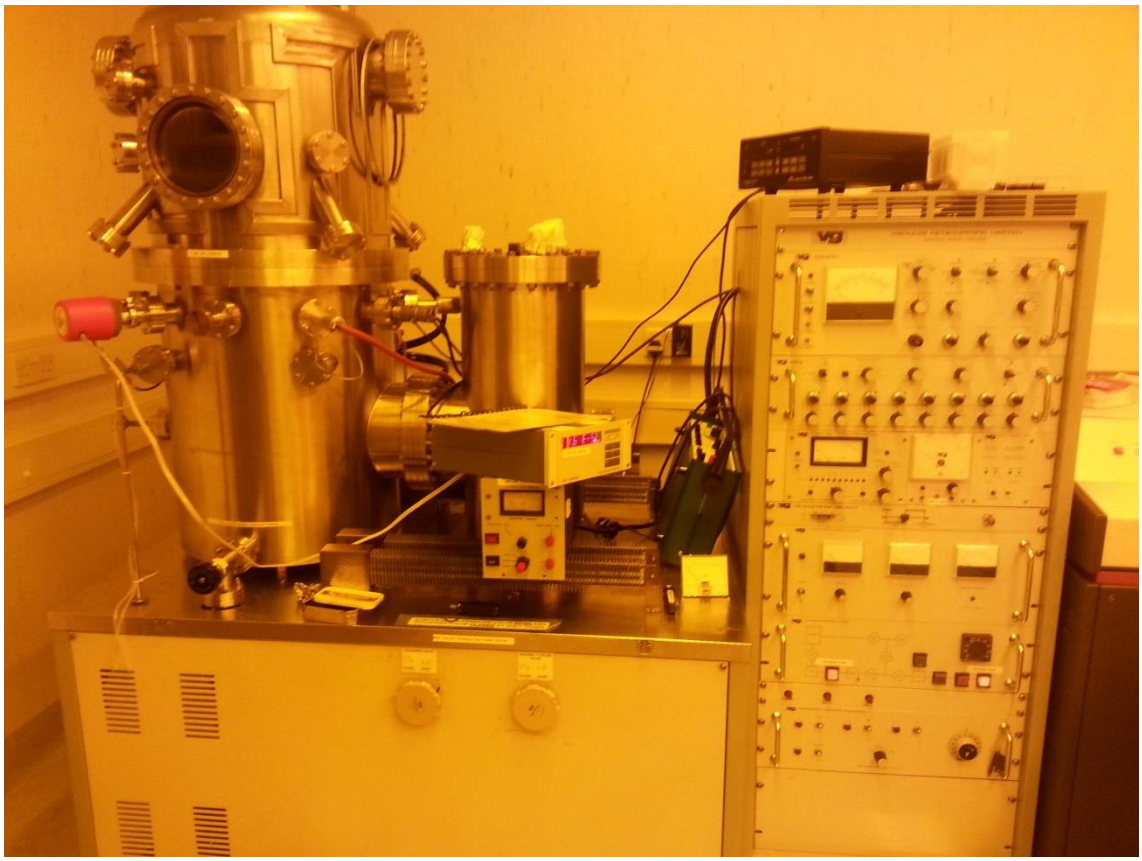

Figure 4.10: The e-beam evaporator equipment

The glass slides were attached via double tape to glass wafers and then placed into the e-beam chamber. The chamber was then pumped down to a high vacuum of $2 \cdot 10^{-5}$Pa and the electron beam positioned onto the target boat containing the material to be deposited. A 50nm titanium layer was first deposited onto the surface of the glass slides, which served as seed layer due to its good adhesion with glass, followed by 100nm of copper (Fig. 4.11). In both cases the deposition rate was monitored and controlled by manipulating the intensity of the electron beam.

Bonding the copper-coated glass slides onto the structured polymer films was achieved by a handheld corona-discharge equipment. Initially, both surfaces to be bonded (PDMS surface and bottom glass surface of the copper-coated glass slide) were treated with corona discharge for 1 minute via repeated passings at 1cm from the surface under treatment. The corona discharge creates an oxygen plasma environment, which changes

temporarily the surface of the PDMS from hydrophobic to hydrophilic enabling it to bond with the glass slide when brought into contact [172].

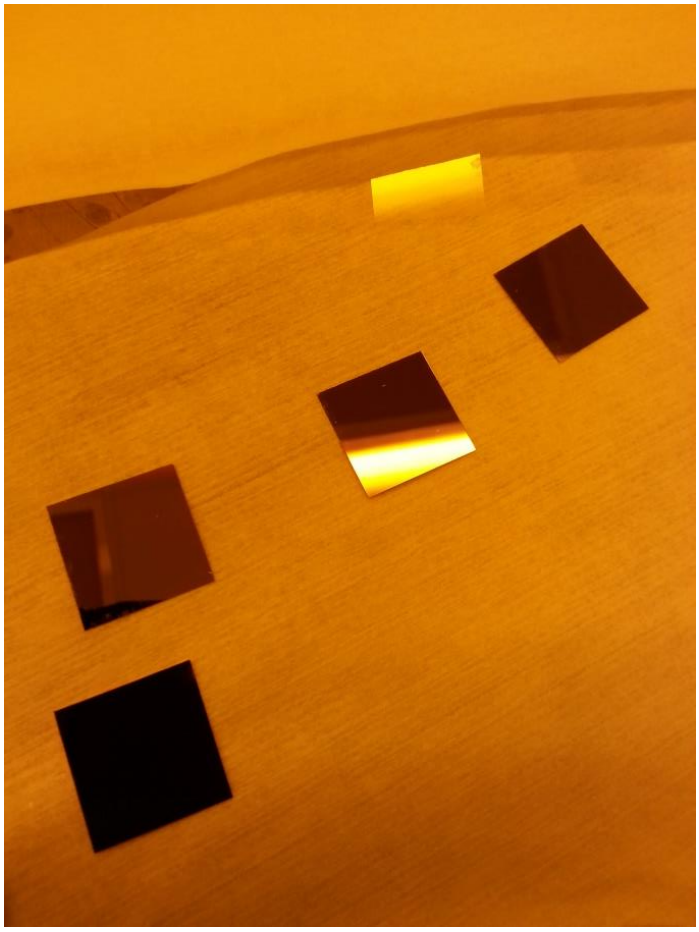

Figure 4.11: Ti/Cu coated glass slides

To further strengthen the bond between the two surfaces, the system was put onto a hot plate at 100^{o}C for 1 hour and a 1kg weight was positioned on top of it. Without treating both surfaces and applying heat via the hot plate, relatively poor and inconsistent bonding results were observed during the de-moulding stage. The addition of the weight also gave overall better bonding results. At the end, the glass wafer with the bonded copper-coated glass slide was then left with the weight undisturbed overnight, to ensure maximum bonding of the two surfaces (Fig. 4.12).

Finally, the total structure of the ultra-thin polymer film bonded unto the copper-coated slide was de-moulded following the same triple bath procedure. To further expedite the de-moulding process in the acetone bath, a blade was utilized to slowly lift the glass copper-coated/polymer layers as the photoresist moulding was dissolving, taking care not to stress the system too much as any excess in force resulted in the breakage of the

glass slides due to over-bending. Every de-moulded layer was then dried via nitrogen blow and inspected and evaluated under the optical profilometer.

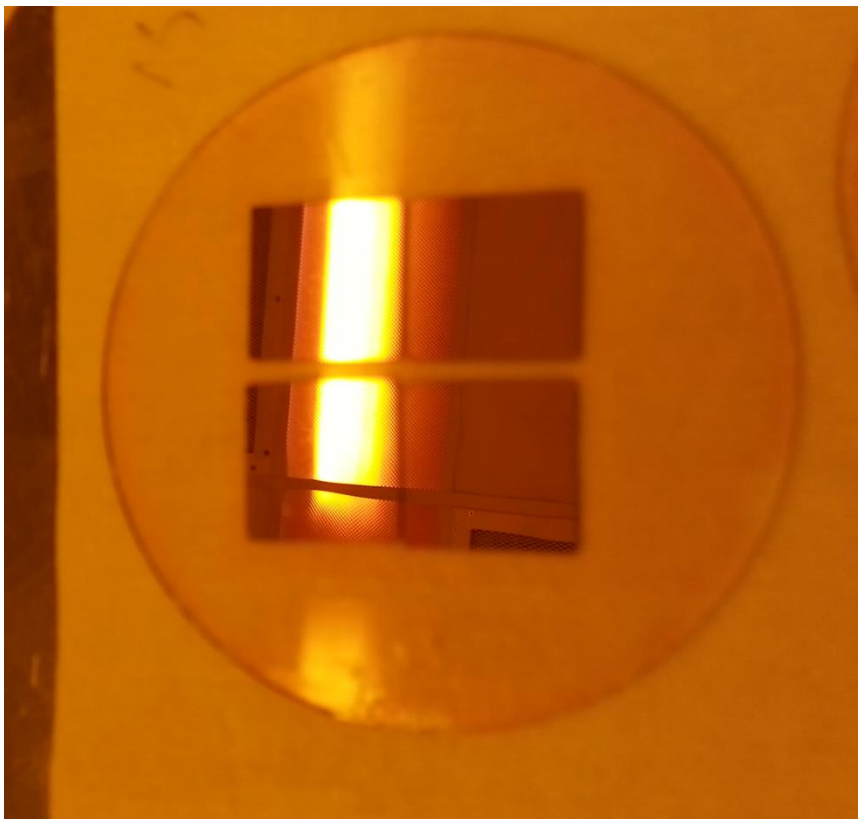

Figure 4.12: Bonded Ti/Cu-coated glass slides on the PDMS blend film prior to de-moulding

4.4 Results and discussion

4.4.1 Photoresist and polymer thickness as a function of spin speed

In the first step of the fabrication process AZ 9260 positive photoresist was spin coated, exposed and developed on pre-cleaned glass wafers. The resist was utilized as a mould for developing the thin structured dielectric layers of the sensor. Initially, during the thinning stage of the spin coating process, the photoresist was spin coated at a variety of spin speeds from 800rpm to 4000rpm (Fig. 4.13) and the resultant thickness of the developed wafers was evaluated under the optical profilometer (5 samples per spin speed).

At the end, the spin speed of 1000rpm was chosen for the coating step due to a better consistency of the developed features over repeated trials and the fact that the resultant pillar features of the developed polymeric films were overall of the same thickness. The thickness of the developed photoresist moulds at this spin speed was approximately

19±1µm; a value that was consistent over photoresist moulds with different features. Photoresist moulds with even the smallest features were successfully developed, with good repeatability, as can be seen in Fig. 4.14.

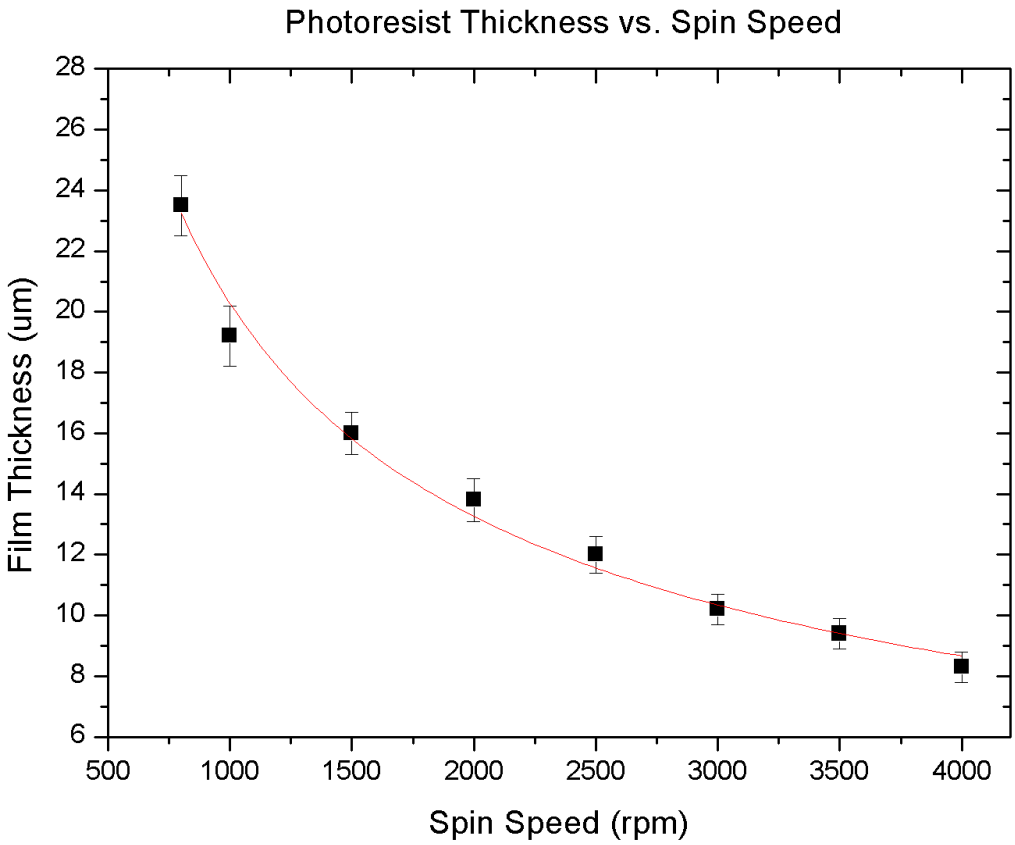

Figure 4.13: Photoresist thickness as a function of spin speed

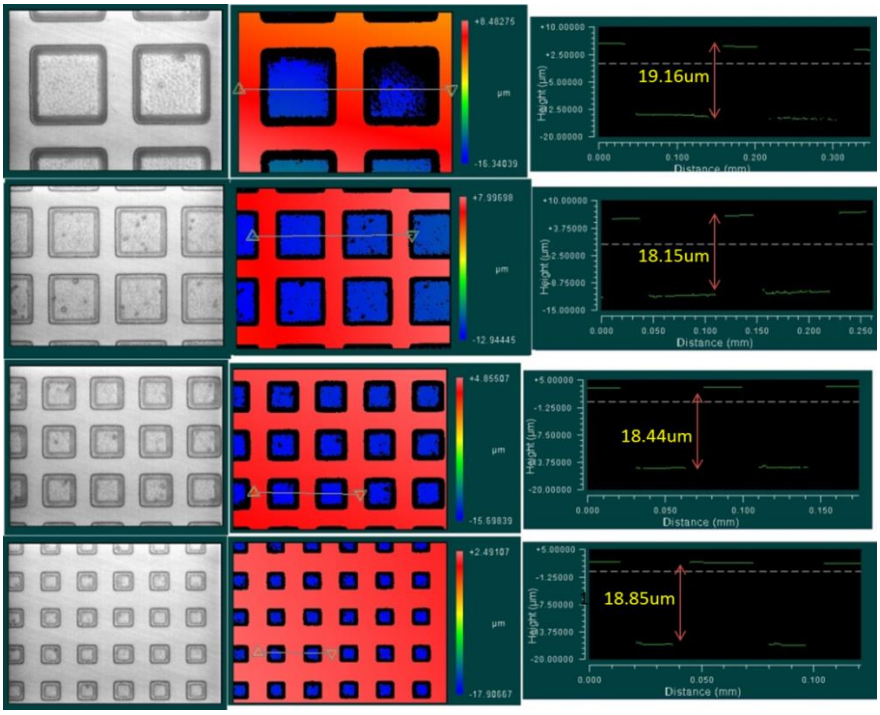

Figure 4.14: Photoresist mould recesses height size over different geometries, from 110µm (top) to 30µm features (bottom)

At the next fabrication stage, the spin-coating, curing, bonding to copper coated-glass slides, and de-moulding of both PDMS and PDMS blends (10:1 and 5:1 types), a range of spin speeds was also tested from 500um to 4000um (Fig. 4.15). The thickness of the base layers of the micro-structured polymeric films was measured via the optical profilometer by cutting a part of the film, which laid flat atop the copper-coated glass slides.

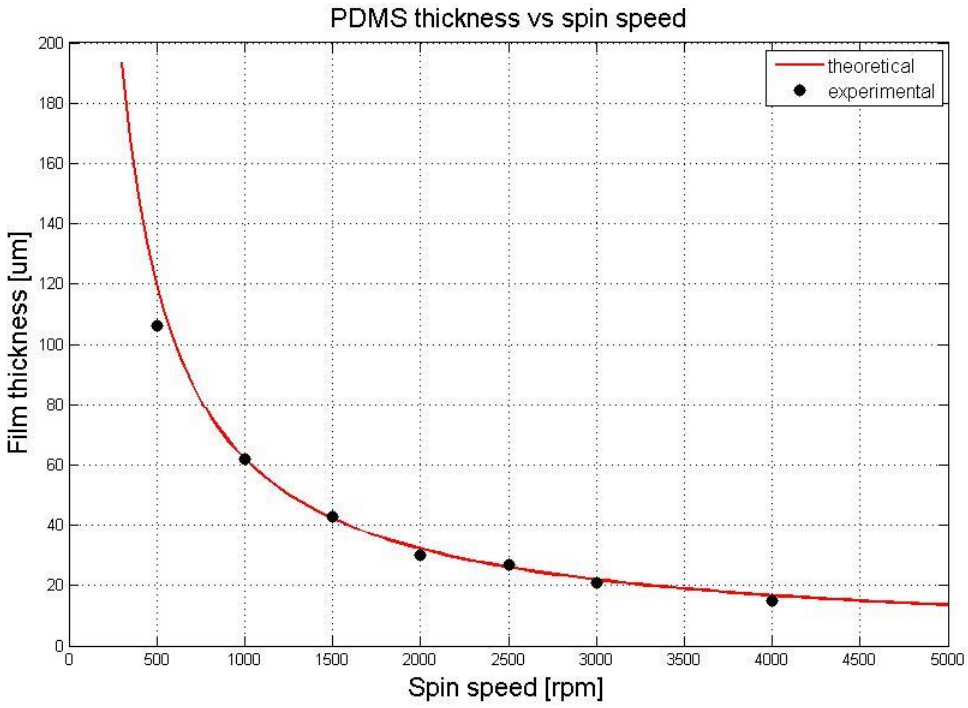

Figure 4.15: PDMS film thickness measurements plotted against the empirical equation 4.5 (red line)

The dependence of PDMS thickness as a function of speed can be estimated by the following empirical equation (Fig. 4.15) [173]:

$$t = \frac{KC^{\beta}[\eta]^{\gamma}}{\omega^{\alpha}} \tag{4.5}$$

Where t is the polymer thickness, ω the spin speed, $[\eta]$ the molecular weight of the polymer measured by its intrinsic viscosity η=4000mPa, C=0.90909 the concentration, K=6.2661 is an overall calibration constant, and α=0.9450, β=5.2707, γ=6.2051 are exponential factors of the formula [174] [175].

The polymeric film thicknesses' recorded experimentally dropped from approximately 106μm at 500rpm to 15μm at 4000rpm (Fig. 4.15, 4.16): a result which is in agreement with PDMS thicknesses recorded in literature [149] [174] [176]. Moreover, no

distinguishable variations were observed for the case of the PDMS blends which exhibited almost identical values at the same spin speed regime.

As mentioned before, scaling down the distance between the two plates of the parallel-plate capacitor sensor leads to an improved sensitivity of the device. Therefore, a spin speed of 4000rpm was chosen for the production of ultra-thin polymeric films with base thicknesses of approximately 15μm. For spin speeds larger than this value, no distinguishable change in thickness of the polymeric films was observed.

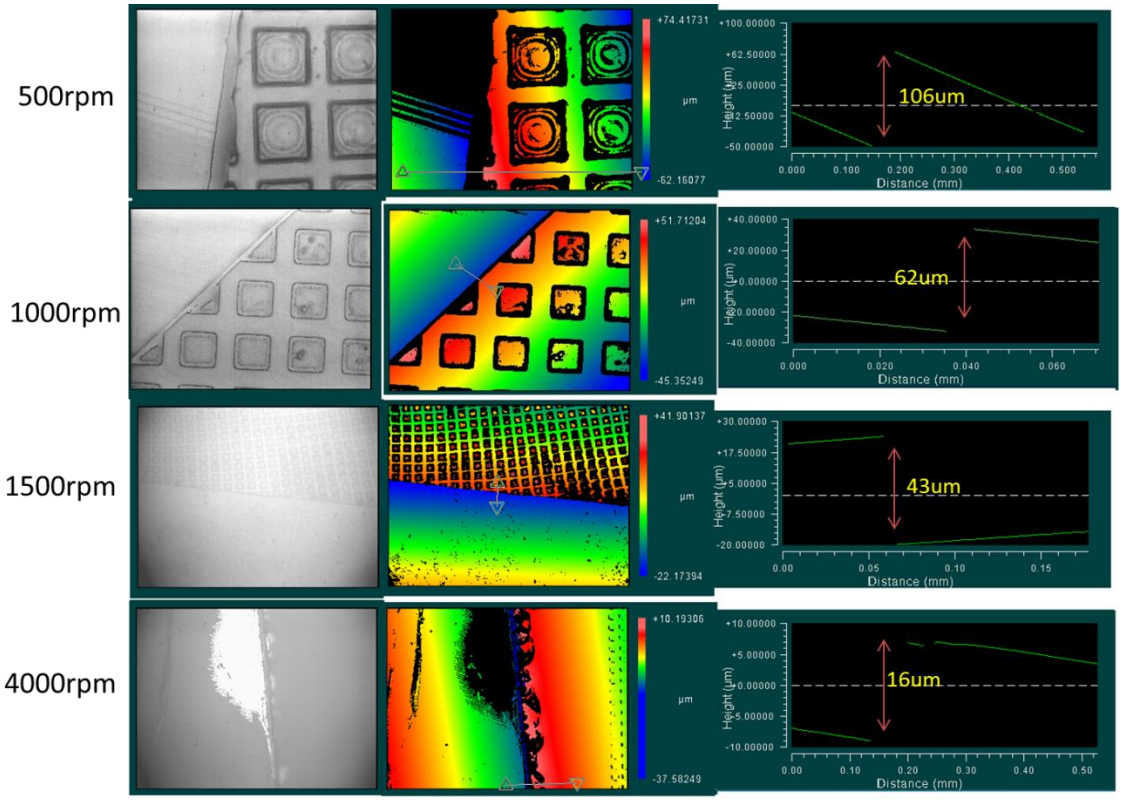

Figure 4.16: Developed PDMS film thickness measurements via optical profilometry

4.4.2 Polymer structures de-moulding results

De-moulding the polymeric films from the mould utilizing the proposed triple bath procedure, yielded excellent results with regards to the quality of the desired features.

Initially, a manual de-moulding by hand was explored which had only minimal success with the stiffer pristine PDMS layers (type 184). In this case, only relative thick (>100μm) PDMS films were successfully de-moulded in the presence of a DI water

bath, which however exhibited severe damage on the pillar geometry as can be seen in Fig.. 4.17. In addition, PDMS films containing pillars with the smallest features were completely destroyed during de-moulding.

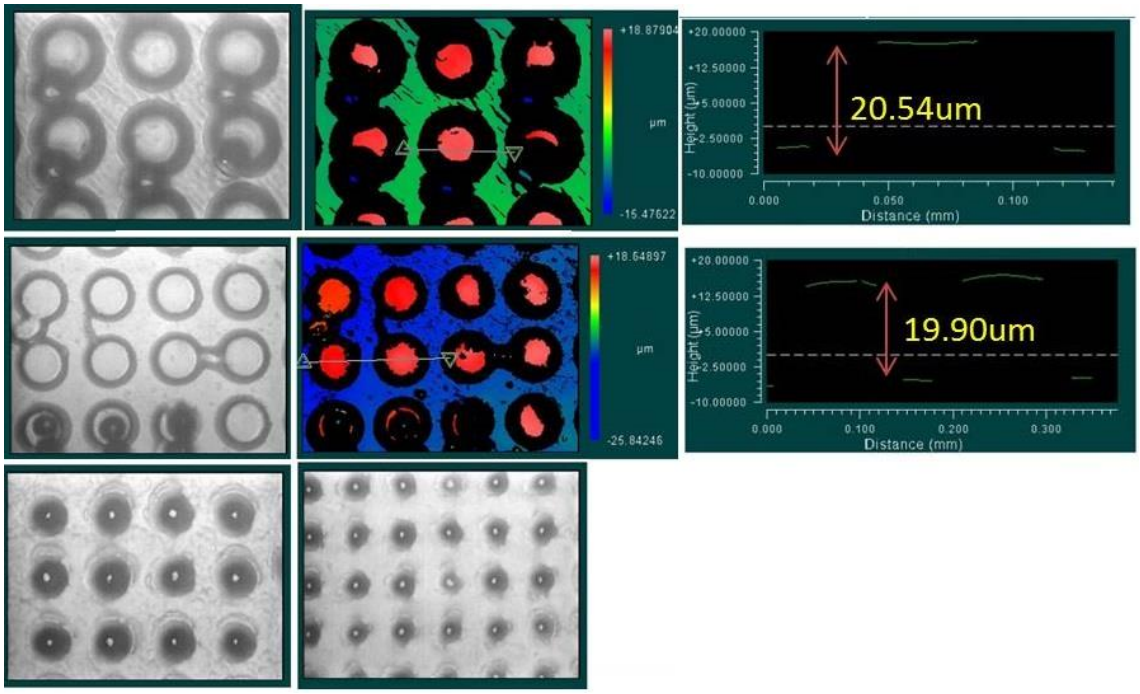

Figure 4.17: Manually de-moulded PDMS structures of a circular pillar-geometry

In contrast, by inserting the wafers containing the spin-coated polymeric films under the acetone bath the photoresist mould was instantly dissolved and allowed a damage-free de-moulding process.

The pillar-geometry was successfully recovered for all categories of moulds utilized, and their height was in agreement with the recess thickness, 19µm, of the photoresist layers (Fig. 4.18). A slight divergence of the pillar size, with regards to the photoresist mould, was the only significant difference observed. The de-moulded structures exhibited a decreased pillar length of approximately 10µm in all feature categories, which however was consistent over repeated trials and amongst different pillar-geometries.

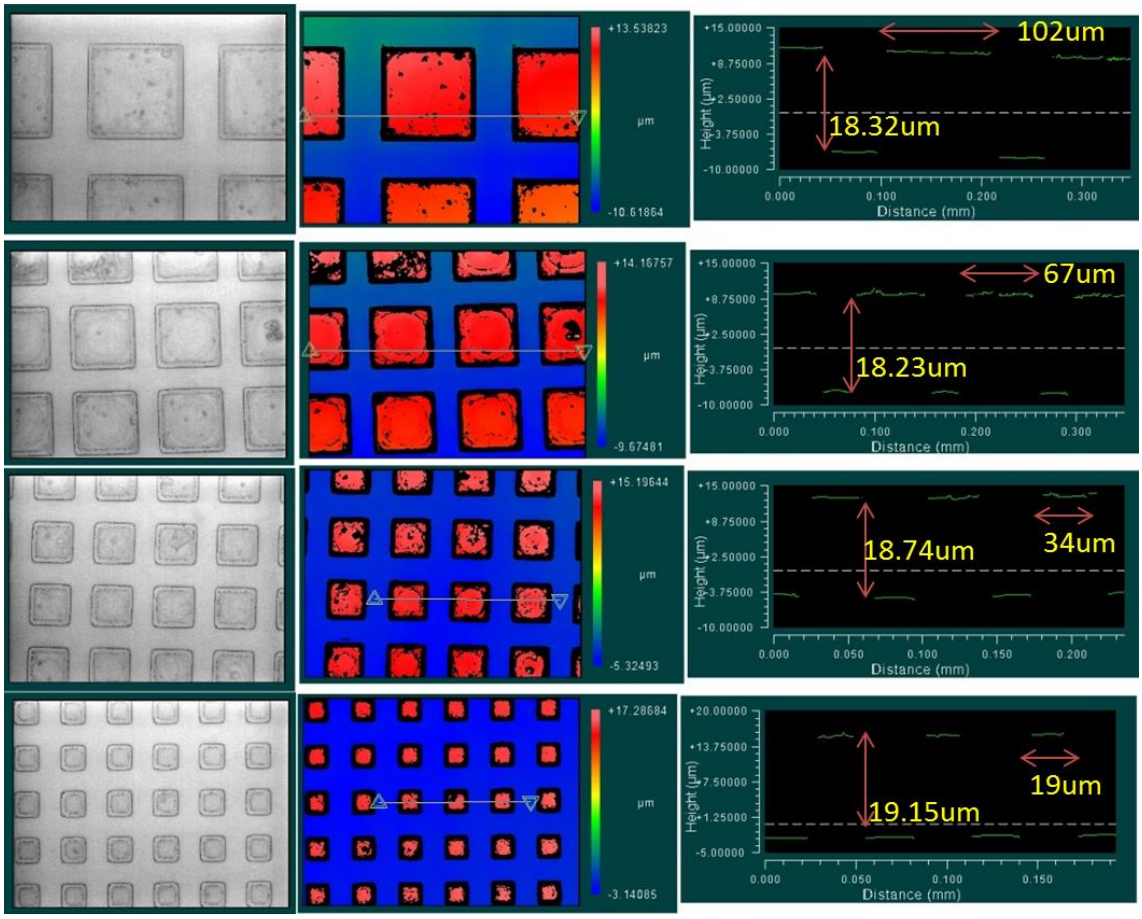

Figure 4.18: De-moulded structured PDMS films via the triple bath process. The pillar geometry of the films was successfully recovered without damage

Finally, in the case of the PDMS blend films, the developed pillars were also recovered successfully, without damage, utilizing the same de-moulding process (Fig. 4.19). Furthermore, the features of the structured composite polymeric films, for both blend types 5:1 and 10:1 respectively, exhibited identical feature sizes, in terms of pillars height and length, as the stiffer pristine PDMS structured films.

In all cases, a number of 5 samples per each polymer type and pillar size were developed and examined under the optical profilometer. Overall, excellent consistency over the pillar sizes was observed with only minor deviations in the range of 3µm for the length of the pillars and less than 1µm in pillar height, between the different sample batches and categories.

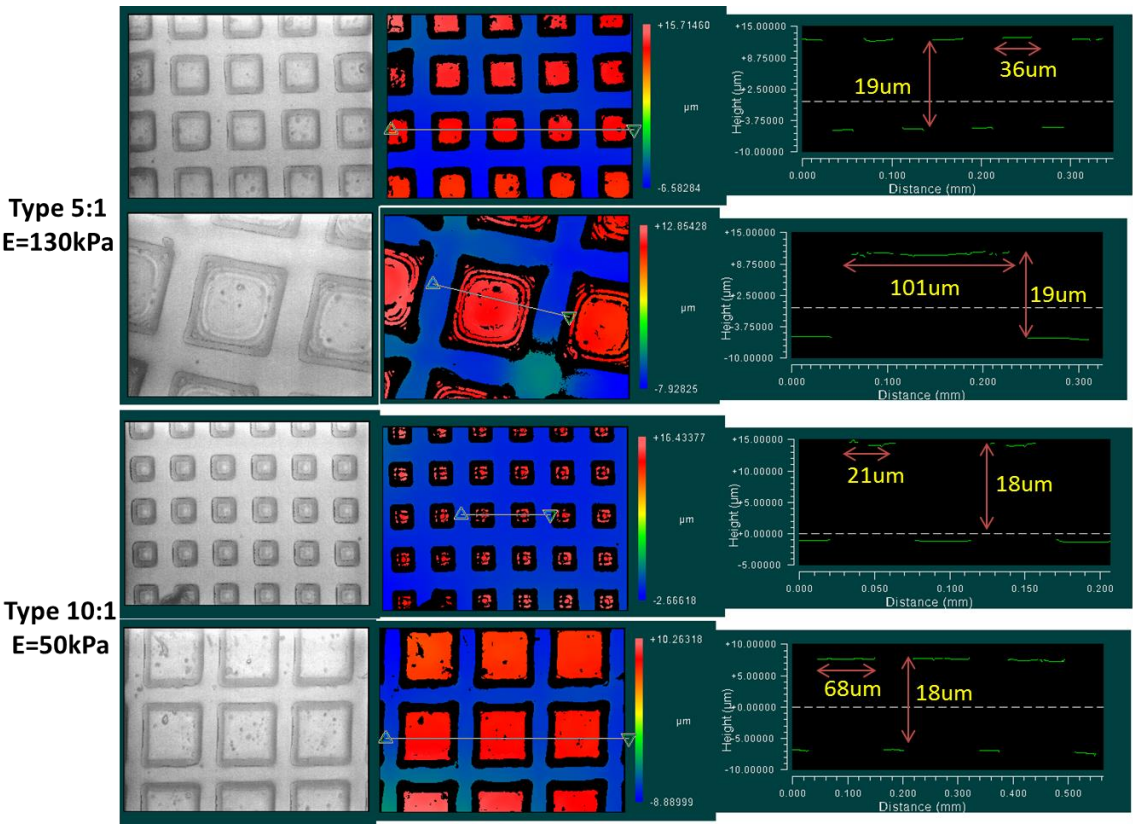

Figure 4.19: De-moulded structured PDMS blend films via the triple bath process. Similarly the structure was not damaged during de-moulding

4.4.3 Capacitance measurements as a function of applied pressure

4.4.3.1 Experimental setup

In order to evaluate the capacitive response of the proposed sensor, capacitance measurements were conducted under different pressure loadings. A 3 inch glass wafer was used as the bottom plate of the parallel-plate capacitor, of which the surface was coated with a thin (150nm in total) titanium/copper conductive, via the e-beam evaporator following the same procedure mentioned before. The conductive wafer provided a completely flat layer on which subsequently the developed copper-coated glass slides with the bonded polymer layer could sit on.

Prior to positioning the samples, thin copper wires were soldered on the conductive surfaces of both the wafer and sample, which served as the input and output bias of the sensor. The wires were connected to a Hewlett Packard 4192a impedance analyser, and the equipment was set on a capacitance measurement mode (minimum capacitance measurement capability 0.01pF) at 1MHz as, at this frequency, the equipment provided the most stable measurements. In addition, prior to measurement the equipment was

calibrated and an average sampling mode was selected (averaging over 10 values), as recommended by the equipment manual.

A set of precision weights were also employed, ranging from 1g to 100g, in order to exert pressures within the desired working range of compression hosiery (Fig. 4.21). By stacking the precision weights under different configurations pressure measurements in the range 0.5-7kPa were achieved.

Figure 4.20: The precision weight set that was utilised to exert the desired pressures

The samples were positioned on top of the copper-coated wafers and repeated capacitance measurements were conducted under different loadings. Both pristine PDMS Sylgard 184 and PDMS blends of Sylgard 184/Sylgard 527 (type 1:5 and type 1:10) samples were measured under this configuration (Fig. 4.21). In addition, samples were measured for each polymer and all type pillar geometries categories, as well as for unstructured flat structures.

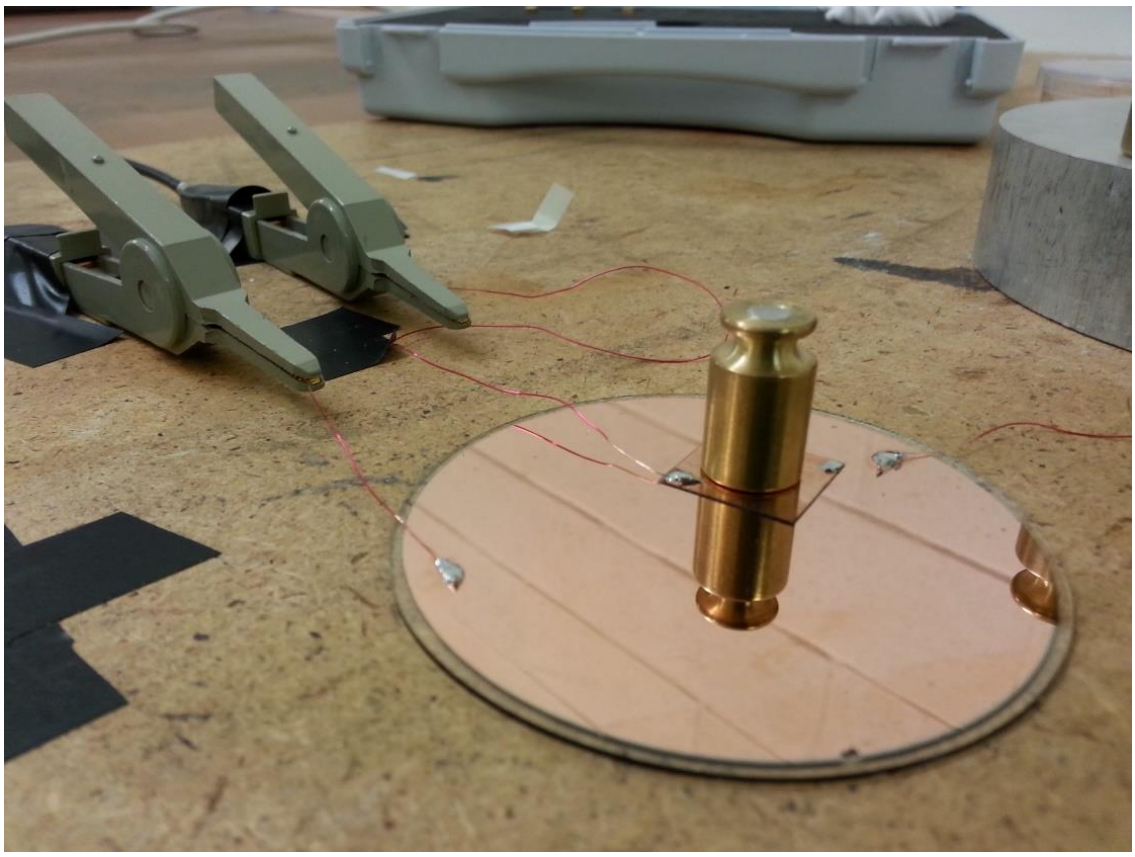

Figure 4.21: Experimental setup connected to the impedance analyser

Due to the viscoelastic nature of the polymer, prior to applying any additional weight the system was left to settle back for a short time to return to its initial state. In the case of pristine PDMS Sylgard 184 samples the required amount of time was found to be approximately 30 seconds, whilst in the case of the softer PDMS blend samples it was approximately 3 minutes. Moreover, to ensure that the samples would not lift due to the presence of the wires and disrupt the initial capacitance of the system, all measurements were taken under the presence of a load exerting an initial small pressure of approximately 0.5kPa that served as the effective initial capacitance of the system and from which all subsequent pressure/capacitance measurements would be conducted.

Finally, in order to conduct repeated measurements of loading and unloading over the same pressure range, a slightly different experimental apparatus was devised to maintain more stable measurements (Fig. 4.22). Moreover this design was developed so as to demonstrate a more compact and practical capacitive pressure sensor that could be potentially embeddable to compression hosiery. In this case, a polyimide film with copper coating was firmly attached on a pre-cleaned glass wafer, and the bottom conductive surface of the copper-coated glass slide/polymeric structured layer was bonded on top of it.

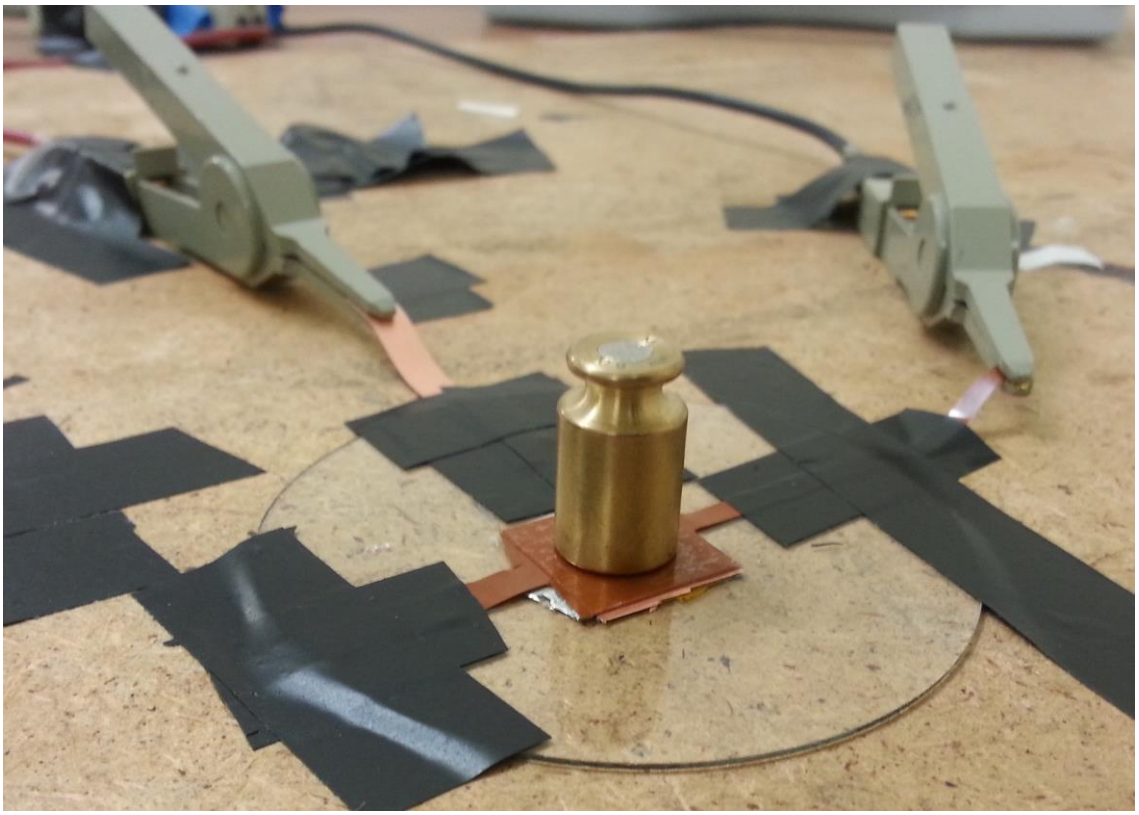

Figure 4.22: The second experimental setup, where polyimide coper-coated films were utilised

The bonding was achieved by doctor-spreading a thin film of conductive silver epoxy upon the copper surface of the polyimide film, where the sensor was firmly attached when the epoxy had solidified. Next a second polyimide film was bonded to a pre-cleaned plain glass slide of the same size as the sensor, to ensure a flat surface and a uniform distribution of the forces exerted, and was positioned on the sensor with its copper-coated surface facing the polymeric film of the sensor. The two parallel plates of the sensor were finally connected to the impedance analyser equipment by polyimide strips of the polyimide films protruding from the sensor that served as the wiring of the system. The sensors polyimide wiring was carefully fixed onto the glass wafer by duct tape, to ensure that both the sensor and its wiring were immobilized on the correct position, thus minimizing parasitic capacitance effects.

4.4.3.2 Sensors pressure sensitivity results

Initially, the capacitive response of the parallel-plate capacitor sensor was evaluated utilizing flat unstructured polymeric films as the deformable layer of the sensor (Fig. 4.23, Region A). As compressive loads were exerted onto the system, the polymeric film in between the two conductive layers would decrease in thickness leading to an

increase of the recorded capacitance. The utilized polymeric films were developed, as mentioned in previous sections, via spin coating at 4000 rpm with a resultant thickness of approximately 15μm.

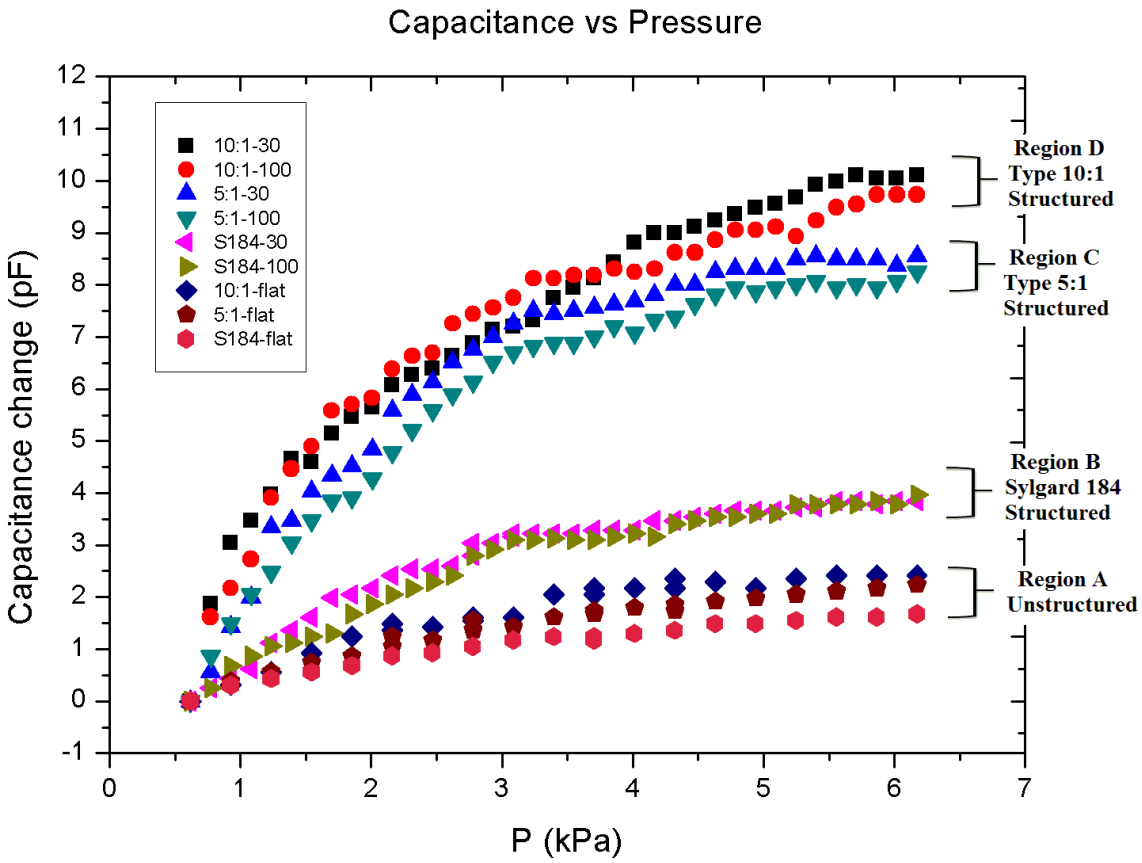

Figure 4.23: Capacitive response of the developed pressure sensors within the working range of compression hosiery. In Region A sensors with unstructured polymer films of pristine PDMS (S184-flat) and PDMS blends of both types (5:1-flat, 10:1-flat) are depicted; while in Regions B,C and D sensors with structured polymeric films of pristine PDMS (S184-30, S184-100) and PDMS blend type 5:1 (5:1-30, 5:1-100) and 10:1 (10:1-30, 10:1-100), respectively, are similarly depicted.

In the case of pristine PDMS Sylgard 184 polymeric films (reported Young modulus 1.7MPa) the change in the capacitive response recorded in the pressure range of 0-6kPa was minimal, with a change of capacitance between initial and stressed state was in the order approximately 1.5pF at the highest pressure applied of 6kPa (Fig. 4.23, Region A, S184-flat data).

A similar behaviour, although slightly improved, was also observed in the case of type 1:10 (reported Young's modulus 50kPa) and type 1:5 type (reported Young's modulus 130kPa) PDMS blends unstructured layers at the same pressure range, whereas the capacitance change for both blend type was in the order of approximately 2pF at pressures of 6kPa (Fig. 4.23, region A, 10:1-flat and 5:1-flat). In both cases, the response of the sensor appeared to be a linear function of pressure, and distinguishable

from noise capacitance change, was measured with a pressure resolution of approximately 1.5kPa.

A significantly enhanced capacitive response of the sensor was however observed when structured polymeric films were utilized as the deformable layer of the parallel-plate capacitor sensor. In this case, as discussed in section 4.2, micro-structuring the polymeric film with a pillar-geometry allows a larger deformation of the dielectric layer of the sensor as the exerted force is confined to a smaller area, leading therefore to an augmented pressure effect. In addition, employing polymeric films with lower Young modulus had an equally significant, if not more important, impact on the sensor sensitivity, as the lower Young modulus of the films allowed an even greater deformation of the structured dielectric layer within the same pressure range.

More specifically, in the case of pristine Sylgard 184 structured polymeric films (Fig. 4.23, Region B), an improved performance was observed as the maximum capacitance change increased to approximately 4pF, whereas the pressure resolution also increased to approximately 1kPa. While in the case of type 1:5 and type 1:10 PDMS blend films (Fig. 4.23, Regions C,D), the observed capacitive response of the sensor was even more pronounced, as the recorded capacitance change reached as high as 10pF with an improved pressure resolution of as low as 0.25kPa.

In both cases, the observed capacitive behaviour of the sensor was found to be non-linear, whereas the capacitance of the system would increase rapidly until the 3kPa pressure load and then increase on a slower rate until the maximum pressure range. Furthermore, a minor improvement of the sensor sensitivity was also observed between the type 1:5 PDMS composite and the type 1:10 PDMS composite, which became more obvious from pressures 4.5kPa and upwards (1:10 type exhibited an increased response of approximately 2pF).

In the case of pristine Sylgard 184 PDMS structured films no noticeable change was observed between samples with pillar features as small as 20μm and samples with pillar features as large as 100μm (Fig. 4.23, S184-30 vs S184-100). In the case of the PDMS blend structured films (for both type 1:5 and 1:10), only a slight increase in the sensor dynamic range, within the error margins, was recorded between samples with smallest pillar features and the largest pillar features (Fig. 4.23, 10:1-30 vs. 10:1-100 and 5:1-30 vs 5:1-100, respectively)

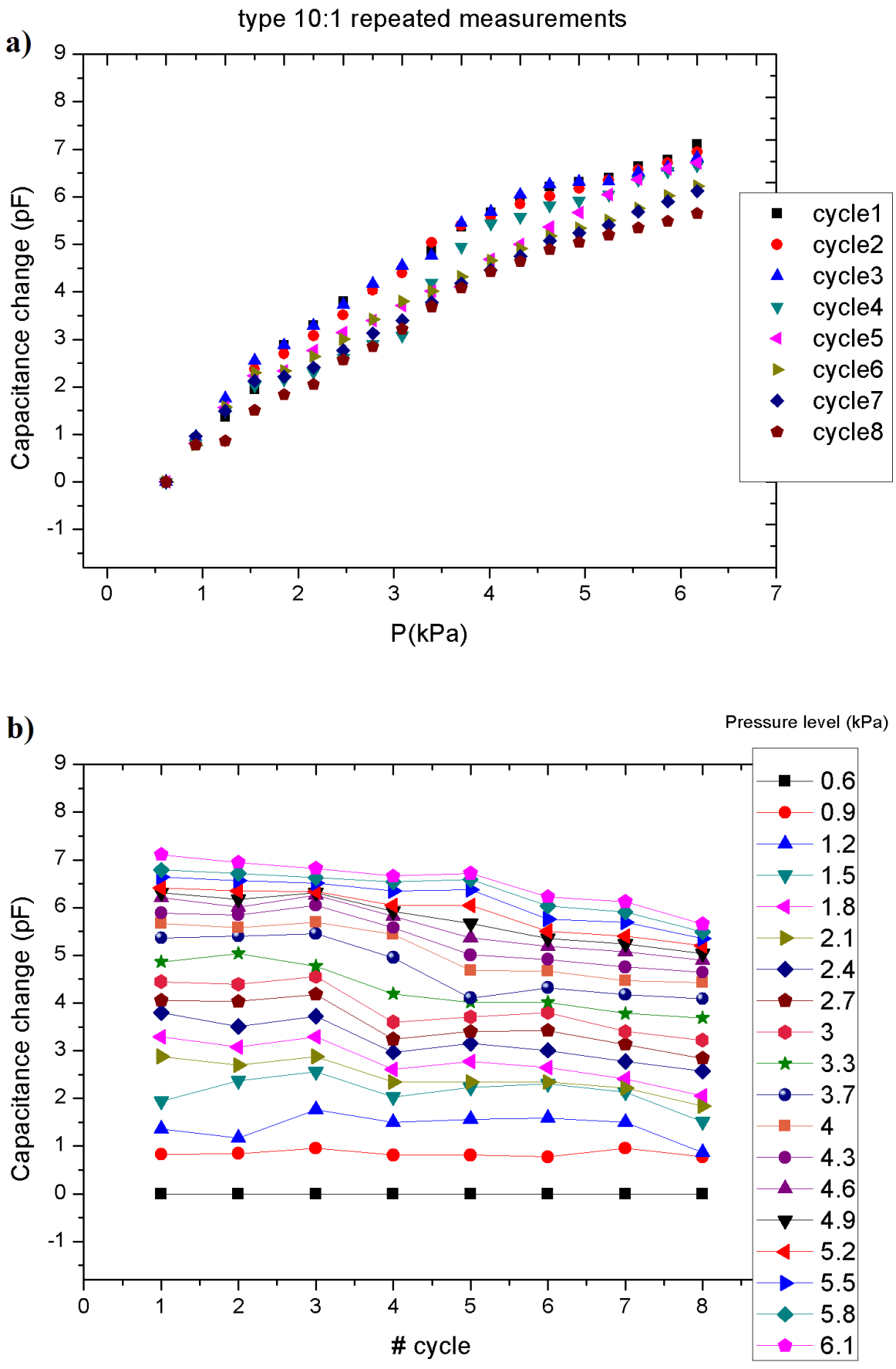

Figure 4.24: Capacitive response of a type 10:1 pressure sensor over repeated measurements: (a) in terms of pressure; (b) in terms of cycle.

The sensor exhibited also a relatively good responsive behaviour when measured repeatedly without presenting any substantial damage to its structure (Fig. 4.24). As mentioned in the previous section 4.3.3.1, a slightly different apparatus was used in this experiment, whereby the sensor was bonded atop copper-coated polyimide films (Fig. 4.22), as it was deemed more stable for repeated measurements and presented a more practical sensor configuration.

In this case, the sensor exhibited a similar capacitive response but with a smaller maximum capacitance change over the same pressure regime (by approximately 3pF). The observed effect could be attributed to the larger bottom electrode plate of the capacitor utilized in the first experimental setup, which may contribute favourably to the sensor performance.

Furthermore, the sensor exhibited a noticeable drop in its dynamic range, as it was measured repeatedly over the same pressure range, which could be attributed to a residual permanent deformation of the pillars caused by the extensive testing without allowing the polymer to fully recover between measurements. Indicative to the above, is a slight decrease of the pillars height (~1μm) after examination by profilometery.

The examination of other measured samples gave however no such permanent deformation of their respective pillars. Another factor that may be responsible for the observed effect may be the experimental apparatus itself.

The manual positioning and stacking of the weights involves involuntary movement that may disrupt and dislodge the sensor structure. Moreover, the permanent deformation observed may as well be solely the consequence of applying accidentally excessive loads to the sensor during the positioning stage. A way to minimize this effect could be achieved by employing a moveable stage and a force gauge to apply the desired loads to the sensor.

Finally, an effort was made to embed the aforementioned sensor configuration to compression hosiery but, due to the rigid and fragile nature of the glass substrates, the sensor structure instantly broke when the garment was attached on a curved surface. Therefore additional work must be conducted to improve the sensor conformity on curved surfaces. Possible solutions to tackle this issue are discussed in the next chapter.

Overall, the parallel-plate capacitor sensor was sensitive enough to distinguish low pressures, within the desired working of compression hosiery, with a relatively good

resolution, especially for the sensors with polymeric films made of the softer micro-structured PDMS blends.

Chapter 5:
Conclusions and future work

5.1 Summary and conclusions

The work in this thesis was focused in developing and evaluating cost-effective flexible pressure sensors, based on conductive and non-conductive polymeric elements, intended to be used and potentially embedded in compression hosiery as a monitoring system of the interface force between garment and skin.

Compressive hosiery and pressure garments were introduced in Chapter 1 and their significance was noted in treating a number of serious medical conditions such as chronic venous insufficiency, varicose veins, venous leg ulcers and hypertrophic scars. The working pressure range of these garments which lies on the low pressure regime of 0-6kPa, as well as the limitations of the current commercial technology employed to monitor their performance, were also discussed.

Stemming from the need of a cost-effective and flexible pressure sensor for this specific application, a number of polymer-based pressure sensors were designed, developed and evaluated to tackle this issue which involved: piezoresistive sensors utilizing MWCNT-PDMS or QTC conductive composites and parallel-plate capacitive sensors employing ultra-thin structured polymeric dielectric mediums with tuneable mechanical properties.

A thorough literature review, regarding both categories of flexible piezoresistive and capacitive pressure sensors, was presented in Chapter 2. The physics governing conduction in filler-polymer composites, such as percolation theory for the carbon-based composites and quantum tunnelling for the QTC composites, as well the working principle of parallel-plate capacitor sensors were discussed.

Materials, fabrication methods and techniques in developing flexible sensors either of a piezoresistive or capacitive nature were presented. This includes the advantages of employing CNTs fillers in carbon-based composites, the superiority of PDMS over other polymers both as the matrix constituent in composites and as a structural material in capacitive sensing, CNT dispersion techniques and others. Moreover, recent research developments on this field and representative examples of flexible piezoresistive and capacitive sensors for both strain and pressure sensing applications were also presented

and compared against their typical MEMS counterparts, with an emphasis on the former's intrinsic strengths.

In Chapter 3, a pressure sensor design was presented that employed a conductive polymeric composite as the sensing element, encapsulated in between a structured and an unstructured configuration of aluminium electrodes. Structuring one of the electrodes, was achieved via a micromilling machine, and provided an augmented pressure effect. Here, two types of conductive composites within the same sensor design were tested and evaluated: a multi-walled carbon nanotubes(MWCNTs)-PDMS composite and a QTC composite.

In the first case, the development of the composite involved a multi-step procedure, which included successive direct sonications and shear mixing, via the use of an organic solvent, in order to disperse the MWCNT filler constituent into the viscous PDMS matrix. The developed composite exhibited the typical step-like conductive behaviour, in agreement with the percolation theory, which attributes the resultant composite conduction in the formation of a percolating network of filler particles in direct contact that spans the material. When the composite was subjected to compression it exhibited a positive piezoresistive effect as expected. The composite exhibited only a minimal response increase of only 50% in resistance change in the pressure range of 0.2-1.2 MPa when a flat electrode layer was used, with a resolution of approximately 200kPa. By utilizing a structured electrode layer the composite response increased to 2.5 orders of magnitude in resistance change over the same pressure range, with a distinguishable pressure resolution as low as 50kPa.

In the second case, a QTC commercial product was utilized that is exclusively developed and distributed by Peratech Inc. The latter composite when subjected to compressive deformation exhibited a large exponential resistance drop in accordance to the quantum tunnelling effect that governs the interaction of its spiky nickel filler particles. QTC pressure sensors exhibited an improved pressure sensitivity under a flat electrode, dropping in resistance by over 6 orders of magnitude over the pressure range of 0.2MPa to 1.2MPa with a pressure resolution of approximately 50 kPa. Similarly a significant improvement in the dynamic range of the sensor was observed when a structured electrode was utilized instead, whereas the same drop in resistance was recorded in a much narrower pressure regime (50-150kPa) with a pressure resolution as low as 10kPa.

Finally, in Chapter 4, a parallel-plate capacitive sensor was presented which employed an ultrathin and structured PDMS blend film as the sensing element, bonded in between two flat conductive and rigid layers. This pressure sensor design was devised as the aforementioned developed piezoresistive sensors failed to detect pressure changes within the working range of compression hosiery.

The development of the sensor involved the use of a patterned sacrificial photoresist mould on which a polymeric film was spin coated and then bonded, via corona discharge, with a copper-coated substrate that served as one of the capacitor plates. De-moulding the polymeric structures undamaged was achieved via a triple bath procedure that effortlessly dissolved the underlying photoresist mould. The polymer was patterned with micropillars to allow a larger deformation of the polymeric film under compressive loads and the total thickness of the film (base layer and pillars) was approximately 33um.

To further increase the deformation of the polymer under compression, and thus the dynamic range of the sensor, a PDMS blend composed of Sylgard 184 and Sylgard 527 was also explored, which exhibits a tuneable Young's modulus from 1.7MPa down to 50kPa. The influences of the Young's modulus of the polymeric dielectric medium and of microstructuring the dielectric medium were characterised. The combination of scaling down the thickness of the polymeric film, structuring its surface and employing a PDMS blend with a much lower Young's modulus resulted into a parallel-plate capacitive sensor with a pressure sensitivity within the working range of compression hosiery (0-6kPa) that exhibited a distinguishable pressure resolution of as low as 0.25kPa.

However additional work is required to make the capacitive sensor flexible, reliable and able to conform to curved surfaces, as well as being embeddable into the garments fabric. Solutions for the above issues are discussed in the next section, as well as strategies on how the pressure sensitivity of the developed piezoresistive sensors could be potentially improved.

5.2 Future work

5.2.1 Improving the sensitivity of MWCNT-PMDS and QTC sensors and an alternative sensor design

Although the developed MWCNT-PDMS composite displays a quantifiable resistance change over compression, its pressure range and sensitivity were not adequate for the working regime of compression hosiery.

A way to potentially increase the composite intrinsic sensitivity could be achieved by employing the PDMS blend of Sylgard 184/Sylgard 527, as the composite polymeric matrix as explained in Chapter 4. This would allow a larger deformation of the composite under smaller pressures and thus an increased piezoresitive effect due to the larger bending of the CNT bundles. Moreover, an additional advantage of utilizing this PDMS blend is its lower viscosity that could deem unnecessary the insertion of an organic solvent during the preparation of the composite, leading thereby to a simpler fabrication protocol, with more consistent results, and possibly a larger resistivity drop beyond the percolation threshold.

Alternatively, the required dynamic range could be potentially achieved if the composite was employed in a different sensor design which would take advantage the tensile stain-resistance dependence of the material instead.

The proposed sensor is depicted in Fig 5.1, and involves the use of a flexible and thin polymeric membrane on top of which a conductive strip of MWCNT-PDMS composite could be casted and patterned. In this case the deflection of the membrane under pressure would subject the MWCNT-PDMS strip to tensile strains, thus leading to a resistance increase of the composite due to the increase of the average spacing of the percolating network, as described in Chapter 2. The sensitivity of the sensor could be further explored by manipulating the amount of deflection of the membrane via employing softer, thinner or larger in size polymer films, or by controlling the amount of strain experienced by the composite via patterning it with different structures.

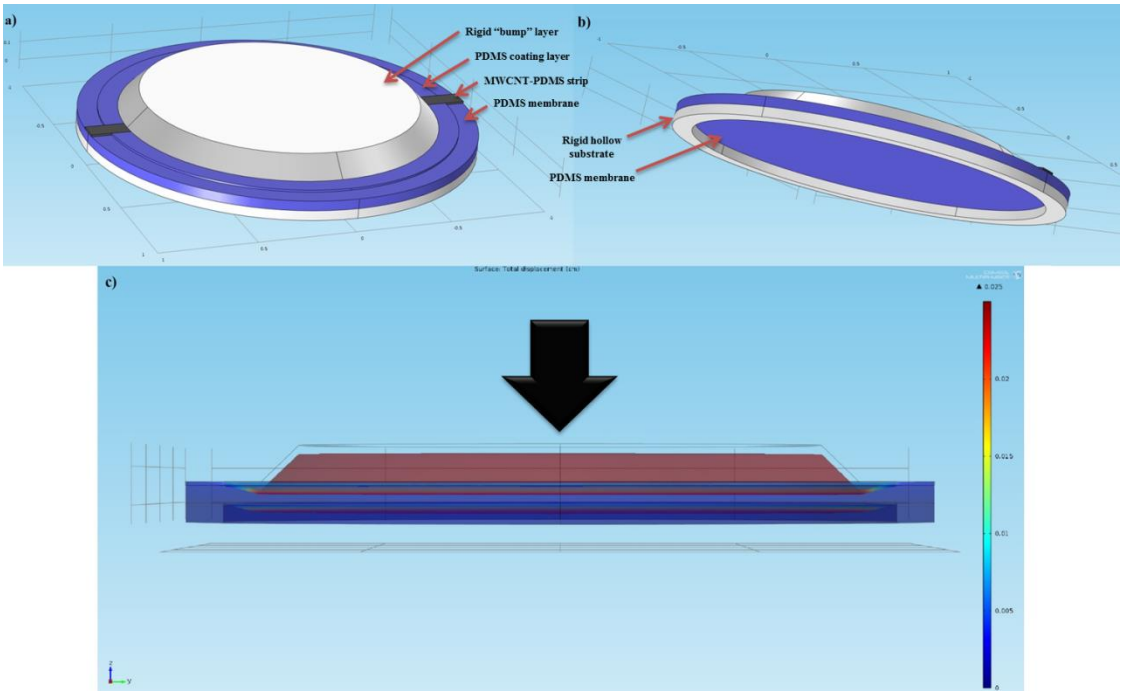

Figure 5.1: (a),(b) A proposed alternative pressure sensor design composed of a rigid "bump" layer that transfers the applied loads to the deflectable membrane, a PDMS-coated MWCNT-PDMS composite strip that spans the surface of the sensor, the PDMS membrane layer and a rigid hollow substrate. (c) Simulation of membrane deflection under 10kPa pressure via COMSOL Multiphysics software. As the PDMS membrane layer deflects, the MWCNT-PDMS strip is subjected to tensile strain

In the case of QTC composites, Peratech Inc. recently started to develop a different custom-made QTC composite ink product [177], with an improved electrical behaviour under deformation, suitable for screen printing. This QTC material contains two types of particles that are uniformly dispersed in a polymeric ink: acicular TiO_2 needles, with a conductive SbO coating, and spherical insulating TiO_2 nanoparticles. Under this configuration, the TiO_2 nanoparticles prevent the conductive acicular TiO_2 needles, which are randomly oriented, of aligning and aggregating, while the compressibility of the material is attributed to the voids existing within particles. Likewise, the material is insulating under normal conditions but displays an exponential rise in conductivity when deformed due to quantum tunneling amongst neighboring TiO_2 needles.

The conductivity under stress of this material could be also explored utilizing the developed sensor design presented in Chapter 3 in the working range of compression hosiery. In addition, the ability of screen printing the material makes it also a good candidate for the proposed sensor design described in the previous paragraph, where the composite conductivity under strain could be similarly exploited.

5.2.2 Improving the conformability of the capacitive pressure sensors and potential for embedding it in compression hosiery

The parallel-plate capacitive pressure sensor developed in this work exhibits a pressure sensitivity within the working regime of compression hosiery, as shown in Chapter 4. However, the rigid nature of the copper-coated glass slides employed as the capacitor plates prevents the sensor in being conformable for curved surfaces; a prerequisite for the application in monitoring the interface force between garment and skin. As a short-term solution to improve the sensor conformity, a direct bonding and fabrication process utilizing a flexible conductive substrate could be explored (Fig. 5.2).

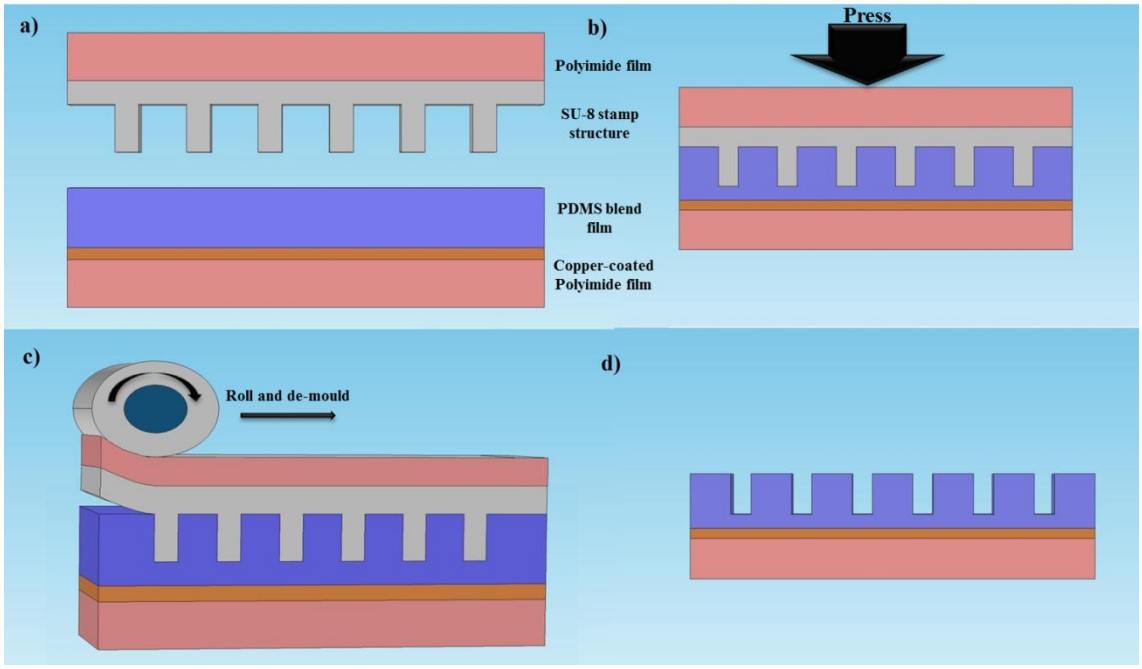

Figure 5.2: Illustration depicting proposed fabrication process of a conformable sensor: a) PDMS blend is spin coated atop a copper-coated flexible polyimide film and development of SU-8 master stamp on polyimide film; b) the stamp is pressed unto the PDMS layer and the system is placed on a hot plate to cross-link the elastomer; c) peeling off the stamp with the help of a roller in a DI water bath; d) resultant structure after de-moulding

This could be accomplished by spin-coating the PDMS blend directly to a flexible copper-coated polyimide film. Patterning the polymeric film could be achieved by utilizing a master stamp that would greatly simplify the process and allow rapid prototyping. As the master stamp, a SU-8 photoresist patterned on top of a polyimide film, with the reverse image of the desired pillar-structure, could be developed that would be pressed on the spin-coated PDMS blend film prior to cross-linking the polymer.

The stamp could then be peeled off from the cured polymer producing as consequence an easier pattering process of the polymeric film, while allowing at the same time a

cost-effective fabrication protocol as the stamp could be reused. To enable a damage-free de-moulding, a thin layer of PVA (poly-vinyl alcohol) could be spin-coated onto the SU-8 which is dissolvable in water [178], and the peel-off process could be conducted in a DI water bath. Finalising the sensor could be accomplished by bonding onto the structured polymer surface, via corona discharge, another flexible copper-coated polyimide film that would serve as the second electrode plate of the capacitor.

A longer term solution in providing a more flexible and conformable sensor, could involve the use of the developed conductive MWCNT-PDMS composite as the electrode plates of the capacitor instead, employing a similar fabrication protocol as mentioned above. Designing the capacitive sensor with flexible CNT-based electrode plates could potentially broaden its sensing capabilities as it would allow in addition a sensitivity under tensile strains besides compressive loads, thus opening the door to other potential applications beyond the scope of medical garments usage alone.

Finally, in order to evaluate the performance of the proposed sensor configuration in compression hosiery, the sensor could be bonded onto the surface of a small pre-cut compression garment strip and electrically connected via conductive threads traversing the fabric as described in Chapter 3 (Fig. 3.3). Initial testing and calibration of the sensor could then be conducted by attaching the garment on a cylindrical object and employing a bladder testing equipment to exert the required forces within the working range of compression hosiery. The next phase of testing should involve the use of a matrix of multiple sensors attached in fixed locations on a compression hosiery (corresponding in the ankle, calf, thigh etc.), which would be applied on a dummy leg to monitor the garment performance and the sensor reliability.

5.2.3 Proposed design of a stand-alone garment-sensor system for low pressure monitoring applications

A more advantageous way of implementing the pressure sensors could be accomplished by designing a stand-alone garment-sensor system, as depicted in Fig 5.3, which could potentially expand the usage of the developed sensors.

In this proposed design concept, instead of attaching the pressure sensors directly onto the compression hosiery or pressure garment, a custom-made garment strip of a flexible

nature (i.e. spandex) could be utilized (the size of a small bandage), which would contain a fixed number of sensors and conductive threads.

By utilizing the depicted configuration of conductive threads two goals are accomplished: each sensor is electrically accessible, while the snake-wise fashion of the conductive threads allows the flexible fabric to stretch unaltered. Moreover this stand-alone garment-sensor system is intended to be the unit cell of a potentially larger system, which would combine a number of these unit cells and produce a matrix of pressure sensors each uniquely accessible. For this cause, a set of metallic clippers could be utilised to encompass the fabric, connect with the individual conductive threads and attach additional unit cells, if desired, to elongate the size of the measuring system.

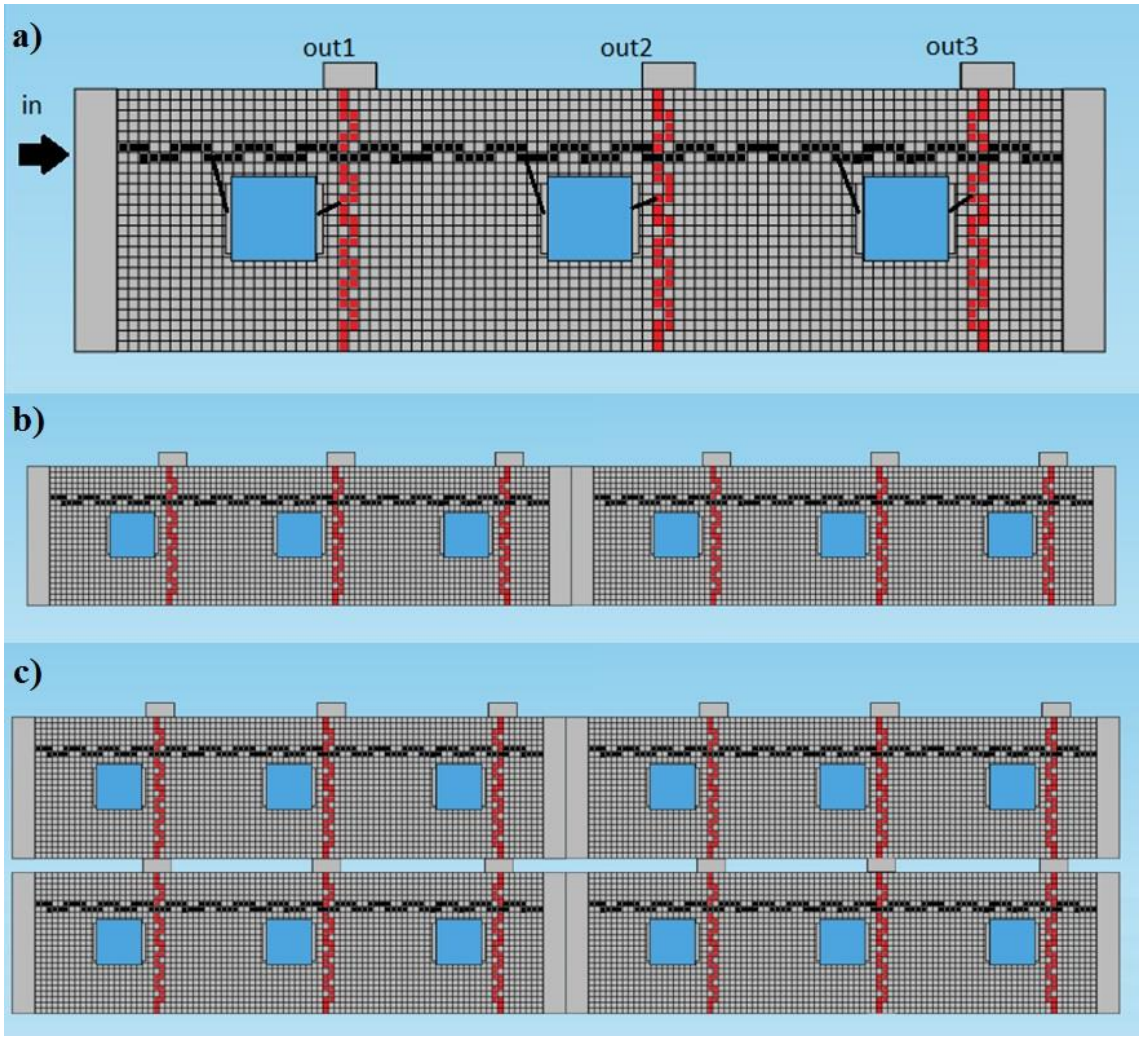

Figure 5.3: Proposed design of (a) stand-alone garment-sensor system as a unit cell and (b),(c) in interconnected multi-cell configurations

In conclusion, under this configuration the size of the pressure monitoring system could be expanded indefinitely, from a single unit cell the size of a small bandage to as large as a vest that could be worn around the body.

Thus, due to the customable size of the sensor system, the potential field of applications of the developed technology would not be limited to compression hosiery alone but could be expanded to other applications such as movement and respiratory monitoring in dynamic conditions, performance evaluation of pressure garments for hypertrophic burn scars on various inaccessible parts of the human body such as shoulder, face and pelvis, to as far as monitoring the radial artery pressure wave around the wrist; applications for which at the moment, to the best of the author's knowledge, no such cost-effective wearable pressure monitoring technology exists.

References

1. *Compression treatment after burns.* Wienert, V. 2003, Textiles and the skin, Vol. 31, pp. 108-113.

2. [Online] www.healthadvancemd.com/eshop/10Expand.asp?ProductCode=8563.

3.[Online] http://www.sgh.com.sg/about-us/newsroom/singapore-health/ Documents/ ONMar Apr09_combined.pdf .

4. *Pressure garments for use in the treatment of hypertrophic scars--a review of the problems associated with their use.* Macintyre L., Baird M. 1, 2006, Burns., Vol. 32, pp. 10-5.

5. *Conservative treatment using compression suits for.* Kloti J, Pochon J. 1982, Burns, Vol. 8, pp. 180–7.

6. *The use of pressure garments on hypertrophic scars.* G., Puzey. 1, 2002, J Tissue Viability, Vol. 12, pp. 11-5.

7. *Use of pressure to treat hypertrophic burn.* Staley MJ, Richard RL. 3, 1997, Adv Wound Care, Vol. 10, pp. 44-6.

8. *Hypertrophic scarring and pressure therapy.* Reid WH, Evans JH, Naismith RS, Tully AE, Sherwin S. S, 1987, Burns, Vol. 13, pp. 29-32.

9. *Pressure therapy for the control of hypertrophic scar formation.* R, Ward. 1991, J Burn Care Rehabil, Vol. 12, pp. 257–62.

10. *Alteration of hypertrophic scars induced by mechanical pressure.* Kischer W, Shetlar M, Shetlar C. 1975, Arch Dermatol, Vol. 111, pp. 60–4.

11. *Effect of different pressure magnitudes on hypertrophic scarin a Chinese population.* Lai Hoi Yan Candy, Li-Tsang Wai Ping Cecilia, Zheng Yong Ping. 8, 2010, Burns, Vol. 36, pp. 1234-41.

12. *British Standard Specification for Graduated compression hosiery.* 6612, British Standards Institute. BS. 1985, pp. 1-10.

13. Conditions, National Clinical Guideline Centre – Acute and Chronic. Venous thromboembolism: reducing the risk of venous thromboembolism (deep vein thrombosis and pulmonary embolism) in patients admitted to hospital. 2010., pp. 45-62 and 44-68.

14. *Medical Elastic Compression Stockings in the Treatment of Venous Insufficiency.* Van Geest, A.J., Franken, Neumann, H.A.M. 2003, Textiles and the skin, pp. 98-107.

15. *Hepatitis C viral dynamics in vivo and the antiviral efficacy of interferon-alpha therapy.* Nuemann AU, Lam NP, Dahari H, Gretch DR, Wiley TE, Layden TJ, Perelson AS. 1998, Science, Vol. 282, pp. 103-7.

16. *Medical compression products: new customers thanks.* Oess, O. 2004, Textile Network, Vol. 4, pp. 62- 65.

17. *Calibration problems encountered while monitoring stump/socket interface pressureswith force sensing resistors: techniques adopted to minimise inaccuracies.* Buis AWP, Convery P. 1997, Prosthet Orthot Int, Vol. 21, pp. 179–82.

18. *Design of pressure garments for hypertrophic scar treatment.* F, Ng. 1995, PhD thesis, De Montfort University.

19. JG, Webster. *Prevention of pressure sores.* s.l. : Bristol: Adam Hilger. pp. 109–41 and 155–74.

20. [Online] http://www.heelift.com/anti-embolism-hosiery.html.

21. *The law of Laplace and its relevance to contemporary medicine and rehabilitation.* JR, Basford. 2002, Arch Phys Med Rehabil, Vol. 83, pp. 1165-1170.

22. *Interface pressure measurements in leg ulcer management.* A., Finnie. 6 Suppl. 23/3–12/4, 2000, Br J Nursing, Vol. 9, pp. 8–10,12,14.

23. *Graduated static ans external compression of the lower limb: a physiological assessment.* Lawrence, D Kakkar, V V. 1980, British Journal of Surgery, Vol. 67, pp. 119-121.

24. *Acceleration of linear flow in the deep veins of the lower extremity of man by local compression".* J R fries. E D, Wilkins. 1949, Journal of Clinical Investigation, Vol. 28, pp. 552-558.

25. *Elastic stockins in the prevention of pulmonary embolism: a preliminary report.* Wilkins, R W Mixxter, G Stanton et al. 1952, New England Journal of Medicine, Vol. 246, pp. 360-364.

26. *The efficiency of graduated compression stockins in the prevention of deep vein thrombosis.* Scurr, J H Ibrahim, S Z Faber, R G et al. 1977, British Journal of Surgery, Vol. 64, pp. 371-373.

27. *Pulmonary embolism: what have we learned since Virchow?* Dalen, J E. 2002, Chest, Vol. 122, pp. 1801-1817.

28. *Graduated compression stockings in the prevention of postoperative venous thromboembolism.* P S Lensing, A W Hirsh, J. 1994, Archives of Internal Medicine, Vol. 154, pp. 67-72.

29. *The effects of graduated compression stocking on cutaneous surface pressure along the path of main superficial veins of lower limbs.* R Liu, Y L Kwok, Y Li, TT Lao, X Zhang. 2006, Wounds, Vol. 18, pp. 150-157.

30. *Prevention of recurrence of venous ulceration: randomized controlled trial of class 2 and class 3 elastic compression.* Nelson, E. A., Harper, D. R., Prescott, R. J., Gibson, B., Brown, D., & Ruckley, C. V. 2006, Journal of Vascular Surgery, Vol. 44, pp. 803-808.

31. *New calibration method for I-scan sensors to enable the precise measurement of pressures delivered by 'pressure garments.* L, Macintyre. 7, 2011, Burns, Vol. 37, pp. 1174-81.

32. *Measurement of interface pressure applied by medical compression garments.* J A Khaburi, A A Dehgani-Sanji, E A Nelson and J Hutchinson. 2011, 2011 International Conference on Mechatronics and Automation (ICMA), pp. 289 - 294.

33. *The use of PicoPress transducer to measure sub-bandage pressure.* J. Al Khaburi, A.A. Dehghani-Sanij, E.A. Nelson and J. Hutchinson,. 2011, International Conference on Biomedical Engineering Systems and Technologies.

34. [Online] [http://www.medigroup.com.au/picopress.

35. [Online] [http://www.tekscan.com/products/industrial/pressure-distribution-measurement-system.

36. *Validation of the Pliance X System in measuring interface pressure generated by pressure garment.* Lai CH, Li-Tsang CW. 6, 2009, Burns, Vol. 35, pp. 845-51.

37. *Design criteria for the measurement of pressure at body surface interfaces.* MW, Ferguson-Pell. 1980, Eng Med, Vol. 9, pp. 209–14.

38. *Review of interface pressure measurement to establish a protocol for their use in the assessment of patient support surfaces.* Wolsley CJ, Hill PD. 2000, J Tissue Viability, Vol. 10, pp. 53–7.

39. *Ian S. The measurement of interface pressure.* Bader D, Bouten C, Colin D, Oomens C. 2005, Pressure ulcer research: current and future perspectives, pp. 51–71.

40. *Piezoresistance effect of silicon.* Kanda, Y. 2, 1991, Sensors and Actuators A: Physical, Vol. 28, pp. 83–91.

41. *Advanced CMOS-based Stress Sensing.* Bartholomeyczik, J. 2006, PhD thesis, University of Freiburg.

42. *Semiconductor strain transducers.* Geyling, F.T. and Forst, JJ. 1960, Bell System Technical Journal, Vol. 39, pp. 705-731.

43. *An integrated MEMS three-dimensional tactile sensor with large force range.* T. Mei, W. J. Li, Y. Ge, Y. Chen, L. Ni, and M. H. Chan. 2000, Sens. Actuators A, Vol. 80, pp. 155–162.

44. *Silicon smart tactile image sensor with pneumatically swollen single diaphragm structure.* H. Takao, K. Sawada, and M. Ishida. 2004, 17th IEEE Int. Conf. Micro Electro Mech. Syst., pp. 846–849.

45. Morris, S. A. *Measurement and Instrumentation Principles.* s.l. : Jordan Hill, GBR: Butterworth-Heinemann, 2001.

46. *Resistivity of a composite conducting polymer as a function of temperature, pressure, and environment: Applications as a pressure and gas concentration transducer.* Lundberg, B. and Sundqvist, B. 3, 1986, J. Appl. Phys, Vol. 60, p. 1074.

47. *Piezoresistivity of heterogeneous solids.* Carmona, F., Canet, R. and Delhaes, P. 7, 1986, J. Appl. Phys., Vol. 61, p. 2550.

48. Callister, W. D. *Material Science and Engineering: An Introduction, 5th ed.* s.l. : John Wiley & Sons Inc, 1999.

49. *Composites in context.* Kelly. s.l. : A. Compos. Sci. Tech., 1985, A. Compos. Sci. Tech., Vol. 23, p. 171.

50. *Criteria for selecting the components of composites.* Ashby, M. F. 1993, Acta Met. Mater., Vol. 41, p. 1313.

51. *Microcontact printing for patterning carbon nanotube/polymer composite films with electrical conductivity.* Ogihara H, Kibayashi H, Saji T. 9, 2012 , ACS Appl Mater Interfaces, Vol. 26;4, pp. 4891-7.

52. Bhattacharya, S.N., Gupta, R.K., and Kamal, M.R. *Polymeric Nanocomposites: Theory and Practice.* s.l. : Hanser, 2008.

53. *Preparation and characterization of polyurethane/multiwalled carbon nanotube composites.* Guo, S., Zhang, C., Wang, W., Liu, T., Tjiu, W.C., He, C., and Zhang, W.-D. 8, 2008, Polymers & polymer composites , Vol. 16 , pp. 501-507.

54. *Very low conductivity threshold in bulk isotropic single-walled carbon nanotube-epoxy composites.* Bryning, M.B., Islam, M.F., Kikkawa, J.M., and Yodh, A.G. 9, 2005, Advanced Materials, Vol. 17, pp. 1186-1191.

55. Margolis, J. M. *Conductive polymers and plastics.* s.l. : Chapman and Hall, 1989.

56. *Carbon based conductive polymer composites.* Zhang, W., Dehghani-Sanij, A.A., and Blackburn, R.S. 10, 2007, Journal of Materials Science, Vol. 42, pp. 3408-3418.

57. *Carbon black filled conducting polymers and polymer blends.* Huang, J.-C. 4, 2002, Advances in Polymer Technology, Vol. 21, pp. 299-313.

58. *Electrical and mechanical properties of carbon-black-filled, electrospun nanocomposite fiber webs.* . Hwang, J., Muth, J., and Ghosh, T. 4, 2007, Journal of Applied Polymer Science, Vol. 104, pp. 2410-2417.

59. *Electron transport processes in conductor-filled polymers.* Sherman, R.D., L.M. Middleman, and S.M. Jacobs. 1, 1983, Polymer Engineering and Science, Vol. 23, pp. 36-46.

60. *Nanoparticle-doped elecrically-conducting polymers for flexible nano-micro systems.* A, Khosla. 2012, The Electrochemichal Society Interface.

61. *Percolation processes.* Broadbent, S.R. and J.M. Hammersley. 1957, Proceedings of the Cambridge Philsophical Society, Vol. 53, pp. 629-641.

62. *Exploring the universal nature of electrical percolation exponents by genetic algorithm fitting with general effective medium theory.* Youngs, I.J. 2002, Journal of Physics D: Applied Physics, Vol. 35, pp. 3127-3137.

63. *Vapour sensing applications and electrical conduction mechanisms of a novel metal-polymer composite* . PJW Hands,. 2003, PhD thesis, Durham University.

64. *Percolation and conduction.* . Kirkpatrick, S. 4, 1973, Reviews of modern physics, Vol. 45, pp. 574-588.

65. *Physical properties of thermoplastic/graphite composites.* Krupa, I. and I. Chodak. 2001, European Polymer Journal, Vol. 37, pp. 2159-2168.

66. *An equation for the conductivity of binary mixtures with anisotropic grain structures.* McLachlan, D.S. 1987, Journal of Physics C: Solid State Physics, Vol. 20, pp. 865-877.

67. *Analytical functions for the AC and DC conductivity of conductor-insulator composites.* McLachlan, D.S. 2, 2000, Journal of Electroceramics, Vol. 5, pp. 93-110.

68. *Measurement and analysis of a model dual-conductivity medium using a generalised effective-medium theory.* McLachlan, D.S. 1988, Journal of Physics C: Solid State Physics, Vol. 21, pp. 1521-1532.

69. *A wireless implantable passive strain sensor system.* F. Umbrecht, M. Wendlandt, D. Juncker, C. Hierold, and J. Neuenschwander. 2005, Proceedings of the 2005 IEEE Sensors Conference, pp. 20–23.

70. *A Carbon Nanotube Strain Sensor for Structural Health Monitoring.* I. Kang, M. J. Schulz, J. H. Kim, V. Shanov, and D. Shi. 3, 2006, Smart Mater. Struct., Vol. 15, pp. 737–748.

71. *Multi-walled Carbon Nanotubes/Poly(L-lactide) Nanocomposite Strain Sensor for Biomechanical Implants.* Y. Liu, S. Chakrabartty, D. S. Gkinosatis, A. K. Mohanty, and N. Lajnef. 2007, Proceedings of Biomedical Circuits and Systems Conference, pp. 119–122.

72. *Carbon Nanotube/Polycarbonate Composites as Multifunctional Strain Sensors.* W. Zhang, J. Suhr, and N. Koratkar. 4, 2006, J. Nanosci. Nanotechnol., Vol. 6, pp. 960–964.

73. *Fabrication of a Thin-Film Strain-Gauge Transducer Using Bi2O3-V2O5.* Perrem, K. Arshak and R. 1, 1993, Sens. Actuators. A: Phys, Vol. 36, pp. 73–76.

74. *Stress softening experiments in silica-filled polydimethylsiloxane provide insight into a mechanism for the Mullins effect.* D. E. Hanson, M. Hawley, R. Houlton, K. Chitanvis, P. Rae, E. B. Orler, and D. A. Wrobleski. 24, 2005, Polymer, Vol. 46, pp. 10989-10995.

75. *Nanoscale Deformation and Nanomechanical Properties of Polydimethylsiloxane (PDMS).* Charitidis, C. A. 2, 2011, Ind. Eng. Chem. Res, Vol. 50, pp. 565-570.

76. *The Mechanical Properties of the Rubber Elastic Polymer Polydimethylsiloxane for Sensor Applications.* J. C. Lotters, W. Olthuis, P. H. Veltink and P. Bergveld. 3, 1997, J. Micromech. Microeng., Vol. 7, pp. 145-147.

77. *Multi-layer Embedment of Conductive and Non Conductive PDMS for All-elastomer MEMS.* J. M. Engel, N. Chen, K. Ryu, S. Pandya, C. Tucker, Y. Yang, C. Liu. 2006, The 12th Solid State Sensors, Actuator and Microsystems Workshop.

78. *Super-Elastic Graphene Ripples for Flexible Strain Sensors.* Y. Wang, R. Yang, Z. Shi, L. Zhang, D. Shi, E. Wang, G. Zhang. 5, 2011, ACS Nano, Vol. 5, pp. 3645-3650.

79. *Highly Sensitive Skin-Mountable Strain Gauges Based entirely on Elastomers.* N. Lu, C. Lu, S. Yang, J. Rogers. 2012, Adv. Funct. Mater, p. ??

80. B.D. Ratner, A.S. Hoffman, F.J. Schoen, J.E. Lemons. *Biomaterials Science: An Introduction to Materials in Medicine.* s.l. : Elsevier Academic Press, 2004.

81. *Transparent, Flexible, Low-Temperature and Solution Processible Graphene Composite Electrode.* H. Chang, G. Wang, A. Yang, X. Tao, X. Liu, Y. Shen, Z. J. Zheng. 2010, Adv. Funct. Mater, Vol. 20, pp. 2893-2902.

82. *Exfoliation of graphite flake and its nanocomposites.* G. H. Chen, D. J. Wu, W. U. Weng, C. L. Wu. 2003, Carbon, Vol. 41, p. 619.

83. *Nanoscale investigation of the structural and chemical changes induced by oxidation on carbon black surfaces: A scanning probe microscopy approach.* J. I. Paredes, M. Gracia, A. Martinez-Alonso, and J. M. D. Tascon. 2005, Journal of Colloid and Interface Science, Vol. 288, pp. 190-199 .

84. *Changing the percolation threshold of carbon black/polymer composite by a coupling treatment of the carbon black.* . Yoon HG, Kwon KW, Nagata K, Takahashi K. 8-9, 2004, Carbon, Vol. 42, pp. 1877-9.

85. *Studies of electrical and mechanical properties of poly(vinyl chloride) mixed with electrically conductive additives.* ALG Saad, HA Aziz, OIH Dimitry. 3, 2004, Journal of applied polymer science, Vol. 91 , pp. 1590-1598.

86. *Carbon Nanowire Made of a Long Linear Carbon Chain Inserted Inside a Multiwalled Carbon Nanotube.* X. Zhao, Y. Ando, Y. Liu, M. Jinno, and T. Suzuki. 18, 2003, Phys. Rev. Lett., Vol. 90, p. 187401.

87. *Exceptionally high Young's modulus observed for individual carbon nanotubes.* M. M. J. Treacy, T. W. Ebbesen, J. M. Gibson. 1996, Nature, Vol. 381, p. 678.

88. *Helical Microtubules of Graphitic Carbon.* Iijima, S. 6348, 1991, Nature, Vol. 354, pp. 56–58.

89. *Processing and Modeling of Conductive Thermoplastic/Carbon Nanotube Films for Strain Sensing.* G. T. Pham, Y.-B. Park, Z. Liang, C. Zhang, and B. Wang. 1, 2008, Compos. B: Eng., Vol. 39, pp. 209–216.

90. *A Review and Analysis of Electrical Percolation in Carbon Nanotube Polymer Composites.* Kovacs, W. Bauhofer and J. Z. 10, 2009, Compos. Sci. Technol, Vol. 69, pp. 1486–1498.

91. *Multi-walled Carbon Nanotubes/Poly(L-lactide) Nanocomposite Strain Sensor for Biomechanical Implants.* Y. Liu, S. Chakrabartty, D. S. Gkinosatis, A. K. Mohanty, and N. Lajnef. 2007, Proceedings of Biomedical Circuits and Systems Conference, pp. 119–122.

92. *Y. Huang and E. Terentjev.* Terentjev, Y. Huang and E. 1, 2008, Int. J. Mate. Form, Vol. 2, pp. 63–74.

93. *Effect of Ball Milling on Morphology of Cup-Stacked Carbon Nanotubes.* Y. A. Kim, T. Hayashi, Y. Fukai, M. Endo, T. Yanagisawa, and M. S. Dresselhaus. 3–4, 2002, Chem. Phys. Lett, Vol. 355, pp. 279–284.

94. *Experimental Investigation of Nanoparticle Dispersion by Beads Milling with Centrifugal Bead Separation.* M. Inkyo, T. Tahara, T. Iwaki, F. Iskandar, C. J. Hogan Jr., and K. Okuyama. 2, 2006, J. Colloid Interface Sci., Vol. 304, pp. 535–540.

95. *Characteristics of Ultrasonic Dispersion of Carbon Nanotubes Aided by Antifoam.* Sano, H. Sato and M. 1–3, 2008, Colloids Surf., A, Vol. 322, pp. 103–107.

96. *Dispersion of Carbon Nanotubes: Mixing, Sonication, Stabilization, and Composite Properties.* Terentjev, Yan Yan Huang and Eugene M. 1, 2012,, Polymers, Vol. 4, pp. 275-295.

97. *Preparation of carbon nanotube bioconjugates for biomedical applicatio.* Liu, Z., et al., et al. 2009, Nat. Protoc., Vol. 4, pp. 1372-1381.

98. *Effects of Surface-Functionalized Multi-Walled Carbon Nanotubes on the Properties of Poly(dimethyl siloxane) Nanocomposites.* T. P. Chua, M. Mariatti, A. Azizan, and A. A. Rashid. 4, 2010, Compos. Sci. Technol, Vol. 70, pp. 671–677.

99. *Effect of Dispersion State of Carbon Nanotube on the Thermal Conductivity of Poly(dimethyl siloxane) Composites* . J. Hong, J. Lee, C. K. Hong, and S. E. Shim. 1, 1010, Curr. Appl. Phys., Vol. 10, pp. 359–363.

100. *Electrical and Dielectric Properties of Hydroxylated Carbon Nanotube−Elastomer Composites.* R. R. Kohlmeyer, A. Javadi, B. Pradhan, S. Pilla, K. Setyowati, J. Chen, and S. Gong. 41, 2009, J. Phys. Chem. C, Vol. 113, pp. 17626–17629.

101. *Poly(3-hexylthiophene) Wrapped Carbon Nanotube/Poly(Dimethylsiloxane) Composites for use in Finger-Sensing Piezoresistive Pressure Sensors.* J. Hwang, J. Jang, K. Hong, K. N. Kim, J. H. Han, K. Shin, and C. E. Park. 1, 2011, Carbon, Vol. 49, pp. 106–110.

102. *A metal polymer composite with unusual properties.* D Bloor, K Donnelly, P J Hands, P Laughlin and D Lussey. 16, 2005, Journal of Physics D: Applied Physics, Vol. 38, p. 2851.

103. Lussey, D. *Peratech Ltd. PCT/GB99/6495069 a. (WO 99/38173)* UK, 1998,.

104. *Multi-Layer Embedment of Conductive and Non-Conductive PDMS for All-Elastomer MEMS.* Jonathan M. Engel, Nannan Chen, Kee Ryu, Saunvit Pandya, Craig Tucker, Yingchen Yang, and Chang Liu. 2006, The 12th Solid State Sensors, Actuator, and Microsystems Workshop.

105. *Flexible strain sensors fabricated with carbon nano-tube and carbon nano-fiber composite thin films.* Fuh-Yu Changa, Ruoh-Huey Wangb, Hsiharng Yangc, Yu-Hsien Lina, Tse-Min Chena, Shu-Jiuan Huangd. 24, 2010, Thin Solid Films, Vol. 518, pp. 7343–7347.

106. *Polyisoprepene-multi-walled carbon nanotube composites for sensing strain.* M.Knite, V.Tupureina, A. Fuith, J. Zavickis,V.Teteris. 2007, Sci.Eng., Vol. 27, p. 1125.

107. *Strain-dependent electrical resistance of multi-walled carbon nanotube/polymer composite films.* M Park, H Kim, JP Youngblood. 5, 2008, Nanotechnology , Vol. 19 , p. 055705.

108. *A strain gauge that uses carbon black and carbon nanotube doped silicone oil encapsulated in a PDMS microchannel.* Ching-Hsiang Cheng, Lidan Xiao, Yin-Nee Cheung, Chen Chao1, Mo Yang, King-Lun Kwok. 2007, 7th IEEE Conference on Nanotechnology, pp. 1199 - 1202.

109. *Nanocomposite Conductive Elastomer: Microfabrication Processes and Applications in Soft-Matter MEMS Sensors.* Liu, Chang. Mater. Res. Soc. Symp. Proc., Vol. 947.

110. *A rubberlike stretchable active matrix using elastic conductors.* 5895, 2008 , Science, Vol. 321, pp. 1468-72.

111. *Resistance-pressure sensitivity and a mechanism study of multiwall carbon nanotube networks/poly(dimethylsiloxane) composites.* C. H. Hu, C. H. Liu, L. Z. Chen, Y. C. Peng, and S. S. Fan. 2008, Appl. Phys. Lett., Vol. 93, p. 033108 .

112. *Effects of carboxyl radical on electrical resistance of multi-walled carbon nanotube filled silicone rubber composite under pressure.* Peng Wang, Shengnan Geng, Tianhuai Ding. 10, 2010, Composites Science and Technology, Vol. 70, pp. 1571–1573.

113. *Poly(3-hexylthiophene) wrapped carbon nanotube/.* Jihun Hwanga, Jaeyoung Janga, Kipyo Honga, Kun Nyun Kimb, Jong Hun Hanc, Kwonwoo Shinc, Chan Eon Park. 1, 2011, Carbon, Vol. 49, pp. 106–110.

114. *Conductive TPU - CNT Composites for Strain Sensing.* Zhang, Rui. 2009, PhD Thesis, Queen Mary university of London.

115. *Polymer-embedded carbon nanotube ribbons for stretchable conductors.* Zhang, Y. Y. et al. 2010, Adv. Mater., Vols. 22,, pp. 3027–3031.

116. *Piezoresistive behavior study on fingersensing silicone rubber/graphite nanosheet nanocomposites.* Chen L, Chen G, Lu L. 6, 2007, Adv Funct Mater, Vol. 17, pp. 898–904.

117. *Supersensitive linear piezoresistive property in carbon nanotubes/silicone rubber nanocomposites.* Dang ZM, Jiang MJ, Xie D, Yao SH, Zhang LQ, Bai J. 024114, 2008, J Appl Phys, Vol. 104, pp. 0–6.

118. *Conductive rubber materials for pressure sensors.* M Hussain, YH Choa, K Niihara. 6, 2001, Journal of materials science letters, Vol. 20, pp. 525-527.

119. [Online] http://www.peratech.com.

120. *Peratech Ltd, Old Repeater Station, 851 Gatherley Road, Brompton on Swale, Richmond, DLIO 7JH.*

121. *Brittle versus ductile transition of nanocrystalline metals.* Yang, F., W. Yang. 13, 2008, J. Solids and Structures, Vol. 45, pp. 3897-3907.

122. *Electrical properties and vapour sensing characteristics of a novel metal-polymer composite.* Graham, Adam. 2008, PhD thesis, Durham University.

123. *Metal–polymer composite sensors for volatile organic compounds: Part 1. Flow-through chemi-resistors.* 1, 2012, Sensors and Actuators B: Chemical, Vol. 162, pp. 400–408.

124. Gardner, J.W. and P.N. Bartlett. *Electronic noses: Principles and applications.* s.l. : Oxford: Oxford University Press, 1999.

125. *Application of capacitance techniques in sensor design.* Heerens, W -C. 1986 , J. Phys. E: Sci. Instrum., Vol. 19, p. 897.

126. Maxwell, J. C. *A treaties on electricity and magnetism.* s.l. : Oxford, 1873.

127. *Smart capacitive sensors, physical, geometrical and electronic aspects",.* Jong, G. De. 1994, PhD thesis, Delft University of Technology.

128. [Online] www.omega.com.

129. Baxter, L. K. *Capacitive sensors: design and applications",.* s.l. : IEEE Press, 1997.

130. *A Ultra-Sensitive, High-Vacuum Absolute Capacitive Pressure Sensor.* Y. Zhang, S. Massoud-Ansari, G. Meng, W. Kim, and N. Najafi. 2001, Technical Digest of the 14th IEEE International Conf. on MicroElectro Mechanical Systems, pp. 166-169.

131. *A Barometric Pressure Sensor with Multiple Elements.* Wise, Y. Zhang and K. D. 1995, Digest IEEE Transducers '95.

132. *An Ultra-Sensitive Capacitive Pressure Sensor with a Bossed Dielectric Diaphragms.* Wise, Y. Zhang and K. D. 1994, Technical Digest of the IEEE Solid-state Sensors and Actuators workshop.

133. *Flexible electronics: stretching our imagination.* LeMieux, M. C. & Bao, Z. N. 2008, Nature Nanotech., Vol. 3, pp. 585-586.

134. *Current concepts: nanomedicine.* Kim, B. Y. S., Rutka, J. T. & Chan, W. C. W. 2010, New Engl. J. Med., Vol. 363, pp. 2434-2443.

135. *Soft robotics for chemists.* Ilievski, F., Mazzeo, A. D., Shepherd, R. F., Chen, X. & WHitesides, G. M.,. 2011, Angew. Chem. Int. Ed., Vol. 50, pp. 1890-1895.

136. *A highsensitive ultra-thin MEMS capacitive pressure sensor.* Zhang, Y., Howver, R., Gogoi, B. and Yazdi, N. 2011, 16th International IEEE in Solid-State Sensors, Actuators and Microsystems Conference, pp. 112-115.

137. *Square Diaphragm CMUT Capacitance Calculation Using a New Deflection Shape Function.* Rahman, M. M. and Chowdhury, S. 2011, Journal of Sensors.

138. *Fabrication and Characterization of a New MEMS Capacitive Microphone using Perforated Diaphragm.* Ganji, B. A. and Majlis, B. Y. 2, 2009, International journal of Engineering, Vol. 22, pp. 153-160.

139. *An integrated MEMS three-dimensional tactile sensor with large force range.* T. Mei, W. J. Li, Y. Ge, Y. Chen, L. Ni, and M. H. Chan. 2000, Sens. Actuators A, Vols. 80,, pp. 155–162.

140. *Silicon smart tactile image sensor with pneumatically swollen single diaphragm structure.* H. Takao, K. Sawada, and M. Ishida. 2004, 17th IEEE Int. Conf. Micro Electro Mech. Syst., pp. 846–849.

141. *A high-sensitive ultra-thin MEMS capacitive pressure sensor.* Y. Zhang, R. Howver, B. Gogoi and N. Yazdi. 2011, 16th International Solid-State Sensors, Actuators and Microsystems Conference, pp. 112 - 115.

142. *Development of polyimide flexible tactile sensor skin.* J. Engel, J. Chen, and C. Liu. 2003, J. Micromech. Microeng., Vol. 13, pp. 359–366.

143. *Measurement of Strain and Strain Rate by Echocardiography.* Marwick, T. H. 7, 2006, J. Am. Coll. Cardiol, Vol. 47, pp. 1313–1327.

144. *Microfabrication of conductive polymer nanocomposite for sensor applications.* Liu, Chaoxuan. 2012, PhD thesis, Louisiana State University.

145. *Wireless flexible capacitive sensor based on ultra-flexible for strain measurement of automobile tires.* Ryosuke Matsuzaki, Akira Todoroki. 1, 2007, Sensors and Actuators A: Physical, Vol. 140, pp. 32–42.

146. *Energy-Efficient Strain Gauges for the Wireless Condition Monitoring Systems* . M. Berndt, Thomas Fellner, Roderich Zeiser and Jürgen Wilde. 2012, 6th European Workshop on Structural Health Monitoring - We.4.C.2.

147. *Soft-Matter Capacitive Sensor for Measuring Shear and Pressure Deformation.* Peter Roberts, Dana D. Damian, Wanliang Shan, Tong Lu, Carmel Majidi. 2013, 2013 IEEE International Conference on Robotics and Automation (ICRA), p. 3529.

148. *Flexible Tactile Sensor Using Polyurethane Thin Film.* Masato Suzuki, Tomokazu Takahashi and Seiji Aoyagi. 2, 2012, Micromachines, Vol. 3, pp. 315-324.

149. *A Flexible Polymer Tactile Sensor: Fabrication and Modular Expandability for Large Area Deployment.* Hyung-Kew Lee, Sun-Il Chang, and Euisik Yoon. 6, 2006, Journal of Microelectromechanical Systems, Vol. 15, pp. 1681 - 1686.

150. *Skin-like pressure and strain sensors based on transparent elastic films of carbon nanotubes.* Darren J. Lipomi, Michael Vosgueritchian, Benjamin C-K. Tee, Sondra L. Hellstrom,Jennifer A. Lee, Courtney H. Fox and Zhenan Bao. 2011, Nature Nanotechnology, Vol. 6, pp. 788–792 .

151. *A full-body tactile sensor suit using electrically conductive fabric and strings.* M. Ibana, Y. Hoshino, K. Nagasaka, T. Ninomiya, S. Kagami, and H. Inoue. 2, Proc. 1996 IEEE/RSJ Int. Conf. Intell., pp. 450–457.

152. *A textile based capacitive pressure sensor.* M. Sergio, N. Manaresi, M. Tartagni, R. Guerrieri, and R. Canegallo,. 2002, Proc. IEEE Sensors, Vol. 2, pp. 1625–1630.

153. *Hybrid resistive tactile sensing.* So, H. Zhang and E. 1, 2002, IEEE Trans.Syst., Vol. 32, pp. 57-65.

154. *A Flexible Capacitive Sensor with Encapsulated Liquids as Dielectrics.* Yasunari Hotta, Yuhua Zhang and Norihisa Miki. 1, 2012, Micromachines , Vol. 3, pp. 137-149.

155. *Design and evaluation of a skin-like sensor with high stretchability for contact pressure measurement.* Debao Zhoua, Haopeng Wanga,. 2013, Sensors and Actuators A: Physical, Vol. 204, pp. 114-121.

156. *A novel PDMS based capacitive pressure sensor.* Riedl, X., Bolzmacher, C., Wagner, R. and Bauer, K., Schwesinger, N. Sensors, 2010 IEEE, pp. 2255 - 2258.

157. *Normal and Shear Force Measurement Using a Flexible Polymer Tactile Sensor With Embedded Multiple Capacitors.* Hyung-Kew Lee, Jaehoon Chung, Sun-Il Chang, and Euisik Yoon. 4, 2008, Journal of Microelectromechanical Systems, Vol. 17, pp. 934 - 942.

158. *Flexible polymer transistors with high pressure sensitivity for application in electronic skin and health monitoring.* Gregor Schwartz, Benjamin C.-K. Tee, Jianguo Mei, Anthony L. Appleton, Do Hwan Kim, Huiliang Wang & Zhenan Bao. 2013, Nature Communications, Vol. 4, p. 1859.

159. *A wearable and highly sensitive pressure sensor with ultrathin gold nanowires.* Shu Gong, Willem Schwalb, Yongwei Wang, Yi Chen, Yue Tang, Jye Si, Bijan Shirinzadeh & Wenlong Cheng. 2013, Nature Communications, Vol. 5, p. 3132.

160. *Simple and rapid synthesis of ultrathin gold nanowires, their selfassembly and application in surface-enhanced Raman scattering.* Feng, H. et al. 2009, Chem. Commun., pp. 1984–1986.

161. [Online] http://www.rapidonline.com/design-technology/qtc-pills-each-06-1298.

162. *Micropatternable Multifunctional Nanocomposite Polymers for Flexible Soft NEMS and MEMS Applications.* Gray, Khosla and B. L. 3, 2012 , ECS Trans. , Vol. 45, pp. 477-494.

163. *Improved Dispersion of Carbon Nanotubes in Polymers at High Concentrations.* Choi, Chao-Xuan Liu 1 and Jin-Woo. 4, 2012, Nanomaterials , Vol. 2, pp. 329-347.

164. *Effect of Surfactants and Manufacturing Methods on the Electrical and Thermal Conductivity of Carbon Nanotube/Silicone Composites.* Jarmila Vilčáková, Robert Moučka 1,2, Petr Svoboda 1,2, Markéta Ilčíková 3, Natalia Kazantseva Martina Hřibová , Matej Mičušík and Mária Omastová. 11, 2012, Molecules , Vol. 17, pp. 13157-13174.

165. *Development of Polydimethylsiloxane Substrates with Tunable Elastic Modulus to Study Cell Mechanobiology in Muscle and Nerve.* Rachelle N. Palchesko, Ling Zhang, Yan Sun, Adam W. Feinberg. 12, 2012, PLos ONE, Vol. 7, p. e51499.

166. *Micro-well arrays for 3D shape control and high resolution analysis of single cells.* Ochsner M, Dusseiller MR, Grandin HM, Luna-Morris S, Textor M, et al. 2007, Lab On A Chip, Vol. 7, pp. 1074-1077.

167. *A hybrid model to determine mechanical properties of soft polymers by nanoindentation.* Liao Q, Huang J, Zhu T, Xiong C, Fang J. 2010 , Mechanics of Materials, Vol. 42, pp. 1043–1047.

168. *A novel method for assessing adherent single-cell stiffness in tension: design and testing of a substrate-based live cell functional imaging device.* Bartalena G, Grieder R, Sharma RI, Zambelli T, Muff R, et al. 2011, Biomed Microdevices, Vol. 13, pp. 291-301.

169. *Process and material properties of polydimethylsiloxane (PDMS) for Optical MEMS.* Schneider F, Draheim J, Kamberger R, Wallrabe U. 2009, Sensors and Actuators A: Physical, Vol. 151, pp. 95–99.

170. *Nanoscale hydrophobic recovery: A chemical force microscopy study of UV/ozone-treated cross-linked poly(dimethylsiloxane).* Hillborg H, Tomczak N, Olah A, Schonherr H, Vancso GJ. 2004, Langmuir, Vol. 20, pp. 785-794.

171. *Hydrophobic recovery of UV/ozone treated poly(dimethylsiloxane): adhesion studies by contact mechanics and mechanism of surface modification.* Olah A, Hillborg H, Vancso GJ. 2005, Applied Surface Science, Vol. 239, p. 410.

172. *PDMS bonding by means of a portable, low-cost corona system.* Kathryn Haubert, Tracy Drierb and David Beebec. 2006, Lab Chip, Vol. 6, pp. 1548-1549.

173. Thompson. "Resist Processing", an Introduction to Microlithography 2nd ed. s.l. : American Chemical Society, pp. 305-313.

174. *Sylgard@l84 Silicone elastomer product information,Dow Corning, Ref. no. 10-1204A-01.*

175. *Elastomer-supported cold welding for room temperature wafer-level bonding.* W.Y . Zhang, G. S. Ferguson , S. Tatic-Lucic. 2004, 17th IEEE International Conference on MEMS, pp. 741 - 744.

176. *The mechanical properties of the rubber elastic polymer polydimethylsiloxane for sensor applications.* J C Lottersy, W Olthuis, P H Veltink and P Bergv. 1997 , J. Micromech. Microeng., Vol. 7, p. 145.

177. *A multi-component nanocomposite screen-printed ink with non-linear touch sensitive electrical conductivity* . Alexander J Webb, Marek Szablewski, David Bloor, Del Atkinson,Adam Graham, Paul Laughlin and David Lussey. 16, 2013, Nanotechnology, Vol. 24, p. 165501.

178. *Fabrication of polymer microstructures for MEMS: sacrificial layer micromolding and patterned substrate micromolding.* Ferrell N, Woodard J, Hansford D. 6, 2007, Biomed Microdevices., Vol. 9, pp. 815-821.